**Title**

Finite Thickness Biological Membranes: Theory and Application



**Author**

Lipel, Zachary Gabriel

**Publication Date**

2023

Peer reviewed|Thesis/dissertation

# Finite Thickness Biological Membranes: Theory and Applications

By

Zachary Gabriel Lipel

A dissertation submitted in partial satisfaction of the

requirements for the degree of

Doctor of Philosophy

in

Chemical Engineering

in the

Graduate Division

of the

University of California, Berkeley

Committee in charge:

Professor Kranthi Kiran Mandadapu, Chair
Professor Rui Wang
Professor Panayiotis Papadopoulos
Professor James Casey

Fall 2023

Finite Thickness Biological Membranes: Theory and Applications

Abstract

Finite Thickness Biological Membranes: Theory and Applications

by

Zachary Gabriel Lipel

Doctor of Philosophy in Chemical Engineering

University of California, Berkeley

Professor Kranthi Kiran Mandadapu, Chair

Biological membranes form the boundaries of cells and most organelles. Therefore, they are crucial for processes such as intracellular vesicle transport, cell signaling, and endocytosis. The shape and function of cells is largely regulated by membrane-environment interactions. As such, it is important to understand the mechanical properties and behaviors of these membranes. For instance, drug delivery methods focus on targeting the cell membrane, and therefore require a detailed understanding of its physics. All biological membranes are composed of lipid bilayers. Each individual lipid has a hydrophobic tail and a hydrophilic head. Therefore, under appropriate physicochemical conditions, lipids will spontaneously assemble into bilayers. The emergent properties of these membranes is a result of the lipid chemistry. The collective in-plane motion of the lipids due to diffusion leads to membrane fluidity while the rigidity resulting from the emergence of the bilayer structure furnishes elasticity. As a result, these membranes are viscoelastic media capable of arbitrarily curved and large deformations. Therefore, a careful mathematical framework that allows for these deformations is required. Most descriptions on the continuum level have described membranes as two-dimensional sheets. More recent developments have begun to resolve the thickness of membrane but often rely on equilibrium approaches.

Here, we present a comprehensive theoretical description of lipid bilayers as three-dimensional bodies. In order to do so, we introduce a spectral methods framework to derive approximate two-dimensional equations describing the membrane that retain its thickness as an explicit parameter. We arrive at a low-order, analytically tractable theory that allows us to explore membrane thickness length scale phenomena on the continuum level. Using this description, we investigate the hydrodynamic response of a finite thickness lipid bilayer by employing the linear response framework. We show that thickness effects lead to a previously unresolved mode of viscous dissipation in the vicinity of the membrane, and finally discuss the biological implications of our findings.

To my brothers Jonah and Gavin,

for your unwavering love and support then, now, and always.

# Contents

# List of Figures

# Acknowledgments

I would like to thank my advisors Drs. Kranthi Mandadapu and Rui Wang for providing me with funding and a space to explore my ideas. I am appreciative of Rui for insightful discussion in the beginning of my PhD.

The path to completing graduate research is never a solitary one. While I may submit this thesis alone, the journey has been profoundly shaped by numerous friends, colleagues, and family members. A special acknowledgment goes to the exceptional graduate students at Berkeley, whose collaboration was a cornerstone of my experience. My heartfelt thanks to my colleagues, Drs. Cory Hargus, Muhammad Hasyim, and Clay Batton, for their invaluable discussions and support over the years. I am particularly indebted to Dr. Yannick Omar and Ahmad Alkadri for our enriching conversations, both within and outside the office. Yannick, your insistence on meticulous research and your kindness have been a beacon in an often challenging environment. Ahmad, your commitment to your work and mathematical precision has been a constant source of inspiration. I cherish our friendship, both in professional and personal realms. I also wish to thank Nikhil Agrawal for bringing joy and light to the otherwise daunting environment of Gilman Hall's basement. Your presence in our office space exemplified the spirit of collaboration and idea-sharing that sets Berkeley's Chemical and Biological Engineering Department apart. I am immensely grateful to Dr. Katie Klymko for her guidance during challenging phases of my research. Her encouragement to persevere was invaluable during times when progress seemed elusive.

Occasionally, we are fortunate enough to encounter singularly remarkable individuals who profoundly alter the trajectory of our lives. I count myself among the lucky few, having met Dr. Dimitrios Fraggedakis during a particularly challenging period in my academic journey. As I faced my qualifying exam, I found myself directionless, merely going through the motions, fearing that my five years of effort would culminate in nothing of significance. However, Dimitrios' arrival in the department that summer marked a turning point. Collaborating with him reignited a passion for learning and comprehension that had nearly diminished. In my professional journey, Dimitrios has been a pivotal figure who more than anyone else taught me the essence of being a scientist. His mentorship enabled me to refine my skills, focus my efforts, and approach problems with a renewed perspective. Most importantly, he showed me how to enjoy science again. Our interactions extended beyond the lab – from casual lunches discussing varied topics, savoring exceptional espressos at 1951, to exploring conferences and enjoying great meals, and even occasional weekend dinners. Through these experiences, Dimitrios exemplified what it means to not just collaborate with a colleague but to foster a lifelong friendship. His approach and philosophy, both in science and life, continue to inspire and guide me.

My time at Berkeley has been made memorable by many wonderful people outside the work environment. To my housemates – Matt, Francis, Alec, and Zach – thank you for the unforgettable memories and traditions at Edwards House, my second home. To my parents, Kathy and Vadim, your enduring work ethic and love have deeply influenced my approach

to both personal and professional pursuits. Your unwavering support has been pivotal in my PhD journey, and I am incredibly grateful for it.

To my brothers, Jonah (Jroob) and Gavin (Goob), your presence in my life is invaluable. I am immensely proud of the remarkable individuals you both are and am fortunate to have your support. It is one of the greatest joys of my life to be your brother and to call you both my closest friends. Every step of this journey is dedicated to you. Lastly, I express my deepest appreciation to my partner, Nicole (Feesh). Your entry into my life towards the end of this journey has been transformative. Your encouragement and belief in me, especially during times of doubt, have been crucial in maintaining my resolve.

# Chapter 1

# Introduction

The plasma membrane is a critical component of living cells, serving as a protective barrier composed primarily of lipids and proteins [1]. This ultra-thin structure, approximately 5 nanometers thick, is responsible for safeguarding the internal contents of cells from the external environment, making it indispensable for the survival of all cells on Earth.

The plasma membrane consists of a lipid bilayer embedded with proteins, imparting specific functions to this membrane. In addition to its role as a protective boundary, the plasma membrane plays key roles in regulating nutrient transport, waste removal, and sensing changes in the surroundings.

Remarkably, the plasma membrane possesses mechanical properties that allow adaptation to changes in cell size and shape without compromising structural integrity. Even in cases of damage, the membrane can quickly self-seal, ensuring the survival of the cell.

All biological membranes share a common structural feature: a lipid bilayer composed of hydrophilic head groups and hydrophobic tails. Lipids in aqueous solutions spontaneously self-assemble, leading to coarse-grained phenomena within membranes, such as bending and tension.

Molecular dynamics simulations have provided valuable insights into lipid bilayers and biomolecules within membranes at the atomic level. However, these simulations have computational limitations, especially for long timescales and length scales relevant to certain biological processes. Additionally, their accuracy depends on empirical force field models [2–5].

To address these challenges, continuum models for biological membranes have been developed. These models offer computational efficiency and can investigate long-term phenomena while integrating fluid dynamics principles. They are based on thermodynamic principles, providing rigorous mathematical foundations [6–11].

Continuum theories have often modeled lipid bilayers as two-dimensional surfaces, and have played a crucial role in elucidating processes at length-scales of approximately $\mathcal{O}(10^2 - 10^3)$ nm. These models have facilitated investigations into phenomena such as membrane budding during endocytosis [12, 13] and the surface diffusion of embedded proteins [14, 15], a process central to cellular signaling. The Helfrich-Canham energy model has been

foundational in this regard, describing bilayer elasticity in terms of curvature, with parameters such as spontaneous curvature and bending modulus [6]. Extensions have introduced anisotropy and inhomogeneity, offering a more realistic representation of biological membranes [16]. More recent advancements have incorporated thermal fluctuations, which are particularly relevant at the nanoscale [17], and significantly impact phenomena such as lipid domain formation and membrane dynamics. Furthermore, two dimensional models have proved essential for understanding membrane budding during endocytosis [18], and have been amenable to including protein-lipid interactions [8] as well as understanding the dynamics of axisymmetric [19] and nonaxisymmetric [13] deformations.

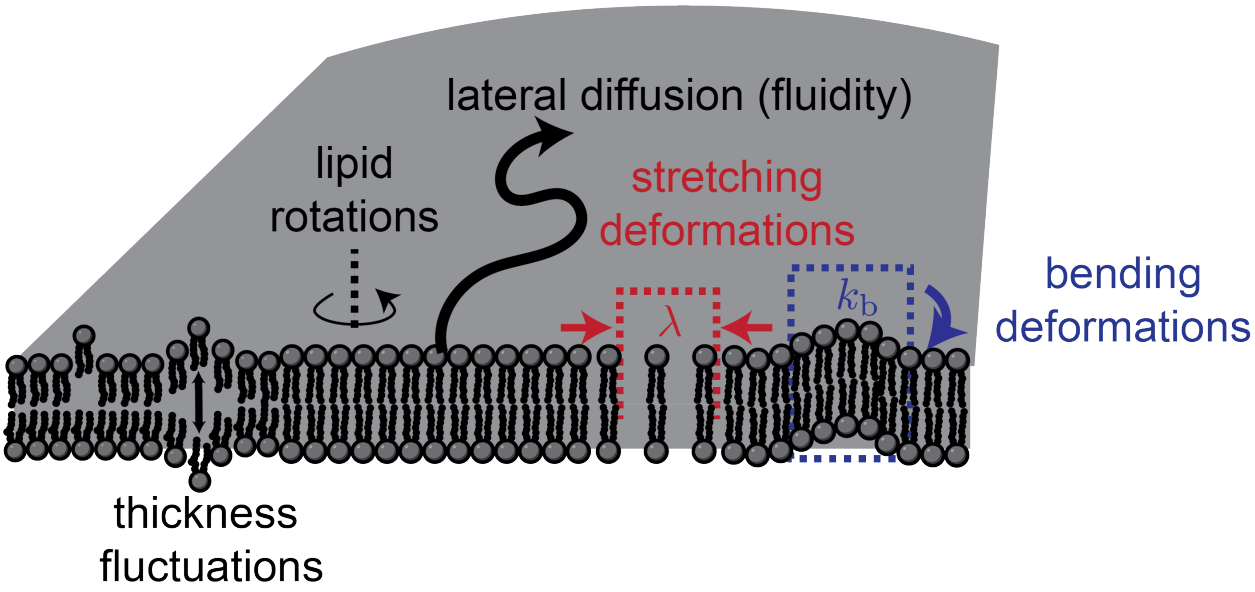


Figure 1.1: Schematic of some of the potential motions possible in lipid bilayers. At the level of individual lipids, we have phenomena such as thickness fluctuations and in-plane diffusion. Upon coarse-graining, these motions lead to collective motions such as in-plane fluidity, areal stretching/compression, and out-of-plane bending.

Two-dimensional models, while useful, have limitations in resolving intramembrane mechanics and membrane-environment coupling when bilayer thickness is a critical factor. For example, thickness is considered to be relevant in the function of mechanosensitive membrane channel proteins [20] as well as membrane fluctuations and dynamics during intercellular binding [21–23]. Expanding upon conventional two-dimensional membrane models, efforts have been made to incorporate finite thickness effects using free energy formalisms to better capture the intricacies of biological membranes [24–26]. Previous studies have successfully harnessed these finite thickness models to investigate a range of phenomena. For instance, these models have been instrumental in exploring the hydrodynamics of membrane-fluid systems [27, 28]. By considering the effects of bilayer thickness, these studies have pro-

vided insights into how fluids interact with membranes and how dynamic processes are influenced by this additional dimension. Moreover, finite thickness models have been applied to investigate nanoscopic density fluctuations within membranes, leveraging structure factor measurements [29–31]. These investigations have shed light on the spatial organization of molecules within lipid bilayers and how fluctuations at the nanoscale impact membrane properties. While these approaches represent significant progress in modeling finite thickness effects on membrane dynamics, they may not fully account for intramembrane mechanics and membrane-fluid couplings consistent with three-dimensional continuum mechanics. While these approaches represent significant progress in modeling finite thickness effects on membrane dynamics, they may not fully account for intramembrane mechanics and membrane-fluid couplings consistent with three-dimensional continuum mechanics [24, 25, 32].

## 1.1 Outline of the thesis

In the development of a lipid membrane theory, our choice of models is guided by the specific phenomena we aim to describe. For instance, when characterizing membrane deformations occurring on timescales of several seconds and spanning hundreds to thousands of nanometers, we turn to the formalism of balance laws in continuum mechanics. This framework proves to be well-suited for capturing such dynamic processes.

Biological membranes can undergo highly intricate morphological shape transitions, as exemplified by the aforementioned endocytosis, which cannot be adequately described using conventional Cartesian, cylindrical, or spherical coordinate systems. Additionally, we aim to apply balance laws on these highly curved and evolving surfaces. To address these challenges, we employ differential geometry, which allows us to express arbitrarily large and curved membrane deformations in generic, curvilinear coordinates. Chapter I provides an overview of this framework, and shows how we can use it to describe the kinematics of the membrane.

Although lipid bilayers are often described as two-dimensional surfaces, they are, in reality, fully three-dimensional bodies. Despite some progress in incorporating bilayer thickness explicitly in continuum mechanical theories, a model for membranes that adequately resolves coupling to the environment and intramembrane mechanics at nanoscopic length and time scales has not yet been developed. To derive such a theory, we employ spectral methods to dimensionally reduce the three-dimensional equations of motion, resulting in effective two-dimensional equations that explicitly consider membrane thickness. We refer to this model as the "$(2+\delta)$-dimensional" theory for lipid bilayers, where $\delta$ refers to the bilayer thickness, which remains constant. The mathematical frameworks necessary to develop this framework are presented in Chapter II. In Chapter III, we apply this theory to the the three-dimensional balance laws and constitutive equations that govern lipid bilayer physics. In doing so we arrive at equations of motion that describe the viscoelastic nature of the membranes and couple them to an immersing bulk medium. In Chapter IV, we present the framework of linear response and use it to derive general base state and perturbation equations for mem-

branes with nearly flat geometries. In the context of biological membranes, we assume that thermal fluctuations in the surrounding medium lead to shape perturbations. By studying the dynamics of these perturbations and characterizing the resulting hydrodynamic response, we gain valuable insights into the nature of the phenomena we resolve with our theory. We then solve these equations and analyze the dynamic response for a membrane in an infinite medium. These analyses allow us to contextualize our results in terms of biological processes at relevant length scales. A key concept we consider is how bilayer thickness affects the non equilibrium physics of membranes, and more importantly, when two-dimensional theories become inadequate. This linear response analysis can naturally lead us into statistical descriptions of membrane fluctuations.

# Chapter 2

# Geometry of finite thickness lipid bilayers

As mentioned in the introduction, lipid bilayers are capable of undergoing highly complex deformations. Therefore, we must introduce a mathematical framework capable of handling such descriptions. Differential geometry is a branch of mathematics that provides the tools for studying the geometry of curves and surfaces. In the context of lipid bilayer membranes, a solid understanding of these fundamental concepts is crucial for analyzing their geometric properties. Here, we first review curvilinear geometry in general three-dimensional space. We then introduce the geometry of the membrane and derive the geometric objects necessary to construct the governing equations in the following chapters, which is facilitated by an assumption of the membrane kinematics. In the following, we will adopt the notation found in [33, 34].

## 2.1 Curvilinear geometry in Euclidean space

In this section, we will describe some notions associated with three-dimensional differential geometry, following the notation in [35]. For now, we will not concern ourselves with time dependence and rather will simply convey a framework to describe arbitrarily deformed bodies. Let $x^i$ (for $i = 1, 2, 3$) refer to a fixed right-handed orthogonal Cartesian coordinate system in a Euclidean 3-space. Let $\zeta^i$ denote an arbitrary (real) curvilinear coordinate system defined by the transformation:

$$x^i = x^i(\zeta^1, \zeta^2, \zeta^3), \qquad \det\left(\frac{\partial x^i}{\partial \zeta^j}\right) \neq 0 \ . \tag{2.1}$$

The condition $\det\left(\frac{\partial x^i}{\partial \zeta^i}\right) \neq 0$ ensures the existence of a unique inverse of the preceding transformation so that:

$$\zeta^i = \zeta^i(x^1, x^2, x^3) \ . \tag{2.2}$$

Any point in three-dimensional euclidean space, $\mathbf{P} \in E^3$ can be described by the either of the parametrizations $\{x^i\}$ and $\{\zeta^i\}$.

This local parametrization $\{\zeta^i\}$ defines a set of natural tangent basis vectors:

$$\boldsymbol{g}_i = \frac{\partial \mathbf{P}}{\partial \zeta^i} = \frac{\partial}{\partial \zeta^i}(x^j \boldsymbol{e}_j) = \frac{\partial x^j}{\partial \zeta^i}\mathbf{e}_j \ , \tag{2.3}$$

where $\boldsymbol{e}_j$ are the Cartesian basis vectors. The box product $[\boldsymbol{g}_1, \boldsymbol{g}_2, \boldsymbol{g}_3] = \det\left(\frac{\partial x^i}{\partial \zeta^i}\right)$ is the determinant of the Jacobian of the transformation from Cartesian to local coordinates, which we assume to be nonzero. Any arbitrary three-dimensional vector $\boldsymbol{u} \in \mathbb{R}^3$ can be decomposed into the basis Eq. (2.3):

$$\boldsymbol{u} = u^i \boldsymbol{g}_i \ . \tag{2.4}$$

Having established this parametrically defined tangent space, we can express the first fundamental form as [33]:

$$\mathrm{d}s^2 = \ \mathrm{d}\boldsymbol{x} \cdot \boldsymbol{x} = \boldsymbol{g}_i \cdot \boldsymbol{g}_j \ \mathrm{d}\theta^i \ \mathrm{d}\theta^j = g_{ij} \ \mathrm{d}\theta^i \ \mathrm{d}\theta^i \ . \tag{2.5}$$

We define the covariant metric tensor, denoted as $g_{ij}$, through the following equation:

$$g_{ij} \coloneqq \mathbf{g}_i \cdot \mathbf{g}_j, \tag{2.6}$$

where $g_{ij}$ encapsulates the metric properties of the tangent space within a curvilinear coordinate system. Furthermore, we introduce the reciprocal, or contravariant basis:

$$\boldsymbol{g}^i = \epsilon^{ijk} \frac{\boldsymbol{g}_j \times \boldsymbol{g}_k}{[\boldsymbol{g}_1, \boldsymbol{g}_2, \boldsymbol{g}_3]} \ , \tag{2.7}$$

where $\epsilon^{ijk}$ is the unit permutator and $[\boldsymbol{g}_1, \boldsymbol{g}_2, \boldsymbol{g}_3] = (\boldsymbol{g}_1 \times \boldsymbol{g}_2) \cdot \boldsymbol{g}_3$ is the box product involving the tangent basis vectors. This definition yields:

$$\boldsymbol{g}_i \cdot \boldsymbol{g}^j = \delta_i^j \ , \tag{2.8}$$

as well as an expression for the contravariant metric tensor:

$$g^{ij} \coloneqq \boldsymbol{g}^i \cdot \boldsymbol{g}^j \ , \tag{2.9}$$

which is the inverse of the metric, satisfying $g_{ij} g^{jk} = \delta_i^k$. As a result, the tangent and reciprocal space metric tensors can be used to raise and lower indices by noting that $\boldsymbol{g}_i = g_{ij} \boldsymbol{g}^j$ and $\boldsymbol{g}^i = g^{ij} \boldsymbol{g}_j$. Therefore, we can extend the expression Eq. (2.4):

$$\boldsymbol{u} = u^i \boldsymbol{g}_i = u^i g_{ij} \boldsymbol{g}^j = u_j \boldsymbol{g}^j \ . \tag{2.10}$$

where we see that the components in each basis are related by $u^i = g^{ij}u_j$, and similarly, $u_i = g_{ij}u^j$. This principle can be extended to arbitrary tensors of the form $\boldsymbol{A} = A_{ij}\,\boldsymbol{g}^i \otimes \boldsymbol{g}^j = A_i{}^j\,\boldsymbol{g}^i \otimes \boldsymbol{g}_j = A^i{}_j\,\boldsymbol{g}_i \otimes \boldsymbol{g}^j = A^{ij}\,\boldsymbol{g}_i \otimes \boldsymbol{g}_j$[1]. In total, the relationships are:

$$c^i = g^{ij}\,c_j \ , \tag{2.11}$$

$$c_i = g_{ij}\,c^j \ , \tag{2.12}$$

$$A^{ij} = g^{ik}A_k{}^j = g^{kj}A^i{}_k = g^{ik}\,g^{lj}A_{kl} \ , \tag{2.13}$$

$$A_{ij} = g_{ik}\,A^k{}_j = g_{kj}\,A_i{}^k = g_{ik}\,g_{lj}A^{kl} \ . \tag{2.14}$$

The covariant derivative of vector components $u^j$ with respect to $\zeta^i$ is defined:

$$u^i|_j = u^i_{,j} + u^k\Gamma^i_{kj} \ , \tag{2.15}$$

where the notation $(\cdot)_{,j}$ refers to partial differentiation, $\partial(\cdot)/\partial\zeta^j$, with respect to the coordinate $\zeta^j$. Equation (2.15) represents how $u^j$ changes along the $\zeta^i$ direction while accounting for the dependence of the local tangent basis on that direction. The Christoffel symbol of the second kind is defined as:

$$\Gamma^i_{kj} \coloneqq \frac{1}{2}g^{in}\left(g_{nj,k} + g_{nk,j} - g_{kj,n}\right) \ . \tag{2.16}$$

This quantity captures the connection and curvature of the local tangent basis in the curvilinear coordinate system.

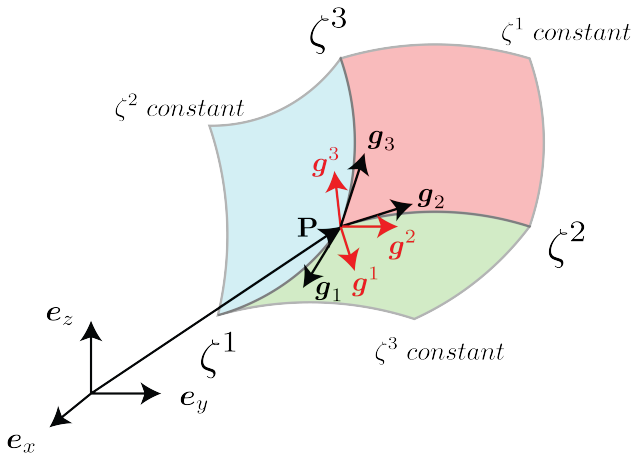


Figure 2.1: Parametrizations of a point **P** in local curvilinear coordinates

This framework equips us to comprehensively describe arbitrarily curved manifolds embedded in Euclidean three-dimensional space. While lipid bilayers inherently possess three-dimensional attributes, our objective is to describe them through the application of effective

[1]In general, $A^i{}_j \neq A_j{}^i$ because not all tensors are symmetric. However, for the most part, tensorial quantities in membrane physics are symmetric.

two-dimensional equations. To achieve this, we will employ kinematic assumptions to map the surface and three-dimensional geometry, allowing us to bridge the gap between the complex three-dimensional reality and the simplified two-dimensional representations.

## 2.2 Geometry and kinematics of finite thickness membranes

Here, we adopt a systematic approach to model a lipid bilayer as a differentiable three-dimensional body, denoted as $\mathcal{M}$. This body is situated within bulk media $\mathcal{B}_\pm$ and bounded by surfaces $\mathcal{S}_\pm$, with the mid-surface represented as $\mathcal{S}_0$, as depicted Fig. 2.2–(a). To describe the geometry of our system effectively, we employ two coupled curvilinear parametrizations: one for the mid-surface $\mathcal{S}_0$ denoted by $(\xi^1, \xi^2) \in \hat{\Omega}$ and another for thickness variation of $\mathcal{M}$ represented by $\xi^3 \in \hat{\Xi}$ to represent the thickness variation of $\mathcal{M}$, where $\hat{\Omega}$ and $\hat{\Xi}$ define their respective parametric domains. It is important to note that these parametrizations, denoted with a "hat" symbol, remain constant over time, making Lagrangian or "convected" coordinates [36, 37].

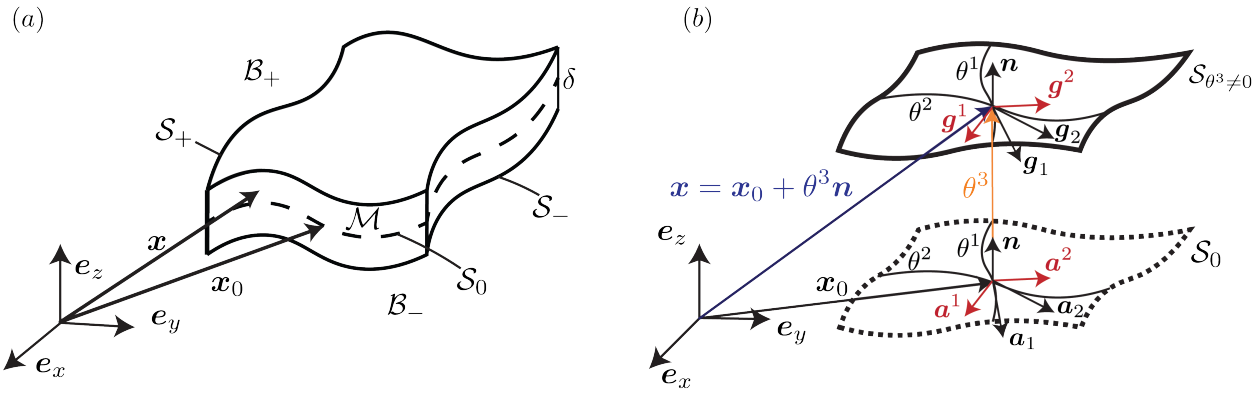


Figure 2.2: (a) Membrane and its bounding surfaces embedded in Euclidean 3-space. (b) Local parametrization of the mid-surface $\mathcal{S}_0$ in the current configuration.

Additionally, we introduce the curvilinear parametrization $(\theta^1, \theta^2) \in \Omega$ for the mid-surface $\mathcal{S}_0$, along with a third parametric coordinate $\theta^3 \in \Xi$ that characterizes $\mathcal{M}$ through its thickness, where $\Omega$ and $\Xi$ are their respective parametric domains. Unlike the Lagrangian parametrization, the $\{\theta^i\}_{i=1,2,3}$ parametrization is considered effectively Eulerian or *surface-fixed* [37]. In this context, $\theta^i = \theta^i(\xi^j, t)$, indicating that these coordinates are explicitly time-dependent. However, there is an important caveat in this terminology that differs from the usual definition. In reality this choice is such that the coordinates $\{\theta^1, \theta^2\}$ correspond to a fixed point on the *mid-surface* while the third coordinate $\theta^3$ is material-fixed. This notion becomes clear when we consider the velocities later on. For now, we consider this

parametrization to by *in-plane Eulerian and out-of-plane Lagrangian* but for brevity we will refer to it as the Eulerian parametrization. Indeed, we will assume later in this section that $\dot{\theta}^3 = 0$, so that we are free to choose $\theta^3 = \xi^3$, which is another statement of the this mixed form. We note that quantities without a distinct symbol are parameterized by $\{\theta^i\}_{i=1,2,3}$ unless otherwise specified.

While the Lagrangian picture is useful for solid deformations, the Eulerian frame proves valuable for fluid motions. In order to bridge the gap between the two perspectives, we define deformations using both the Lagrangian and Eulerian pictures. These concepts become particularly clear when we note that material points on the body are frame independent, meaning that they can be expressed in either set of coordinates. Therefore, we can equivalently express the reference configuration as, $\mathcal{M}_0 = \left\{\hat{\boldsymbol{X}}(\xi^i) : \xi^i \in \hat{\Omega} \times \hat{\Xi}\right\} = \{\boldsymbol{X}(\theta^i(\xi^j, t), t = 0) : \theta^i \in \Omega \times \Xi\}$. Likewise, the current configuration can be characterized by both pictures, $\mathcal{M} = \left\{\hat{\boldsymbol{x}}(\xi^i, t) : \xi^i \in \hat{\Omega} \times \hat{\Xi}\right\} = \{\boldsymbol{x}(\theta^i(\xi^j, t), t) : \theta^i \in \Omega \times \Xi\}$. The reference and current configurations are then connected by the deformation gradient $\boldsymbol{F}$ [38] (see Fig. 2.3). A point on the mid-surface $\mathcal{S}_0$ is similarly given by: $\boldsymbol{x}_0\big(\theta^\alpha\big(\xi^\beta, t\big), t\big) = \hat{\boldsymbol{x}}_0(\xi^\alpha, t)$, as shown in Figs. 2.2 and 2.3. Furthermore, we define the mid-surface as the collection of points where the thickness coordinate is zero, *e.g.* $\boldsymbol{x}_0(\theta^1, \theta^2, t) = \boldsymbol{x}(\theta^1, \theta^2, \theta^3 = 0, t)$. This dual approach allows us to navigate between the Lagrangian and Eulerian descriptions of our system, enabling our ability to analyze and understand the behavior of lipid bilayers in the context of both solid and fluid deformations.

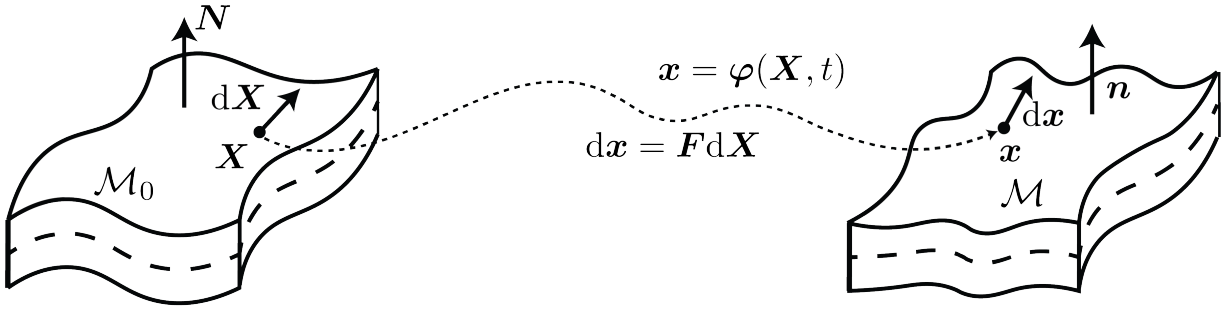


Figure 2.3: Schematic of the mapping from the reference to the current configuration.

With these foundations in place, we can define essential geometric quantities as in Sec. 2.1. The mid-plane parametrization $\{\theta^\alpha\}_{\alpha=1,2}$ induces an in-plane, covariant basis $\{\boldsymbol{a}_\alpha\}_{\alpha=1,2}$ on $\mathcal{S}_0$:

$$\boldsymbol{a}_\alpha = \left.\frac{\partial \boldsymbol{x}_0}{\partial \theta^\alpha}\right|_t . \tag{2.17}$$

This basis allows us to define the normal $\mathcal{S}_0$ as $\boldsymbol{n} = \boldsymbol{a}_1 \times \boldsymbol{a}_2 / ||\boldsymbol{a}_1 \times \boldsymbol{a}_2||$, where $||\boldsymbol{v}|| = \sqrt{\sum_i^n (v_i)^2}$ denotes the $L^2$ norm of a vector $\boldsymbol{v} \in \mathbb{R}^n$. Together, these vectors form a basis in

$\mathbb{R}^3$:

$$\{\check{\boldsymbol{g}}_i\}_{i=1,2,3} = \{\boldsymbol{a}_1, \boldsymbol{a}_2, \boldsymbol{n}\} \ . \tag{2.18}$$

The dual basis on the mid-surface is defined:

$$\boldsymbol{a}^\alpha = \epsilon^{\alpha\gamma} \frac{\boldsymbol{a}_\gamma \times \boldsymbol{n}}{[\boldsymbol{a}_1, \boldsymbol{a}_2, \boldsymbol{n}]} \ , \tag{2.19}$$

where $\epsilon^{\alpha\gamma}$ is the two-dimensional unit permutator. As before, these definitions allow us to define the surface metric and its inverse:

$$a_{\alpha\beta} = \boldsymbol{a}_\alpha \cdot \boldsymbol{a}_\beta \ , \tag{2.20}$$

$$a^{\alpha\beta} = \boldsymbol{a}^\alpha \cdot \boldsymbol{a}^\beta \ , \tag{2.21}$$

which again can be used to raise and lower indices of vectors and tensors ($\boldsymbol{u}$, $\boldsymbol{A}$) living on $\mathcal{S}_0$ according to:

$$u^\alpha = a^{\alpha\beta}\, u_\beta \ , \tag{2.22}$$

$$u_\alpha = a_{\alpha\beta}\, u^\beta \ , \tag{2.23}$$

$$A^{\alpha\beta} = a^{\alpha\gamma} A_\gamma^{\ :\beta} = a^{\gamma\beta} A^\alpha_{\ :\gamma} = a^{\alpha\gamma}\, a^{\lambda\beta} A_{\gamma\lambda} \ , \tag{2.24}$$

$$A_{\alpha\beta} = a_{\alpha\gamma}\, A^\gamma_{\ :\beta} = a_{\gamma\beta}\, A_\alpha^{\ :\gamma} = a_{\alpha\gamma}\, a_{\lambda\beta} A^{\gamma\lambda} \ . \tag{2.25}$$

We introduce the covariant derivative on the mid-surface as:

$$u^\alpha_{:\beta} = u^\alpha_{,\beta} + u^\gamma\ {}^0\Gamma^\alpha_{\gamma\beta} \ , \tag{2.26}$$

where the colon notation denotes the covariant derivative of a vectorial quantity and ${}^0\Gamma^\alpha_{\gamma\beta}$ is the Christoffel symbol of the second kind that lives on the mid-surface and is defined in terms of the surface metric tensors [33, 39]. For a tensor, we define:

$$A^\alpha_{\lambda;\beta} = A^\alpha_{\lambda,\beta} + A^\gamma_\lambda\ {}^0\Gamma^\alpha_{\gamma\beta} - A^\alpha_\gamma\ {}^0\Gamma^\gamma_{\beta\lambda} \ . \tag{2.27}$$

The three-dimensional tangent, or covariant, basis $\{\boldsymbol{g}_i\}_{i=1,2,3}$ on $\mathcal{M}$ follows Eq. (2.3)

$$\boldsymbol{g}_i = \left.\frac{\partial \boldsymbol{x}}{\partial \theta^i}\right|_t \ . \tag{2.28}$$

The metric tensor induced by this basis is defined again by Eq. (2.6) and the dual, contravariant basis is constructed through Eq. (2.7). We can further express the metric tensor on the tangent plane to $\mathcal{S}_0$ as

$$\boldsymbol{i} = \boldsymbol{a}_\alpha \otimes \boldsymbol{a}^\alpha \ , \tag{2.29}$$

and the three-dimensional metric or identity tensor as

$$\boldsymbol{I} = \boldsymbol{g}_i \otimes \boldsymbol{g}^i \ . \tag{2.30}$$

The curvature tensor of the mid-surface is defined as:

$$\boldsymbol{b} = b_{\alpha\beta}\, \boldsymbol{a}^\alpha \otimes \boldsymbol{a}^\beta = (\boldsymbol{a}_{\alpha,\beta} \cdot \boldsymbol{n})\ \boldsymbol{a}^\alpha \otimes \boldsymbol{a}^\beta \ . \tag{2.31}$$

The mean curvature $H$ and Gaussian curvature $K$ of the mid-surface are defined as:

$$H = \frac{1}{2}\,\mathrm{tr}\,\boldsymbol{b} \ , \tag{2.32}$$

$$K = \det \boldsymbol{b} \ , \tag{2.33}$$

The curvature tensor can also be decomposed into an orthogonal basis:

$$\boldsymbol{b} = \sum_{\alpha=1}^{2} \kappa_\alpha \boldsymbol{l}_\alpha \otimes \boldsymbol{l}^\alpha \ , \tag{2.34}$$

where $\kappa_\alpha$ and $\boldsymbol{l}_\alpha = \boldsymbol{l}^\alpha$ are the principal curvatures and orthonormal eigenvectors, respectively. Equation (2.34) implies that the mean and Gaussian curvatures can be expressed as:

$$H = \frac{1}{2}\left(\kappa_1 + \kappa_2\right) \ , \tag{2.35}$$

$$K = \kappa_1 \kappa_2 \ . \tag{2.36}$$

These results will prove crucial in Sec. 3.2.2.

We are now in place to introduce the kinematic assumptions underlying the theory. Our goal is to find the position and velocity vectors in the Eulerian representation. To do so, we will assume that any point along the normal to the mid-surface remains on the normal and maintains a constant distance from the mid-surface during deformation. This restriction is known as Kirchoff-Love (K-L) kinematics [40, 41]. This restriction is in particular on the Lagrangian position:

$$\hat{\boldsymbol{x}}\big(\xi^i, t\big) = \hat{\boldsymbol{x}}_0(\xi^\alpha, t) + \hat{\boldsymbol{n}}(\xi^\alpha, t)\, \xi^3 \ , \tag{2.37}$$

where we have $\xi^3 \in (-\delta/2, \delta/2)$. The Lagrangian form of the velocity follows as:

$$\hat{\boldsymbol{v}} = \hat{\boldsymbol{x}}_{,t} = \left.\frac{\partial \hat{\boldsymbol{x}}}{\partial t}\right|_{\xi^i} = \left.\frac{\partial \hat{\boldsymbol{x}}_0}{\partial t}\right|_{\xi^\alpha} + \left.\frac{\partial \hat{\boldsymbol{n}}_0}{\partial t}\right|_{\xi^\alpha} \xi^3 \ , \tag{2.38}$$

which implies that the mid-surface velocity is given by:

$$\hat{\boldsymbol{v}}_0(\xi^\alpha, t) = \hat{\boldsymbol{x}}_{0,t}(\xi^\alpha, t) \ . \tag{2.39}$$

The velocity can be decomposed into in-plane and normal components as:

$$\hat{\boldsymbol{v}}_0 = \hat{v}_0^\alpha \boldsymbol{a}_\alpha + \hat{v}_0^3 \hat{\boldsymbol{n}} \ . \tag{2.40}$$

Along with Eq. (2.37), this implies that the time-derivative of the normal is:

$$\hat{\boldsymbol{n}}_{,t} = -\left(\hat{v}^3_{0,\alpha} + \hat{v}^\lambda_0 \hat{b}_{\lambda\alpha}\right) \hat{\boldsymbol{a}}^\alpha \ , \tag{2.41}$$

where we have used the results $\hat{\boldsymbol{n}}_{,t} \cdot \hat{\boldsymbol{n}} = 0$ and $(\hat{\boldsymbol{a}}_\alpha)_{,t} = \hat{\boldsymbol{v}}_{0,\alpha}$. The Lagrangian velocity then reads:

$$\hat{\boldsymbol{v}}\big(\xi^i, t\big) = \hat{\boldsymbol{x}}_{,t}\big(\xi^i, t\big) = \hat{\boldsymbol{v}}_0 - \left(\hat{v}^3_{0,\alpha} + \hat{v}^\lambda_0 \hat{b}_{\lambda\alpha}\right) \hat{\boldsymbol{a}}^\alpha \, \xi^3 \ , \tag{2.42}$$

We now seek to utilize these results to define the equivalent restrictions in the Eulerian parametrization.

We begin by choosing an appropriate representation of the position vector. A suitable expression is:

$$\boldsymbol{x}\big(\theta^i, t\big) = \boldsymbol{x}_0(\theta^\alpha, t) + \boldsymbol{n}(\theta^\alpha, t)\, \theta^3 \ , \tag{2.43}$$

as this form describes the same body $\mathcal{M}$ as given by the Lagrangian description $\hat{\boldsymbol{x}}$ (see Fig. 2.3). This geometry is depicted in Fig. 2.2. A consequence of this is that the functional representations of geometric quantities (*e.g.* $\boldsymbol{g}_i$, $\boldsymbol{b}$, $H, \dots$) in the Eulerian parametrization is equivalent to those in the Lagrangian system.

The velocity follows from Eq. (2.43):

$$\boldsymbol{v}\big(\theta^i, t\big) = \frac{\partial}{\partial t}\boldsymbol{x}\big(\theta^i, t\big)\bigg|_{\theta^j} + \frac{\partial}{\partial \theta^k}\boldsymbol{x}\big(\theta^i, t\big)\bigg|_t \left.\frac{\partial \theta^k}{\partial t}\right|_{\xi^j} \ . \tag{2.44}$$

Furthermore, since the parametrizations describe the same body, the velocities, like the positions, are related by:

$$\boldsymbol{v}(\theta^i(\xi^j, t), t) = \hat{\boldsymbol{v}}(\xi^i, t) \ . \tag{2.45}$$

This is satisfied under the assumptions [42]:

$$\theta^\alpha = \theta^\alpha\big(\xi^\beta, t\big) \ , \tag{2.46}$$

$$\dot{\theta}^3 = 0 \ , \tag{2.47}$$

which is consistent with the notion that this parametrization is in-plane Eulerian and out-of-plane Lagrangian. To see this, note that the position should satisfy,

$$\boldsymbol{x}_0(\theta^\alpha, t + \mathrm{d}t) = \boldsymbol{x}_0(\theta^\alpha, t) + v_0^3(\theta^\alpha, t)\boldsymbol{n}(\theta^\alpha, t)\mathrm{d}t \ , \tag{2.48}$$

implying that in the absence of any normal velocity, $\left(\bar{\theta}^1, \bar{\theta}^2\right)$ corresponds to a fixed point on the mid-surface rather than a fixed material point. This aligns with the usual Eulerian perspective for three-dimensional fluids. The assumption, Eq. (2.46), ensures that the velocity varies at most linearly with the thickness coorindate $\theta^3$:

$$\boldsymbol{v} \cdot \boldsymbol{a}_\alpha \sim \theta^3 \ . \tag{2.49}$$

The second assumption, Eq. (2.47), implies that the normal velocity is constant through the thickness:

$$\boldsymbol{v} \cdot \boldsymbol{n} \neq f(\theta^3) \ . \tag{2.50}$$

We are free to make the choice $\theta^3 = \xi^3$, though in general any time-independent function would be possible. However, this assumption leads to the expression:

$$\boldsymbol{v}\big(\theta^i, t\big) = \frac{\mathrm{d}}{\mathrm{d}t}\boldsymbol{x}_0(\theta^\alpha, t) + \frac{\mathrm{d}}{\mathrm{d}t}\boldsymbol{n}(\theta^\alpha, t)\theta^3 \tag{2.51}$$

$$= \boldsymbol{v}_0(\theta^\alpha, t) + \boldsymbol{v}_1(\theta^\alpha, t)\,\theta^3 \ . \tag{2.52}$$

This form shows explicitly the linear dependence of the velocity on the thickness coordinate, as depicted in Fig. 2.4. Interestingly, this result suggests that we can capture membrane deformations where there exists surface in-plane motion even when the mid-surface is stationary in-plane. This is noteworthy because this is the case during bending [43], where the bounding surfaces must compress and extend in order to elastically deform out-of-plane. Strict two-dimensional theories [10, 11, 36] capture at most the in-plane flows. Current finite thickness models [27, 28] fail to properly resolve this surface motion, which affects potential boundary conditions (see Secs.3.4 and 3.6).

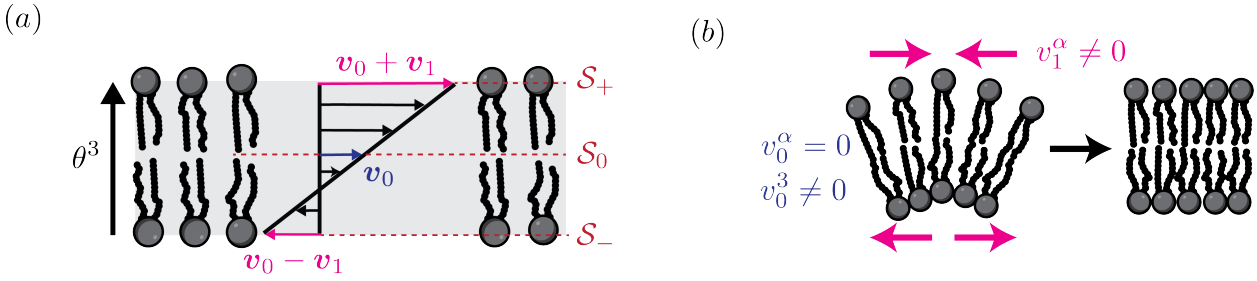


Figure 2.4: (a) Schematic of lipid in-plane flows. The velocity varies linearly with the thickness direction. (b) Deformation where surface motion is possible without in-plane motion.

The mid-surface velocity is:

$$\boldsymbol{v}_0(\theta^\alpha, t) = \frac{\mathrm{d}}{\mathrm{d}t}\boldsymbol{x}_0(\theta^\alpha, t) = \hat{\boldsymbol{v}}_0\big(\xi^\beta(\theta^\alpha, t)\big) \ , \tag{2.53}$$

and we define the first-order velocity as:

$$\boldsymbol{v}_1(\theta^\alpha, t) = \frac{\mathrm{d}}{\mathrm{d}t}\boldsymbol{n}(\theta^\alpha, t) = \hat{\boldsymbol{n}}\big(\xi^\beta(\theta^\alpha, t)\big) \ . \tag{2.54}$$

Therefore, we can write the Eulerian velocity as:

$$\boldsymbol{v}\big(\theta^i, t\big) = v_0^\alpha \boldsymbol{a}_\alpha + v_0^3 \boldsymbol{n} + v_1^\alpha \boldsymbol{a}_\alpha \, \theta^3 \ , \tag{2.55}$$

where the first-order components are:

$$v_1^\alpha = \boldsymbol{a}^\alpha \cdot \dot{\boldsymbol{n}} = -\left(v_{0,\beta}^3 + v_0^\lambda b_{\lambda\beta}\right) a^{\alpha\beta} \ . \tag{2.56}$$

To close, we note that the covariant basis is found from Eq. (2.43):

$$\boldsymbol{g}_\alpha = \boldsymbol{a}_\alpha - b_\alpha^\beta \boldsymbol{a}_\beta \theta^3 \ , \tag{2.57}$$

$$\boldsymbol{g}_3 = \boldsymbol{n} \ , \tag{2.58}$$

where we used $\boldsymbol{n}_{,\beta} = -b_\beta^\alpha \boldsymbol{a}_\alpha$ [33, 34]. This implies that the normal vectors of the bounding surfaces $\mathcal{S}_\pm$ are $\pm\boldsymbol{n}$. Following Eq. (2.7) and using Eqs. (2.57), (2.58), (2.32), and (2.33), the contravariant basis is:

$$\begin{aligned} \boldsymbol{g}^\alpha &= \epsilon^{\alpha\beta\gamma} \frac{\boldsymbol{g}_\beta \times \boldsymbol{g}_\gamma}{1 - \theta^3 H + (\theta^3)^2 K} \ , \\ &= \left(\delta_\beta^\alpha \theta^3 b_\beta^\alpha + (\theta^3)^2 b_\gamma^\alpha b_\beta^\gamma\right) \boldsymbol{a}^\beta + \mathcal{O}(\theta^3 |\boldsymbol{b}|)^3 \ , \end{aligned} \tag{2.59}$$

$$\boldsymbol{g}^3 = \boldsymbol{g}_3 = \boldsymbol{n} \ . \tag{2.60}$$

These basis vectors can be used to find the metric tensors and the Christoffel symbols using Eqs. (2.6), (2.9), and (2.16).

## 2.3 Summary

In this chapter, we have characterized the geometry and kinematics of finite thickness lipid bilayers. Using the language of differential geometry, we were able to map general points within the membrane to the mid-surface by assuming K-L kinematics, which restricts the permissible bilayer deformations. Using these results, we will now derive the equations of motion for finite thickness lipid bilayers. In order to do so, we introduce a procedure known as dimension reduction that is motivated by order of magnitude assumptions and the kinematic results presented here.

# Chapter 3

# Dimension reduced equations of motion

In the previous chapter, we presented a mathematical framework suitable to describe the deformations of lipid bilayers. By constraining the kinematics, we arrived at expressions for the necessary geometric concepts to proceed with deriving the equations of motion. In this chapter, we first review the three-dimensional balance laws, that of mass, linear momentum, and angular momentum. We then introduce the dimension reduction framework, where we show how to arrive at approximate two-dimensional equations from the original three-dimensional laws. By introducing order-of-magnitude assumptions, we arrive at equations of motion describing the membrane.

## 3.1 Three-dimensional balance laws

In this section, we provide a summary of the three-dimensional balance laws. We begin by introducing the mass, linear, and angular momentum balances. For the angular momentum balance, we provide a derivation for the curvilinear statement. We then describe the interface conditions between the body $\mathcal{M}$ and the bulk domains $\mathcal{B}^{\pm}$ that are required for the later chapters of the thesis.

**Mass balance** In the Eulerian description, the local form of the mass balance reads [44]

$$\dot{\rho} + \rho \, \mathrm{div}(\boldsymbol{v}) = 0 \, , \tag{3.1}$$

where $\rho$ is the mass density, $\dot{\rho} = \mathrm{d}\rho/\mathrm{d}t$ denotes the material time derivative of $\rho$, and $\boldsymbol{v}$ is the velocity vector. In the Lagrangian description, the mass balance is [44]

$$\frac{\hat{\rho}_{\mathrm{r}}}{\hat{\rho}} = \frac{d\hat{v}}{d\hat{V}} \, , \tag{3.2}$$

where $\hat{\rho}_{\mathrm{r}}$ and $d\hat{V}$ are the density and an infinitesimal volume in some reference configuration, respectively, and $d\hat{v}$ is the corresponding infinitesimal volume in the current configuration. Typically we employ the Eulerian description due to the in-plane fluidity of the membrane. Regardless, Eq. (3.2) will prove necessary to derive the $(2+\delta)$-dimensional mass balance in Sec. 3.3.1.

**Linear momentum balance** The linear momentum balance in the Eulerian description is [44]:

$$\rho\dot{\boldsymbol{v}} = \mathrm{div}(\boldsymbol{\sigma}) + \boldsymbol{f} \ , \tag{3.3}$$

where $\dot{\boldsymbol{v}} = d\boldsymbol{v}/dt$ is the material time derivative of $\boldsymbol{v}$, $\boldsymbol{\sigma}$ is the material stress tensor, and $\boldsymbol{f}$ the body force per unit volume, respectively.

**Angular momentum balance** For lipid bilayers, it is necessary to derive the angular momentum balance for curvilinear geometries. Consider an arbitrary subregion of the membrane $\mathcal{P} \subset \mathcal{M}$ with boundary $\partial\mathcal{P}$. Assume there exists a stationary reference configuration $\mathcal{M}_0$ in which $\mathcal{P}$ occupies $\mathcal{P}_0 \in \mathcal{M}$. The global form of the angular momentum balance reads,

$$\frac{d}{dt}\int_{\mathcal{P}} \boldsymbol{x} \times \rho\boldsymbol{v} dv = \int_{\partial\mathcal{P}} \boldsymbol{x} \times \boldsymbol{t} da + \int_{\mathcal{P}} \boldsymbol{x} \times \rho\boldsymbol{b} dv \ . \tag{3.4}$$

The material time derivative can be applied to the inertial term,

$$\begin{aligned} \frac{d}{dt}\int_{\mathcal{P}} \boldsymbol{x} \times \rho\boldsymbol{v} dv &= \int_{\mathcal{P}} \boldsymbol{x} \times \left(\rho\dot{\boldsymbol{v}} + \boldsymbol{v}(\dot{\rho} + \rho\mathrm{div}(\boldsymbol{v})\right) dv \\ &= \int_{\mathcal{P}} \boldsymbol{x} \times \rho\dot{\boldsymbol{v}} dv \ , \end{aligned} \tag{3.5}$$

where we have used the mass balance to arrive at the final result. We further recall that for two arbitrary vectors $\boldsymbol{b}$ and $\boldsymbol{l}$, the cross product is a linear operation related to a unique, skew-symmetric tensor such that $\boldsymbol{b} \times \boldsymbol{l} = \boldsymbol{W}_b \boldsymbol{l}$. Thus, we rewrite $\boldsymbol{x} \times \boldsymbol{t} = \boldsymbol{W}_x \boldsymbol{\sigma}^T \boldsymbol{n}$, where we invoke the well-known Cauchy tetrahedron argument to write the traction in terms of the stress tensor. From here we can rewrite the traction contribution to Eq. (3.4) by way of the Divergence Theorem [44, 45]:

$$\int_{\partial\mathcal{P}} \boldsymbol{x} \times \boldsymbol{t} da = \int_{\mathcal{P}} \boldsymbol{g}_i \times (\boldsymbol{\sigma}^T \boldsymbol{g}^i) + \boldsymbol{x} \times \mathrm{div}(\boldsymbol{\sigma}) dv \ . \tag{3.6}$$

Inserting Eqs. (3.5) and (3.4) into Eq. (3.4) and invoking the linear momentum balance Eq. (3.3) furnishes the result:

$$\boldsymbol{g}_i \times (\boldsymbol{\sigma}^T \boldsymbol{g}^i) = \boldsymbol{0} \ . \tag{3.7}$$

By writing the stress tensor in a generic basis $\{\boldsymbol{g}'_i\}_{i=1,2,3}$ as $\boldsymbol{\sigma} = \sigma'^{ij}\,\boldsymbol{g}'_i \otimes \boldsymbol{g}'_j$, we find that Eq. (3.7) also implies the usual symmetry condition of the stress tensor [44]:

$$\sigma'^{ij} = \sigma'^{ji} \ . \tag{3.8}$$

The form in Eq. (3.7) is particularly convenient when applying the dimension reduction procedure to the angular momentum balance in Sec. 3.3.4.

**Constitutive models** In this context, it is important to note that the governing equations, specifically Eqs.(3.1),(3.3), and (3.7), require the specification of constitutive relations that define the stress tensor. For now, we adopt a generic form for this relationship, as expressed by:

$$\boldsymbol{\sigma} = \boldsymbol{\mathcal{F}}\left(\rho, \boldsymbol{C}, \boldsymbol{D}, \ldots\right) \ , \tag{3.9}$$

Here, $\boldsymbol{C}$ is the right Cauchy Green strain tensor and $\boldsymbol{D}$ is the symmetric part of the velocity gradient. In Sec. 3.5, we will delve into the application of constitutive models that describe the viscous-elastic material response of lipid membranes.

**Boundary conditions** The membrane $\mathcal{M}$ is embedded into the bulk domains with bounding surfaces $\mathcal{S}_\pm$ as shown in Fig. 2.2. At the interfaces, we impose continuity of velocities and tractions, i.e.

$$\boldsymbol{v}|_{\mathcal{S}_\pm} = \boldsymbol{v}_{\mathcal{B}_\pm}|_{\mathcal{S}_\pm} \ , \qquad \forall \boldsymbol{x} \in \mathcal{S}_\pm \ , \tag{3.10}$$

$$\boldsymbol{\sigma}^T\big|_{\mathcal{S}_\pm}\boldsymbol{n}_\pm = \boldsymbol{\sigma}_{\mathcal{B}}^T\big|_{\mathcal{S}_\pm}\boldsymbol{n}_\pm \ , \quad \forall \boldsymbol{x} \in \mathcal{S}_\pm \ , \tag{3.11}$$

where $\boldsymbol{v}_{\mathcal{B}}$ denotes the velocities in the bulk domains and $\boldsymbol{n}_\pm$ are the normal vectors to $\mathcal{S}_\pm$, pointing towards $\mathcal{B}_\pm$ [46] (see Fig. 2.2). It is possible to formulate the no-slip and no-penetration conditions in Eq. (3.10) in terms of displacements rather than velocities. However, motivated by the fluidity of lipid membranes, we treat the velocities as the primary variables. In general, the traction continuity condition in Eq. (3.11) requires the total stress tensor including the Maxwell stress [42, 47], but in this thesis we will consider mechanics alone. By defining the mechanical tractions acting on $\mathcal{S}_\pm$ from the bulk domains as $\boldsymbol{t}_\pm = \boldsymbol{\sigma}_{\mathcal{B}}^T\big|_{\mathcal{S}_\pm}\boldsymbol{n}_\pm$, Eq. (3.11) can be recast as

$$\boldsymbol{\sigma}^T\big|_{\mathcal{S}_\pm}\boldsymbol{n}_\pm = \boldsymbol{t}_\pm \ , \quad \forall \boldsymbol{x} \in \mathcal{S}_\pm \ . \tag{3.12}$$

## 3.2 Dimension reduction procedure

In this section, we introduce the dimension reduction procedure, a fundamental step in our research framework. To begin, we establish the weighted inner product of two functions,

denoted as $f(\Theta)$ and $g(\Theta)$, are both $L_2$ functions [48], where an $L^2$ function is one that is square integrable with respect to some measure $\mu$, *e.g.* $\int_X |f|^2 d\mu$ and where $\Theta$ spans the interval $[-1, 1]$. We choose the measure $d\mu = g(\Theta)\mathrm{d}\Theta$, where $g(\Theta) = 1/\sqrt{1-\Theta^2}$. This implies that the inner product is defined as:

$$\langle f(\Theta), g(\Theta)\rangle = \frac{1}{\pi}\int_{-1}^{1} f(\Theta)g(\Theta)\frac{1}{\sqrt{1-\Theta^2}}\mathrm{d}\Theta \ . \tag{3.13}$$

The significance of this inner product lies in its ability to establish the orthogonality relationship among Chebyshev polynomials, denoted as $P_n(\Theta)$, where $n$ is a non-negative integer. This relationship is expressed as follows [49]:

$$\langle P_k(\Theta), P_l(\Theta)\rangle = \beta_k \delta_{kl} \ , \tag{3.14}$$

Here, $\delta_{kl}$ represents the Kronecker delta function, and the coefficients $\beta_k$ take the form:

$$\beta_k = \begin{cases} 1 & \text{if } k = 0 \ , \\ \frac{1}{2} & \text{otherwise} \ . \end{cases} \tag{3.15}$$

These Chebyshev polynomials constitute a complete set of orthogonal polynomials, offering us the capability to represent a function $f(\Theta) \in L_2$ as an infinite series:

$$f(\Theta) = \sum_{k=0}^{\infty} f_k P_k(\Theta) \ . \tag{3.16}$$

In Eq. (3.16), $f_k$ signifies the expansion coefficients.

We define the vector-valued and nonlinear differential operator $\boldsymbol{\mathcal{L}}(\boldsymbol{w}(\theta^i, t); \boldsymbol{p}(\theta^i, t))$, where $\boldsymbol{w}(\theta^i, t)$ represents a sufficiently smooth vector-valued function defined on our manifold $\mathcal{M}$. Additionally, we have the vector-valued parameters $\boldsymbol{p}(\theta^i, t) = \boldsymbol{p}_k(\theta^i, t) k = 1, \ldots, N\mathrm{p}$.

Furthermore, consider $\boldsymbol{u}(\theta^i, t)$ as the solution to the differential equation:

$$\boldsymbol{\mathcal{L}}(\boldsymbol{u}; \boldsymbol{p}) = \boldsymbol{0} \ , \tag{3.17}$$

where for clarity, we have omitted the explicit dependence on the parametrization and time. To facilitate our analysis, we find it convenient to express $\boldsymbol{u}$ in terms of the basis $\{\check{\boldsymbol{g}}_i\}_{i=1,2,3}$, as defined in Eq. (2.18). Notably, this basis is independent of the thickness direction $\theta^3$, allowing us to express $\boldsymbol{u}$ as:

$$\boldsymbol{u} = \check{u}^i(\theta^j, t)\check{\boldsymbol{g}}_i(\theta^\alpha, t) \ . \tag{3.18}$$

Leveraging Eq. (3.16), we can expand the components $\check{u}^i_k(\theta^i, t)$ in terms of Chebyshev polynomials:

$$\check{u}^i = \sum_{k=0}^{\infty} \check{u}^i_k(\theta^\alpha, t) P_k(\Theta), \quad \text{with } \Theta = \frac{2}{\delta}\theta^3 \in (-1, 1). \tag{3.19}$$

In Eq. (3.19), it is important to note that the unknown coefficients $\check{u}^i_k(\theta^\alpha, t)$ are solely dependent on the in-plane parametrization, while the influence of the thickness direction is encapsulated within the Chebyshev polynomials.

To facilitate dimension reduction, we truncate the series expansions in Eq. (3.19) at a finite order $N_i$. This truncation represents a crucial approximation, forming the basis of dimension reduction. It is worth noting that this approximation should be validated post-truncation. Nonetheless, for thin bodies, it is often reasonable to assume minimal variation along the thickness direction.

Upon truncating the series expansion in Eq. (3.19) and inserting it into Eq. (3.17), we can derive a set of equations. These equations are obtained by taking the inner product of Eq. (3.17) with the $l$-th Chebyshev polynomial, leading to the following set of equations:

$$\check{\boldsymbol{g}}_j(\theta^\alpha, t) \cdot \left\langle \boldsymbol{\mathcal{L}}\left( \sum_{i=1}^{3} \left[ \sum_{k=0}^{N_i} \check{u}^i_k(\theta^\alpha, t)\, P_k(\Theta) \right] \check{\boldsymbol{g}}_i(\theta^\alpha, t); \boldsymbol{p} \right), P_l(\Theta) \right\rangle = 0 \ , \quad j \in [1, 2, 3] \, , \ \forall l \in [0, N_j] \ , \tag{3.20}$$

It is important to emphasize that in Eq. (3.20), we do not apply Einstein's summation convention.

These equations, as derived in Eq.(3.20), yield a total of $N_i + 1$ equations for each of the three components of $\boldsymbol{u}$. Significantly, these equations no longer depend on the thickness direction $\theta^3$. Hence, they are regarded as dimensionally-reduced equations [42, 50]. These "$(2 + \delta)$-dimensional" equations capture information about the thickness direction without explicit dependence on the thickness coordinate.

Before proceeding, it is essential to clarify several key points about our methodology, which shed light on the assumptions and considerations underlying our approach.

Firstly, in Eq. (3.20), we selected the basis $\{\check{\boldsymbol{g}}_i\}_{i=1,2,3}$ due to its independence from the coordinate $\theta^3$. This choice simplifies the evaluation of inner products, although it is not an absolute requirement. Additionally, when evaluating Eq. (3.20), we expand the parameters $\boldsymbol{p}_i$ using Chebyshev polynomials. We note here that this choice is not unique and is rather made out of convenience as the Chebyshev polynomials have analytically simple relationships between different orders. However, any complete set of orthogonal polynomials would suffice. The expansion was omitted for clarity, but it is important to highlight that there is no strict need to truncate these expansions. To ensure the manageability of Eq. (3.20), it is imperative

to maintain low truncation orders, denoted as $N_i$. This approach allows us to obtain exact solutions up to the specified order, eliminating the necessity for further approximations. However, it is essential to underscore that the appropriateness of these low-order expansions depends on the specific problem at hand and warrants careful validation.

### 3.2.1 Expansion choices

To apply the dimension reduction methodology as delineated in Sec. 3.2, it becomes imperative to represent all variables and parameters featured in the pertinent differential equations using Chebyshev polynomials as the basis functions. In the context of the equilibrium equations expounded in Sec. 3.1, it is essential to establish expansions for various physical quantities, including the position and velocity vectors, density, stress tensor, and body force. Inspired by the fluid behavior observed in lipid membranes, these expansions have been formulated within the Eulerian parametrization framework, although it is noteworthy that a corresponding formulation within the Lagrangian parametrization framework is equally feasible. Our endeavor commences with the recasting of the expressions governing the position and velocity vectors, as articulated in Eqs. (2.43) and (2.55), in terms of Chebyshev polynomials:

$$\boldsymbol{x}\big(\theta^i, t\big) = \boldsymbol{x}_0(\theta^\alpha, t)P_0(\Theta) + \frac{\delta}{2}\boldsymbol{n}(\theta^\alpha, t)P_1(\Theta) \ , \tag{3.21}$$

$$\boldsymbol{v}\big(\theta^i, t\big) = \boldsymbol{v}_0(\theta^\alpha, t)P_0(\Theta) + \frac{\delta}{2}v_1^\alpha(\theta^\alpha, t)\boldsymbol{a}_\alpha(\theta^\alpha, t)P_1(\Theta) \ , \tag{3.22}$$

where we used $\theta^3 = \frac{\delta}{2}\Theta$, $\Theta \in (-1, 1)$, and the Chebyshev polynomial definitions:

$$P_0(\Theta) = 1 \ , \tag{3.23}$$

$$P_1(\Theta) = \Theta \ , \tag{3.24}$$

$$P_{n+1}(\Theta) = 2\Theta P_n(\Theta) + P_{n-1}(\Theta) \tag{3.25}$$

Note that in Eqs. (3.21) and (3.22) all quantities but the Chebyshev polynomials exclusively depend on the in-plane parametrization.

To ascertain a suitable expansion for the density $\rho$, it is crucial to acknowledge that $\rho$ is entirely determined by the deformations of the manifold $\mathcal{M}$. Consequently, imposing constraints on the allowable deformations in compliance with the K-L kinematics also places constraints on the permissible variations of density. This implies that the density cannot be truncated independently, necessitating the consideration of a generic series expansion as expressed below:

$$\rho\left(\theta^i, t\right) = \sum_{k=0}^{\infty} \rho_k\left(\theta^\alpha, t\right) P_k(\Theta) \ . \tag{3.26}$$

We can also arrive at Eq. (3.26) by invoking analogous arguments involving the Eulerian representation of the mass balance equation and the constraint placed on the velocity vector, as articulated in Eq. (2.55). Consequently, the expansion coefficients $\rho_k(\theta^\alpha, t)$ can be determined by employing the mass balance equations in either the Eulerian form (Eq. (3.1)) or the Lagrangian form (Eq. (3.2)), in conjunction with the assumption of K-L kinematics as outlined in Eqs. (2.37) or (2.55). A comprehensive discussion of this process will be provided in Sec. 3.3.1.

In a manner analogous to the density, the choice of expansion order for the stress tensor cannot be arbitrary. Instead, it is dictated by the reactive stresses [42] and the constitutive model as given in Eq. (3.9). For a detailed treatment of the reactive stresses, we refer to [42]. Here, we will concern ourselves with the constitutive components. To that end, we adopt the series expansion:

$$\boldsymbol{\sigma}\left(\theta^i, t\right) = \sum_{k=0}^{\infty} \check{\sigma}_k^{\alpha\beta}\left(\theta^\alpha, t\right) \boldsymbol{a}_\alpha\left(\theta^\alpha, t\right) \otimes \boldsymbol{a}_\beta\left(\theta^\alpha, t\right) P_k(\Theta) \ , \tag{3.27}$$

where the utilization of the mid-surface basis $\{\check{\boldsymbol{g}}_i\}_{i=1,2,3}$ proves convenient as it facilitates the separation of coordinates into in-plane and thickness components.

Finally, we consider the body forces $\boldsymbol{f}$ a set of parameters, so we use a generic series expansion,

$$\boldsymbol{f}\left(\theta^i, t\right) = \sum_{k=0}^{\infty} \boldsymbol{f}_k(\theta^\alpha, t) P_k(\Theta) \ . \tag{3.28}$$

Now that we have determined our expansion orders, we discuss the assumptions involved in the framework. This is particularly important as it allows us to truncate our expansions accordingly.

### 3.2.2 Order of magnitude approximations

In this section, we introduce physically motivated assumptions aimed at rendering the $(2+\delta)$-dimensional theory more manageable. These assumptions enable the neglect of higher-order expansion coefficients based on their order of magnitude in the dimensionally-reduced balance laws and equations of motion, as presented in Secs. 3.3 and 3.4. These omissions pertain solely to coordinates independent of the $\theta^3$ dimension.

The initial assumption, grounded in geometric considerations, postulates that the principal curvatures $\kappa_\alpha$ are significantly smaller than the thickness of the thin film, thus satisfying the condition:

$$\left(\delta\kappa_\alpha\right)^2 \ll 1 \ , \quad \alpha = 1, 2 \ . \tag{3.29}$$

Eq.(3.29) implies that both the mean and principal curvatures, as defined in Eqs.(2.35) and(2.36), are also markedly smaller than the thickness of the thin film:

$$(\delta H)^2 \ll 1 \ , \tag{3.30}$$
$$\delta^2 |K| \ll 1 \ . \tag{3.31}$$

Equation (3.29) also enables us to derive order of magnitude estimates for contractions of the curvature tensor $\boldsymbol{b}$ with both tensors and vectors. To demonstrate this, we begin by recalling the spectral decomposition of $\boldsymbol{b}$ as provided in Eq.(2.34) and consider an arbitrary tensor $\boldsymbol{A} = A^{\alpha}_{\ .\beta} \boldsymbol{l}_\alpha \otimes \boldsymbol{l}^\beta$. For $m \geq 0$, we can then express this contraction as follows:

$$(\delta \boldsymbol{b})^m : \boldsymbol{A} = \sum_{\alpha=1}^{2} (\delta \kappa_\alpha)^m A^{\alpha}_{\ .\alpha}, \tag{3.32}$$

where the *colon* notation represents the double contraction operation. Since $\boldsymbol{i} \colon \boldsymbol{A} = A^{\alpha}_{\ .\alpha}$, Eq.(3.32) implies the following relationship:

$$(\delta \boldsymbol{b})^m : \boldsymbol{A} = \mathcal{O}\left((\delta \kappa)^m\right) (\boldsymbol{i} \colon \boldsymbol{A}) \, , \tag{3.33}$$

where $\kappa = \max_\alpha |\kappa_\alpha|$. Utilizing the assumption from Eq.(3.29), Eq.(3.33) specifically indicates:

$$(\delta \boldsymbol{b})^n : \boldsymbol{A} \ll (\delta \boldsymbol{b})^{n-2} : \boldsymbol{A} \ , \quad n \geq 2. \tag{3.34}$$

Similarly, for the contraction $\boldsymbol{c} \cdot (\delta \boldsymbol{b})^m \boldsymbol{a}^\alpha$, $m \geq 0$, where $\boldsymbol{c} = c^\gamma \boldsymbol{l}_\gamma$ represents an arbitrary vector, we can express it as follows:

$$\boldsymbol{c} \cdot (\delta \boldsymbol{b})^m \boldsymbol{a}^\alpha = (c^\gamma \boldsymbol{l}_\gamma) \cdot \left( \sum_{\beta=1}^{2} (\delta \kappa_\beta)^m \, , \boldsymbol{l}^\beta \otimes \boldsymbol{l}_\beta \right) \boldsymbol{a}^\alpha = \sum_{\alpha=1}^{2} c^\beta \, (\delta \kappa_\beta)^m \, (\boldsymbol{l}_\beta \cdot \boldsymbol{a}^\alpha) \, , \tag{3.35}$$

which further implies:

$$\boldsymbol{c} \cdot (\delta \boldsymbol{b})^m \boldsymbol{a}^\alpha = \mathcal{O}\left((\delta \kappa)^m\right) \boldsymbol{c} \cdot \boldsymbol{i} \boldsymbol{a}^\alpha, \tag{3.36}$$

and consequently:

$$\boldsymbol{c} \cdot (\delta \boldsymbol{b})^n \boldsymbol{a}^\alpha \ll \boldsymbol{c} \cdot (\delta \boldsymbol{b})^{n-2} \boldsymbol{a}^\alpha \ , \quad n \geq 2 \ . \tag{3.37}$$

Additionally, we assume that there exist characteristic in-plane length scales denoted as $\ell_{\mathrm{v}}$, $\ell_{\mathrm{s}}$, and $\ell_{\mathrm{c}}$, respectively, over which the velocity, stress and curvature change. The scales are taken to be similar to each other, or $\ell_{\mathrm{v}} \sim \ell_{\mathrm{s}} \sim \ell_{\mathrm{c}}$. In general, these length scales are

coupled in a physical manner so that this assumption is plausible. Furthermore, we make the assumption that

$$\left(\frac{\delta}{\ell_{\mathrm{v}}}\right)^2 \ll 1 \ , \tag{3.38}$$

$$\left(\frac{\delta}{\ell_{\mathrm{s}}}\right)^2 \ll 1 \ , \tag{3.39}$$

$$\left(\frac{\delta}{\ell_{\mathrm{c}}}\right)^2 \ll 1 \ , \tag{3.40}$$

so that the characteristic length scales of all expanded variables are much larger than the membrane thickness. This is also a limiting assumption in constructing a continuum theory, and its violation necessitates a molecular approach. We continue by assuming that the first order in-plane velocity coefficients are are smaller than the zeroth order, mid-surface velocities:

$$\left(\frac{\delta v_1^\alpha}{v_0^\beta}\right)^2 \ll 1 \ , \tag{3.41}$$

though it should be noted that it is possible cases exist where this condition is violated, and thus it should be verified *a-posteriori*.

To further make the theory analytically tractable, we require assumptions about the stress tensor coefficients in Eq. (3.27). We again note that we concern ourselves with the in-plane components prescribed by constitutive relations. Order of magnitude assumptions about the components $\check{\sigma}^{i3} = \check{\sigma}^{3i}$ are given in [42]. Here, we simply state that these components are in part fixed by the traction boundary conditions Eq. (3.12) and the stress tensor symmetries Eq. (3.8).

We suppose that there exists some non-dimensional parameter $|\mathcal{A}| < 1$ that satisfies:

$$\check{\sigma}_k^{\alpha\beta} = \mathcal{O}(A^{\mathcal{Z}_k}) \ , \tag{3.42}$$

where $\mathcal{Z}_k$ has some dependence on the order of the coefficient, $k$. For example, such a small parameter might be the mean curvature, $\delta H$ or a non-dimensional length scale, i.e. $\delta/\ell_c$. We make the assumption that the stress tensor coefficients with $k \geq 2$ are at most as large as the zeroth and first order coefficients:

$$\mathcal{Z}_k \geq \mathcal{Z}_0 \quad \mathcal{Z}_k \geq \mathcal{Z}_1 \ , \qquad \forall \ k \geq 2 \ . \tag{3.43}$$

These assumptions can be verified *a-posteriori*.

We have now provided several conditions for the applicability of the $(2+\delta)$-dimensional theory. We require that the curvature is smaller than the thickness of the membrane (Eqs (3.29)–(3.31)). Furthermore, we assume that there exist characteristic length scales

over which the stress, velocity, and curvature change, and that these scales are both comparable to each other and much larger than the thickness (Eqs. (3.40) and (3.39)). The final kinematic assumption (Eq. (3.41)) states that the first order velocity coefficient is much less than the zeroth order, or mid-plane, velocity. Finally, we consider the stress coefficients to not increase in magnitude with polynomial order (Eq. (3.43)). With these restrictions in place, we now proceed with deriving the dimensionally reduced balance laws.

## 3.3 $(2+\delta)$-dimensional Balance laws

Here, we use the dimension reduction procedure outlined in the preceding section to derive the balance laws for a thin, finite thickness membrane. We begin with the mass balance in Sec. 3.3.1. We continue by presenting the form of the stress vectors in Sec. 3.3.2, which we subsequently use to derive the general linear and angular momentum balances in Secs. 3.3.3 and 3.3.4.

### 3.3.1 Balance of mass

In order to derive the reduced mass balance, we make use of both the Lagrangian and the Eulerian forms in Eqs. (3.2) and (3.1), respectively. The Lagrangian statement allows us to determine the how the density coefficients relate to that on the mid-surface, which itself is solved for via the Eulerian form.

Let us assume that for all points on the mid-surface, $\hat{\boldsymbol{x}}_0 \in \mathcal{S}_0$ we have a constant density $\hat{\rho}$ through the thickness if the body is flat, e.g. if $\hat{H} = \hat{K} = 0$. We take this state to be th reference configuration for all surface points. Under the assumption of constant thickness, the Lagrangian mass balance reads [39, 51, 52]:

$$\frac{\hat{\rho}_{\mathrm{r}}}{\hat{\rho}} = \frac{\mathrm{d}\hat{a}_0}{\mathrm{d}\hat{A}_0}\left(1 - \delta\hat{H}\Theta + \frac{\delta^2}{4}\hat{K}\Theta^2\right) \ , \tag{3.44}$$

where $\mathrm{d}\hat{A}_0$ and $\mathrm{d}\hat{a}_0$ are infinitesimal area elements on the mid-surface in the reference and current configurations, respectively. Given that the reference is flat and the density is constant through the thickness, we have that:

$$\hat{\rho}_{\mathrm{mid}} = \hat{\rho}_{\mathrm{r}}\,\frac{\mathrm{d}\hat{A}_0}{\mathrm{d}\hat{a}_0} \ , \tag{3.45}$$

so that we can write the mass balance as:

$$\hat{\rho} = \hat{\rho}_{\mathrm{mid}}\left(1 - \delta\hat{H}\Theta + \frac{\delta^2}{4}\hat{K}\Theta^2\right)^{-1} \ . \tag{3.46}$$

Eq. (3.46) is a scalar equation and is thus invariant to changes in parametrization. Thus, it can be written in the Eulerian form as:

$$\rho = \rho_{\text{mid}} \left(1 - \delta H \Theta + \frac{\delta^2}{4} K \Theta^2\right)^{-1} \ . \tag{3.47}$$

Because the denominator is a rational polynomial in $\delta H$ and $\delta^2 K$ and noting that $\Theta \in [-1, 1]$, we can Taylor expand about $\delta H = \delta^2 K = 0$ in light of the order of magnitude assumptions Eqs. (3.30) and (3.31) to yield:

$$\rho = \rho_{\text{mid}} \left(1 - \Theta \delta H + \frac{\Theta^2}{4}(4H^2 - K)\right) \tag{3.48}$$

When we compare to the expansion Eq. (3.26), this result implies the following for the coefficients:

$$\frac{\rho_0}{\rho_{\text{mid}}} = 1 \ , \tag{3.49}$$

$$\frac{\rho_1}{\rho_{\text{mid}}} = \delta H \ , \tag{3.50}$$

$$\frac{\rho_2}{\rho_{\text{mid}}} = \frac{\delta^2}{8}(4H^2 - K) \ , \tag{3.51}$$

where we have again made use of the order of magnitude assumptions in Sec. 3.2.2.

Equation (3.48) can be used along with the Lagrangian mid-surface mass balance Eq. (3.45) to find $\rho_{\text{mid}}$. However, the fluid nature of the lipid bilayer motivates the use of the Eulerian form. From here, we note that in general, solving for $\rho_{\text{mid}}$ in the Eulerian mass balance would necessitate solving for its time dependence. Instead, we assume that the mid-surface is incompressible, noting that membranes tend to stretch at most $2 - 3\%$ before tearing [53, 54]. To that end, we have that:

$$\rho_0 - \rho_2 \neq f(t) \ , \tag{3.52}$$

and we further note that $\rho_0 \gg \rho_2$. Therefore, we are left with the approximation:

$$\rho_0 \approx \rho_{\text{mid}} \ . \tag{3.53}$$

To arrive at an equation for $\rho_0$, we take the inner product of the Eulerian form of the mass balance in Eq. (3.1) with the zeroth Chebyshev polynomial:

$$\left\langle \frac{\mathrm{d}\rho}{\mathrm{d}t}, P_0(\Theta) \right\rangle + \langle \rho \mathrm{div}(\boldsymbol{v}), P_0(\Theta) \rangle = 0 \ . \tag{3.54}$$

Recall that the thickness coordinate is independent of time. This implies that:

$$\left\langle \frac{\mathrm{d}\rho}{\mathrm{d}t}, P_0(\Theta) \right\rangle = \frac{\mathrm{d}}{\mathrm{d}t}\langle \rho, P_0(\Theta)\rangle = \frac{\mathrm{d}\rho_0}{\mathrm{d}t} \ . \tag{3.55}$$

To evaluate the second term, we express the divergence of the velocity as:

$$\mathrm{div}(\boldsymbol{v}) = \boldsymbol{v}_{,i} \cdot \boldsymbol{g}^i \ , \tag{3.56}$$

where we express the velocity from Eq. (2.55) in terms of Chebyshev polynomials:

$$\boldsymbol{v}\big(\theta^i, t\big) = \boldsymbol{v}_0(\theta^\alpha, t)P_0(\Theta) + \frac{\delta}{2}\boldsymbol{v}_1(\theta^\alpha, t)P_1(\Theta) \tag{3.57}$$

$$= \left(v_0^\beta \boldsymbol{a}_\beta + v_0^3 \boldsymbol{n}\right) P_0(\Theta) + \frac{\delta}{2} v_1^\beta \boldsymbol{a}_\beta P_1(\Theta) \ . \tag{3.58}$$

Upon expanding the partial derivatives in Eq. (3.56), we find:

$$\boldsymbol{v}_{,\alpha} = \left[w^\beta_{\ .\alpha}\, \boldsymbol{a}_\beta + \left(v_0^\beta b_{\beta\alpha} + v^3_{0,\alpha}\right)\boldsymbol{n}\right] P_0(\Theta) + \frac{\delta}{2}\left[v^\beta_{1:\alpha}\boldsymbol{a}_\beta + v_1^\beta b_{\beta\alpha}\boldsymbol{n}\right] P_1(\Theta) \ , \tag{3.59}$$

$$\boldsymbol{v}_{,3} = v_1^\alpha \boldsymbol{a}_\alpha P_0(\Theta) \ , \tag{3.60}$$

where we have used the surface covariant derivative from Eq. (2.26) and defined:

$$w^\beta_{\ .\alpha} = v^\beta_{0:\alpha} - v_0^3 b^\beta_\alpha \ , \tag{3.61}$$

Eqs. (3.57) and (3.58), we find:

$$\boldsymbol{v}_{,\alpha} \cdot \boldsymbol{g}^\alpha = w^\beta_{\ .\alpha}\left(\boldsymbol{a}_\beta \cdot \boldsymbol{g}^\alpha\right) + \frac{\delta}{2} v^\beta_{1:\alpha}\left(\boldsymbol{a}_\beta \cdot \boldsymbol{g}^\alpha\right)\Theta \ , \tag{3.62}$$

$$\boldsymbol{v}_{,3} \cdot \boldsymbol{n} = 0 \ , \tag{3.63}$$

and using the expansion of the dual basis vectors in Eq. (2.7):

$$\boldsymbol{a}_\beta \cdot \boldsymbol{g}^\alpha = \delta^\alpha_\beta + \frac{\Theta}{2} b^\alpha_\beta + \frac{\Theta^2}{4} b^\alpha_\gamma b^\gamma_\beta \tag{3.64}$$

$$\approx P_0(\Theta) + P_1(\Theta)\frac{\delta}{2} b^\alpha_\beta + P_2(\Theta) b^\alpha_\gamma b^\gamma_\beta \frac{\delta^2}{8} \tag{3.65}$$

$$\boldsymbol{a}_\beta \cdot \boldsymbol{g}^\alpha \Theta \approx P_0(\Theta)\frac{\delta}{4} b^\alpha_\beta + P_1(\Theta)\delta^\alpha_\beta + P_2(\Theta)\left(\frac{\delta}{4} b^\alpha_\beta + \frac{\delta^2}{16} b^\alpha_\gamma b^\gamma_\beta\right) \ . \tag{3.66}$$

Together, Eqs. (3.62) and (3.66) yield the following expression for the divergence of the velocity:

$$\operatorname{div}(\boldsymbol{v}) \approx P_0(\Theta) w^{\alpha}_{\cdot\alpha} + P_1(\Theta)\frac{\delta}{2}\big(w^{\beta}_{\cdot\alpha} b^{\alpha}_{\beta} + v^{\alpha}_{1:\alpha}\big) + P_2(\Theta)\frac{\delta^2}{8}\Big(b^{\alpha}_{\gamma} b^{\gamma}_{\beta} w^{\beta}_{\cdot\alpha} + b^{\alpha}_{\beta} v^{\beta}_{1:\alpha}\Big) \ , \tag{3.67}$$

where we have used the approximation Eq. (3.41). Putting Eq. (3.67) together with the Eqs. (3.48) and (3.51), we have to first order the result:

$$\rho\operatorname{div}(\boldsymbol{v}) \approx P_0(\Theta)\rho_0 w^{\alpha}_{\cdot\alpha} + P_1(\Theta)\rho_0\left(\frac{\delta}{2} w^{\beta}_{\cdot\alpha} b^{\alpha}_{\beta} + \frac{\delta}{2} v^{\alpha}_{1:\alpha} - \delta H w^{\beta}_{\cdot\alpha}\right) . \tag{3.68}$$

Thus, using Eqs. (3.55) and (3.68) and defining $\rho_s \coloneqq \delta\rho_0$, the zeroth order Eulerian mass balance reads:

$$\frac{\mathrm{d}\rho_s}{\mathrm{d}t} + \rho_s\big(v^{\alpha}_{0:\alpha} - 2v^3_0 H\big) \ , \tag{3.69}$$

where we have substitute the definition in Eq. (3.61). We note that this form of the mass balance is well known for two-dimensional viscous fluids [11, 55]. Also, $\rho_s$ has units mass per unit area, and can be considered the effective surface density within our framework. Thus, we can solve for the zeroth order coefficient using this equation and the rest using the results from the Lagrangian form.

### 3.3.2 The stress vectors

It is common to express the linear and angular moment balances for thin bodies in terns of stress vectors [10, 39]. Using the same convention, we first derive the $(2+\delta)$-dimensional stress vectors using the dimension reduction procedure. Next, we use these results to derive the linear and angular momentum balances in Secs. 3.3.3 and 3.3.4.

We define the stress vector acting on a surface perpendicular to the plane tangent to $\boldsymbol{g}^i$ as:

$$\boldsymbol{T}^i \coloneqq \boldsymbol{\sigma}\boldsymbol{g}^i \ , \tag{3.70}$$

which implies the stress tensor can be written:

$$\boldsymbol{\sigma} = \boldsymbol{T}^i \otimes \boldsymbol{g}_i \ . \tag{3.71}$$

From here, we assume that due to our order of magnitude assumptions in Sec. 3.2.2, we can truncate the stress tensor in-plane components at $k = 1$, an approximation which we justify when we consider the constitutive models for the membrane in Sec. 3.5. Furthermore, we assume that the out-of-plane components go to $k = 1$ so as to satisfy the traction conditions at the top and bottom surfaces. This yields the following definitions:

$$\boldsymbol{T}^{\alpha} = \boldsymbol{\sigma}\boldsymbol{g}^{\alpha} = \sum_{k=0}^{2} P_k(\Theta)\boldsymbol{T}_k^{\alpha} \ , \tag{3.72}$$

$$\boldsymbol{T}^{3} = \boldsymbol{\sigma}\boldsymbol{n} = \sum_{k=0}^{1} P_k(\Theta)\boldsymbol{T}_k^{3} \ . \tag{3.73}$$

Using the expansion for the dual basis vectors Eq. (3.27) and the stress expansion Eq. (3.27), we find that the stress vectors are:

$$\boldsymbol{T}^{\alpha} \approx \left( P_0(\Theta)\left( \check{\sigma}_0^{\alpha j} + \frac{\delta}{2} b_{\beta}^{\alpha} \check{\sigma}_1^{\beta j} \right) + P_1(\Theta)\left( \check{\sigma}_0^{\alpha j} \ + \frac{\delta}{2} b_{\beta}^{\alpha} \check{\sigma}_1^{\beta j} \right) + P_2(\Theta)\frac{\delta}{4}\check{\sigma}_1^{\beta j} \right) \check{\boldsymbol{g}}_j \ , \tag{3.74}$$

$$\boldsymbol{T}^{3} = \left( P_0(\Theta)\check{\sigma}_0^{3j} + P_1(\Theta)\check{\sigma}_1^{3j} \right) \check{\boldsymbol{g}}_j \ , \tag{3.75}$$

from which we identify:

$$\boldsymbol{T}_0^{\alpha} = (\check{\sigma}_0^{\alpha j} + \frac{\delta}{2} b_{\beta}^{\alpha} \check{\sigma}_1^{\beta j}) \check{\boldsymbol{g}}_j \ , \tag{3.76}$$

$$\boldsymbol{T}_1^{\alpha} = (\check{\sigma}_0^{\alpha j} \ + \frac{\delta}{2} b_{\beta}^{\alpha} \check{\sigma}_1^{\beta j}) \check{\boldsymbol{g}}_j \ , \tag{3.77}$$

$$\boldsymbol{T}_2^{\alpha} = (\frac{\delta}{4} \check{\sigma}_1^{\beta j}) \check{\boldsymbol{g}}_j \ , \tag{3.78}$$

$$\boldsymbol{T}_0^{3} = (\check{\sigma}_0^{3j}) \check{\boldsymbol{g}}_j \ , \tag{3.79}$$

$$\boldsymbol{T}_1^{3} = (\check{\sigma}_1^{3j}) \check{\boldsymbol{g}}_j \ . \tag{3.80}$$

With the stress vectors defined, we are now in place to derive the reduced linear momentum balance.

### 3.3.3 The balance of linear momentum

We begin with the three-dimensional balance in Eq. (3.3). We discuss the inertial, stress divergence, and body force contributions separately. In this section we will omit some of the algebraic steps.

**Inertia** To evaluate the inertia term, we use the results for the velocity and density expansions given by Eq.(3.57), Eq. (3.48), and (3.53). First, recall the material time derivative:

$$\dot{\boldsymbol{v}}\big(\theta^i, t\big) = \frac{\mathrm{d}}{\mathrm{d}t}\boldsymbol{v}\big(\theta^i, t\big) = \frac{\partial}{\partial t}\boldsymbol{v}\big(\theta^i, t\big)\bigg|_{\xi^k} \ . \tag{3.81}$$

Applying this to the velocity, we arrive at:

$$\dot{\boldsymbol{v}} = \left(\dot{v}_0^\alpha \boldsymbol{a}_\alpha + v_0^\alpha \dot{\boldsymbol{a}}_\alpha + \dot{v}_0^3 \boldsymbol{n} + v_0^3 \dot{\boldsymbol{n}}\right) P_0(\Theta) + \frac{\delta}{2}\left(\dot{v}_1^\alpha \boldsymbol{a}_\alpha + v_1^\alpha \dot{\boldsymbol{a}}_\alpha\right) P_1(\Theta) \ , \tag{3.82}$$

Using the results in [11, 42, 56], we find that:

$$\dot{v}_0^\alpha = v_{0,t}^\alpha \tag{3.83}$$
$$\dot{v}_1^\alpha = v_{1,t}^\alpha + v_0^\beta v_{1:\beta}^\alpha - v_1^\beta v_{0,\beta}^\alpha \ , \tag{3.84}$$
$$\dot{v}_0^3 = v_{0,t}^3 + v_{0,\alpha}^3 v_0^\alpha \ , \tag{3.85}$$
$$\dot{\boldsymbol{a}}_\alpha = \boldsymbol{v}_{0,\alpha} \ , \tag{3.86}$$

where using the surface covariant derivative definition furnishes the following:

$$\boldsymbol{v}_{0,\alpha} = \left(v_{0:\alpha}^\beta - v_0^3 b_\alpha^\beta\right)\boldsymbol{a}_\beta + \left(v_{0,\alpha}^3 + v_0^\beta b_{\beta\alpha}\right)\boldsymbol{n} \ . \tag{3.87}$$

Finally, we use this result to find:

$$\boldsymbol{a} = \dot{\boldsymbol{v}} = \dot{\boldsymbol{v}}_0 P_0(\Theta) + \frac{\delta}{2}\dot{\boldsymbol{v}}_1 P_1(\Theta) \tag{3.88}$$
$$= \dot{\boldsymbol{v}}_0 P_0(\Theta) + \frac{\delta}{2}\ddot{\boldsymbol{n}} P_1(\Theta) \ , \tag{3.89}$$

where we have the following definitions [42]:

$$\dot{\boldsymbol{v}}_0 = \left(v_{0,t}^\alpha + v_0^\beta v_{0:\beta}^\alpha - 2v_0^3 v_0^\beta b_\beta^\alpha - v_0^3 v_{0,\beta}^3 \, a^{\alpha\beta}\right)\boldsymbol{a}_\alpha + \left(v_{0,t}^3 + 2v_0^\alpha v_{0,\alpha}^3 + v_0^\alpha v_0^\beta b_{\beta\alpha}\right)\boldsymbol{n} \ , \tag{3.90}$$
$$\ddot{\boldsymbol{n}} = \left(v_{1,t}^\alpha + v_0^\beta v_{1,\beta}^\alpha + v_1^\beta v_{0:\beta}^\alpha - v_1^\beta v_0^3 b_\beta^\alpha - v_1^\beta v_{0,\beta}^\alpha\right)\boldsymbol{a}_\alpha + \left(v_1^\alpha v_{0,\alpha}^3 + v_1^\alpha v_0^\beta b_{\beta\alpha}\right)\boldsymbol{n} \ . \tag{3.91}$$

We can combine these results with the density expansion Eqs. (3.48) and the relation Eq. (3.53) to find the inertial contribution to first order:

$$\delta\rho\boldsymbol{a} \overset{1}{\approx} \rho_{\mathrm{s}}\dot{\boldsymbol{v}}_0 P_0(\Theta) + \left(\rho_{\mathrm{s}}\delta H \dot{\boldsymbol{v}}_0 + \frac{\delta\rho_{\mathrm{s}}}{2}\ddot{\boldsymbol{n}}\right) P_1(\Theta) \ , \tag{3.92}$$

where we have followed the order of magnitude assumptions implicitly.

**Stress divergence** The stress divergence can be analyzed by noting:

$$\mathrm{div}(\boldsymbol{\sigma}) = \boldsymbol{T}^i_{,i} + \boldsymbol{T}^j \Gamma^i_{ji} \ , \tag{3.93}$$

where the Christoffel symbol of the second kind is defined in Eqs. (2.16). The derivative terms read:

$$\boldsymbol{T}^i_{,i} = \boldsymbol{T}^\alpha_{,\alpha} + \boldsymbol{T}^3_{,3} \tag{3.94}$$
$$= \left(\boldsymbol{T}^\alpha_{0,\alpha} + \frac{2}{\delta}\boldsymbol{T}^3_1\right) P_0(\theta) + \boldsymbol{T}^\alpha_{1,\alpha} P_1(\theta) \ . \tag{3.95}$$

In terms of Chebyshev polynomials, the relevant Christoffel symbols are:

$$\Gamma^{\beta}_{\alpha\beta} = {}^{0}\Gamma^{\beta}_{\alpha\beta} - \delta H_{,\alpha} P_1(\Theta) - \frac{\delta^2}{8} b^{\delta}_{\alpha;\beta} b^{\beta}_{\delta} P_2(\Theta) \tag{3.96}$$

$$\Gamma^{\alpha}_{3\alpha} = -2H - \delta\left(2H^2 - K\right) P_1(\Theta) + \frac{\delta^2}{8} b^{\varepsilon}_{\alpha} b^{\lambda}_{\varepsilon} b^{\alpha}_{\lambda} P_2(\Theta) \ , \tag{3.97}$$

where we have made use of the Mainardi-Codazzi equations [33]:

$$b^{\beta}_{\alpha;\beta} = 2H_{,\alpha} \tag{3.98}$$

Using these results the divergence of the stress tensor to first order is:

$$\begin{aligned} \operatorname{div}(\boldsymbol{\sigma}) \approx & \left( \boldsymbol{T}^{\alpha}_{0:\alpha} + \frac{2}{\delta}\boldsymbol{T}^{3}_{1} - 2H\boldsymbol{T}^{3}_{0} - \frac{\delta}{2}\boldsymbol{T}^{\alpha}_{1} H_{,\alpha} \right) P_0(\theta) + \\ & \left( \boldsymbol{T}^{\alpha}_{1:\alpha} - 2H\boldsymbol{T}^{3}_{1} - \delta\left( \boldsymbol{T}^{\alpha}_{0} + \frac{1}{2}\boldsymbol{T}^{\alpha}_{2} \right) H_{,\alpha} - \delta\boldsymbol{T}^{3}_{0}\left(2H^2 - K\right) \right) P_1(\theta) \ . \end{aligned} \tag{3.99}$$

**Body forces** Truncating the body force term in Eq. (3.28) yields:

$$\boldsymbol{f} = \boldsymbol{f}_0 P_0(\Theta) + \boldsymbol{f}_1 P_1(\Theta) \ . \tag{3.100}$$

**Dimensionally reduced balance of linear momentum** Before writing down the final result, we make use of the boundary conditions in Eq. (3.12) and the stress vector definitions Eqs. (3.3.2). Putting the two together and rearranging, we have the following relationships:

$$\boldsymbol{T}^{3}_{0} = \frac{1}{2}(\boldsymbol{t}_{+} - \boldsymbol{t}_{-}) \ , \tag{3.101}$$

$$\boldsymbol{T}^{3}_{1} = \frac{1}{2}(\boldsymbol{t}_{+} + \boldsymbol{t}_{-}) \tag{3.102}$$

We can combine Eqs. (3.92), (3.99), (3.100), and (3.101) to yield the zeroth and first order linear momentum balances:

$$\rho_{\mathrm{s}} \dot{\boldsymbol{v}}_0 = \delta \boldsymbol{T}^{\alpha}_{0:\alpha} - \frac{\delta^2}{2} H_{,\alpha} \boldsymbol{T}^{\alpha}_{1} + (\boldsymbol{t}_{+} + \boldsymbol{t}_{-}) - \delta H(\boldsymbol{t}_{+} - \boldsymbol{t}_{-}) + \boldsymbol{f}_{\mathrm{s}} \ , \tag{3.103}$$

$$\begin{aligned} \rho_{\mathrm{s}}\delta H \dot{\boldsymbol{v}}_0 + \frac{\rho_{\mathrm{s}}\delta}{2}\ddot{\boldsymbol{n}} = & \delta \boldsymbol{T}^{\alpha}_{1:\alpha} - \delta^2 H_{,\alpha}\left( \boldsymbol{T}^{\alpha}_{0} + \frac{1}{2}\boldsymbol{T}^{\alpha}_{2} \right) \\ & - \delta H(\boldsymbol{t}_{+} + \boldsymbol{t}_{-}) - \frac{\delta^2}{2}\left(2H^2 - K\right)(\boldsymbol{t}_{+} - \boldsymbol{t}_{-}) + \delta \boldsymbol{f}_1 \ , \end{aligned} \tag{3.104}$$

where we have multiplied through by $\delta$ and defined $\boldsymbol{f}_s \coloneqq \delta \boldsymbol{f}_0$ as the body force per unit area.

### 3.3.4 The balance of angular momentum

We begin this section by recalling three-dimensional, curvilinear angular momentum balance in Eq. (3.7). Using the expansions for the tangent and dual bases in Sec. 2.2, we express the balance as:

$$\boldsymbol{g}_i \times \left(\boldsymbol{\sigma}^T \boldsymbol{g}^i\right) \overset{1}{=} P_0(\theta)\left(\boldsymbol{a}_\alpha \times \boldsymbol{T}_0^\alpha - \frac{\delta}{4} b_\alpha^\gamma \boldsymbol{a}_\gamma \times \boldsymbol{T}_1^\alpha + \boldsymbol{n} \times \boldsymbol{T}_0^3\right) \tag{3.105}$$

$$+ P_1(\theta)\left(\boldsymbol{a}_\alpha \times \boldsymbol{T}_1^\alpha - \frac{\delta}{2} b_\alpha^\gamma \boldsymbol{a}_\gamma \times \left(\boldsymbol{T}_0^\alpha + \frac{1}{2}\boldsymbol{T}_2^\alpha\right) + \boldsymbol{n} \times \boldsymbol{T}_1^3\right) \ . \tag{3.106}$$

where we have truncated at first order. The normal components of these equations imply, respectively, the following:

$$\boldsymbol{T}_0^\alpha \cdot \boldsymbol{a}^\beta - \frac{\delta}{4} b_\gamma^\alpha \boldsymbol{T}_1^\gamma \cdot \boldsymbol{a}^\beta \quad \text{is symmetric} \ , \tag{3.107}$$

$$\boldsymbol{T}_1^\alpha \cdot \boldsymbol{a}^\beta - \frac{\delta}{4} b_\gamma^\alpha (\boldsymbol{T}_2^\gamma + \boldsymbol{T}_1^\gamma) \cdot \boldsymbol{a}^\beta \quad \text{is symmetric} \ . \tag{3.108}$$

Note that this preserves the original symmetry statement in Eq. (3.8). Thus, a three dimensional constitutive model that satisfies the symmetry requirement also obeys Eq. (3.107). Therefore, this equation does not need to be considered in practice as long as a suitable constitutive model is chosen.

In order to proceed, we define the following quantities, which resemble the equivalent definitions in strict surface theories [10, 36, 39, 57]:

$$N^{\alpha\beta} = \delta \boldsymbol{T}_0^\alpha \cdot \boldsymbol{a}^\beta \ , \tag{3.109}$$

$$M^{\alpha\beta} = -\frac{\delta^2}{4} \boldsymbol{T}_1^\alpha \cdot \boldsymbol{a}^\beta \ . \tag{3.110}$$

Specifically, $N^{\alpha\beta}$ are the in-plane mid-surface stress components, which are constant through the thickness. These components, as we will see in Sec.3.5, can be attributed to elastic stretching forces due to membrane tension or in-plane viscous stemming from membrane fluidity. The components $M^{\alpha\beta}$ are moment-inducing stresses that are responsible for the bending response of the membrane. The first symmetry statement in Eq. (3.107) can be rewritten:

$$\check{\sigma}_0^{\alpha\beta} = N^{\alpha\beta} + b_\gamma^\alpha M^{\gamma\beta} \quad \text{is symmetric} \ , \tag{3.111}$$

which is the same statement found in Naghdi's shell theory [39] as well as strict surface theories [10, 11, 36], though now the definitions of the components are different due to our explicit inclusion of thickness.

The zeroth and first order in-plane components of the balance in Eq. (3.106) are, respectively:

$$\boldsymbol{T}_0^\alpha \cdot \boldsymbol{n} - \frac{\delta}{4} b_\gamma^\alpha \boldsymbol{T}_1^\gamma \cdot \boldsymbol{n} - \frac{1}{2}(\boldsymbol{t}_+ - \boldsymbol{t}_-) \cdot \boldsymbol{a}^\alpha = 0 \ , \tag{3.112}$$

$$\boldsymbol{T}_1^\alpha \cdot \boldsymbol{n} - \frac{\delta}{4} b_\gamma^\alpha (\boldsymbol{T}_2^\gamma + \boldsymbol{T}_0^\gamma) \cdot \boldsymbol{n} - \frac{1}{2}(\boldsymbol{t}_+ + \boldsymbol{t}_-) \cdot \boldsymbol{a}^\alpha = 0 \ \ , \tag{3.113}$$

where we have incorporated the definitions given in Eqs. (3.101). Equation (3.112) shows that we again preserve the three-dimensional symmetry condition in (3.8), or that:

$$\check{\sigma}_n^{\alpha 3} \quad \text{is symmetric} \ . \tag{3.114}$$

In order to compare this to strict surface theories, we define the following quantities:

$$S^\alpha = \delta \boldsymbol{T}_0^\alpha \cdot \boldsymbol{n} \ , \tag{3.115}$$

$$R^\alpha = -\frac{\delta^2}{4} \boldsymbol{T}_1^\alpha \cdot \boldsymbol{n} \ . \tag{3.116}$$

Employing Eq. (3.115) and (3.116), Eq. (3.112) becomes:

$$S^\alpha + b_\gamma^\alpha R^\gamma - \frac{\delta}{2}(\boldsymbol{t}_+ - \boldsymbol{t}_-) \cdot \boldsymbol{a}^\alpha = 0 \ , \tag{3.117}$$

$$R^\alpha - \frac{\delta^2}{4} b_\gamma^\alpha \left(\delta \boldsymbol{T}_2^\gamma \cdot \boldsymbol{n} + S^\gamma\right) + \frac{\delta^2}{8}(\boldsymbol{t}_+ + \boldsymbol{t}_-) \cdot \boldsymbol{a}^\alpha = 0 \ \ , \tag{3.118}$$

which importantly shows that:

$$R^\alpha = \mathcal{O}\big(\delta^3 \kappa \boldsymbol{T}_2^\alpha + \delta^2 (\boldsymbol{t}_+ + \boldsymbol{t}_-)\big) \ . \tag{3.119}$$

While the form of Eq. (3.112) seems to differ from strict surface theories [10, 11, 36, 39], it is in fact equivalent. Revealing this requires a detailed analysis of the component-form equations of motion, which we present in Sec. 3.4.

## 3.4 Material independent $(2+\delta)$-dimensional equations of motion

Before proceeding with the derivation of the $(2+\delta)$-dimensional equations of motion, it is important to revisit the core variables in our theoretical framework. Equation (3.51) reveals that the expansion coefficients of density can be expressed in terms of the mid-surface density and curvature. Therefore, we only need to solve for one of these expansion coefficients, making it reasonable to consider the mid-surface density $\rho_{\mathrm{s}}$, as defined in Sec. 3.3.1, as one of our fundamental unknowns.

Regarding the stress tensor components presented in Eq. (3.27), they are determined by the constitutive model in Eq. (3.9). As a result, these stress tensor components are not considered fundamental unknowns. Specifically, the in-plane stress tensor components $\check{\sigma}^{\alpha\beta}$ are dictated by the constitutive response of the membrane, which, in turn, depends on the strain tensor or velocity gradient. According to the assumption of K-L kinematics, the strain tensor and velocity gradient are fully determined by the mid-surface position vector $\boldsymbol{x}_0$ or, equivalently, the mid-surface velocity vector $\boldsymbol{v}_0$. Therefore, we consider $\boldsymbol{v}_0$ as a fundamental unknown and determine $\boldsymbol{x}_0$ by integrating Eq. (2.53).

In the present work, the components $\check{\sigma}^{i3} = \check{\sigma}^{3i}$ are assumed to be fixed by the applied surface tractions $\boldsymbol{t}_\pm$ as well as the symmetry conditions Eq. (3.8). In general, these components also depend on stresses that enforce K-L kinematics [58, 59], but we leave details of such a treatment to [42], where it is demonstrated that these stresses can be solved for entirely implicitly.

In order to arrive at the equations of motion, we first express the zeroth order linear momentum balance, Eq. (3.103), in terms of its in-plane and normal components:

$$\begin{aligned}\rho_{\mathrm{s}}\left(v^\alpha_{0,t} + v^\beta_0 v^\alpha_{0:\beta} - 2v^3_0 v^\beta_0 b^\alpha_\beta - v^3_0 v^3_{0,\beta}\, a^{\alpha\beta}\right) &= N^{\gamma\alpha}_{;\gamma} - S^\gamma b^\alpha_\gamma + 2H_{,\gamma} M^{\gamma\alpha} \\ &\quad + \left(\boldsymbol{t}^+ + \boldsymbol{t}^-\right)\cdot\boldsymbol{a}^\alpha - \delta H\left(\boldsymbol{t}^+ - \boldsymbol{t}^-\right)\cdot\boldsymbol{a}^\alpha + \boldsymbol{f}_{\mathrm{s}}\cdot\boldsymbol{a}^\alpha\ , \end{aligned} \tag{3.120}$$

$$\begin{aligned}\rho_{\mathrm{s}}\left(v^3_{0,t} + 2v^\alpha_0 v^3_{0,\alpha} + v^\alpha_0 v^\beta_0 b_{\beta\alpha}\right) &= N^{\alpha\beta} b_{\alpha\beta} + S^\alpha_{:\alpha} + \left(\boldsymbol{t}^+ + \boldsymbol{t}^-\right)\cdot\boldsymbol{n} \\ &\quad - \delta H\left(\boldsymbol{t}^+ - \boldsymbol{t}^-\right)\cdot\boldsymbol{n} + \boldsymbol{f}_{\mathrm{s}}\cdot\boldsymbol{n}\ , \end{aligned} \tag{3.121}$$

where we have used the definitions in Eqs. (3.109), (3.110), (3.115), (3.116) and have neglected terms using Eq. (3.119). The term $-\frac{\delta^2}{2}H_{,\alpha}\boldsymbol{T}^\alpha_1\cdot\boldsymbol{a}^\beta = 2H_{,\gamma}M^{\gamma\alpha}$ in Eq. (3.120), couples curvature gradients to moments, and is arises from the finite thickness nature of the membrane.

Assuming an appropriate constitutive model, Eqs. (3.120) and (3.121) depend on $\rho_s$, $\boldsymbol{v}_0$, and $S^\alpha$ alone. While the in-plane equations allow us to solve for the mid-surface velocities and the out-of-plane equation for the surface density, we require an additional equation to solve for the stress components $S^\alpha$. We find such an equation using the first order linear and angular momentum balances. First, we note that the first-order stress vector divergence can be expressed as:

$$-\frac{\delta^2}{4}\boldsymbol{T}^\alpha_{1:\alpha}\cdot\boldsymbol{a}^\beta = M^{\gamma\beta}_{;\gamma} - R^\gamma b^\beta_\gamma\ . \tag{3.122}$$

We can substitute into this the first order linear momentum balance Eq. (3.104), and plug the result into the zeroth order angular momentum balance Eq. (3.117). Solving for the stress components yields:

$$S^\alpha = -M^{\gamma\alpha}_{;\gamma} + \frac{\delta}{2}\left(\boldsymbol{t}^+ - \boldsymbol{t}^-\right)\cdot\boldsymbol{a}^\alpha - \frac{\delta}{4}\left(\rho_{\mathrm{s}}\delta H\dot{\boldsymbol{v}}_0 + \frac{\rho_{\mathrm{s}}\delta}{2}\ddot{\boldsymbol{n}} + 2\delta H\left(\frac{1}{2}\left(\boldsymbol{t}^+ + \boldsymbol{t}^-\right)\right) - \delta\boldsymbol{f}_1\right)\cdot\boldsymbol{a}^\alpha\ , \tag{3.123}$$

where we have used the order of magnitude assumptions to neglect the terms $\frac{\delta^3}{8}\left(2H^2-K\right)\left(\boldsymbol{t}_+-\boldsymbol{t}_-\right)\cdot\boldsymbol{a}^\alpha$ and $\frac{\delta^3}{4}H_{,\beta}\left(\boldsymbol{T}_0^\beta+\frac{1}{2}\boldsymbol{T}_2^\beta\right)\cdot\boldsymbol{a}^\alpha$ in comparison with others in Eq. (3.123).

Equation (3.123) represents the final equation necessary to solve for $S^\alpha$ in the $(2+\delta)$-dimensional theory. In strict surface theories [10, 11, 36], the equivalent result is $S^\alpha=-M^{\beta\alpha}_{;\beta}$. However, here we observe contributions from inertia as well as external tractions coupled to curvature. In our later analysis in Sec. 4.1, we will assume that neglecting inertia is a reasonable assumption, which is the case for lipid membrane systems [60]. However, the applied surface tractions are in general nonnegligible, and have been shown to significantly alter membrane behavior [61–63].

We now have in place the equations of motion for finite thickness membranes. The mass balance is given by Eq. (3.3.1) and the linear momentum balance in Eqs. (3.103), (3.104), and (3.123). In order to proceed, we will prescribe material responses for the membrane and will derive, the dimensionally reduced constitutive laws. This will allow us to write down the component form equations of motion that we will analyze using linear response.

## 3.5 $(2+\delta)$-dimensional constitutive equations

In the preceding sections, we derived the dimensionally reduced mass, linear momentum, and angular momentum balances under the assumption of K-L kinematics. Additionally, we imposed order of magnitude assumptions, given in Sec. 3.2.2, motivated by length scales present in cellular systems. We were able to arrive at material-independent component form equations of motion where thickness is explicitly resolved. However, in order to solve for the unknowns, namely the velocity $\boldsymbol{v}_0$, the surface density $\rho_s$, and the stress components $S^\alpha$, we require the specification of constitutive models that describe the material response of the membrane.

Motivated by the arguments presented in [11], we assume the membrane is a compressible, viscous fluid. To that end, the stress tensor Eq. 3.9 is split up into two parts:

$$\boldsymbol{\sigma}=\boldsymbol{\sigma}_{\text{visc}}+\boldsymbol{\sigma}_{\text{elas}}\ , \tag{3.124}$$

where the first term on the right-hand side describes the viscous response of the membrane and the second the elastic response. In the following sections, we will derive the dimensionally reduced forms for the stress components. In particular, we will provide the terms: $N^{\alpha\beta}$, $M^{\alpha\beta}$ for each material response model.

### 3.5.1 Elastic response

It is well documented [6, 10, 11, 53, 64, 65] that membranes exhibit elastic behavior, capable of stretching in-plane and bending out-of-plane. In strict two-dimensional theories, the elastic stresses typically are derived using the Helfrich Hamiltonian [6]. However, such a picture assumes a two-dimensional isolated body in thermodynamic equilibrium. It was shown in [11]

that the local equilibrium hypothesis could be applied to derive equations of motion using linear, irreversible thermodynamics. In this treatment, membrane compression and bending are separately penalized. Bending is a fundamentally two-dimensional phenomena [43] that approximates the effects of coupled compression and extension of opposing surfaces. As a result, we are motivated to assume the following model for the stress:

$$\boldsymbol{\sigma}_{\text{elas}} = 2k_{\text{c}}(J-1) \ , \tag{3.125}$$

where $k_{\text{c}}$ is the compression modulus and the $J$ denotes the volume change with respect to some stress free configuration [38, 66]. We note that this is the same as proposed in [67]. The volume change (3.2) can be expressed as:

$$J = \frac{\mathrm{d}v}{\mathrm{d}V} = \frac{\mathrm{d}\theta^3}{\mathrm{d}\theta^3}\frac{da}{dA} \ , \tag{3.126}$$

where $\mathrm{d}v$ and $\mathrm{d}V$ are the volume changes in the current and reference configurations, respectively and in which we used the assumption of constant thickness. We note that this is a restatement of the Lagrangian mass balance Eq. (3.2) using the current configuration, which is permitted because all the quantities are invariant to changes in parametrization. Thus, assuming a flat reference configuration, Eq. (3.126) can be expressed relative to the mid-surface as:

$$J = J_0(1 - \delta H\Theta + \frac{\delta^2}{4}K\Theta) \ , \tag{3.127}$$

where we recognize $J_0 = \mathrm{d}a_0/\ \mathrm{d}A_0 = \hat{\rho}_{\text{mid}}/\rho_{\text{mid}}$ as the mid-surface area stretch. In terms of Chebyshev polynomials, this reads:

$$J = P_0(\Theta)J_0 - P_1(\Theta)\delta H J_0 + P_2(\theta)\frac{\delta^2}{8}J_0 \ , \tag{3.128}$$

where we have applied the assumptions in Sec. 3.2.2. Using Eqs. (3.76), (3.109), (3.110), we arrive at the following for the elastic stress and moment stress components:

$$N^{\alpha\beta}_{\text{elas}} = 2k_{\text{c}}\delta(J_0-1)a^{\alpha\beta} + k_{\text{b}}\left(\frac{1}{2}Ka^{\alpha\beta} - Hb^{\alpha\beta}\right) \ , \tag{3.129}$$

$$M^{\alpha\beta}_{\text{elas}} = k_{\text{b}}Ha^{\alpha\beta} + \frac{k_{\text{b}}}{2}b^{\alpha\beta}(J_0-1) \ , \tag{3.130}$$

where $k_{\text{b}} \coloneqq k_{\text{c}}\delta^3/2$ is the membrane bending modulus. However, in most cases, lipid bilayers are considered area incompressible as they tear after $2-3\%$ areal stretching [53, 54]. Therefore, we take $J_0 = 1$ and end with the following elastic stress components:

$$N^{\alpha\beta}_{\text{elas}} = \lambda a^{\alpha\beta} + k_{\text{b}}\left(\frac{1}{2}Ka^{\alpha\beta} - Hb^{\alpha\beta}\right) \ , \tag{3.131}$$

$$M^{\alpha\beta}_{\text{elas}} = k_{\text{b}}Ha^{\alpha\beta} \ , \tag{3.132}$$

where $\lambda$ is a Lagrange multiplier that enforces mid-surface incompressibility. We will reserve comparison of these stresses for Sec. 3.6.

### 3.5.2 Viscous response

Lipid bilayers are typically assumed to have the viscous response of Newtonian fluid [14, 68], which is experimentally supported [69]. Direct two-dimensional theories employ the method of Scriven [55] to model membrane in plane as a shear surface fluid [9, 11, 28]. Therefore, we attempt to arrive at an effective model by dimension reducing the three-dimensional stress for a Newtonian fluid. The full stress contribution for an compressible medium can be split into shear and volumetric contributions:

$$\boldsymbol{\sigma}_{\text{visc}} = \boldsymbol{\sigma}_{\text{visc,shear}} + \boldsymbol{\sigma}_{\text{visc,vol}} \ , \tag{3.133}$$

$$\boldsymbol{\sigma}_{\text{visc,shear}} = \eta^m \left( \nabla \boldsymbol{v} + \nabla \boldsymbol{v}^{\mathrm{T}} \right) \ , \tag{3.134}$$

$$\boldsymbol{\sigma}_{\text{visc,vol}} = \zeta^{\mathrm{m}} \mathrm{div}(\boldsymbol{v}) \ , \tag{3.135}$$

where $\eta^m$ and $\zeta^m$ are the three-dimensional membrane shear and volume viscosities [70, 71], respectively. The velocity gradient can be expressed:

$$\nabla \boldsymbol{v} = \boldsymbol{v}_{,i} \otimes \boldsymbol{g}^i \ . \tag{3.136}$$

Implementing this and recalling the expansion Eq. (3.58), we can write the shear part of the stress as:

$$\begin{aligned} \boldsymbol{\sigma}_{\text{visc,shear}} = 2\eta^{\mathrm{m}} \Big[ & P_0(\Theta) \left\{ \left( d_0^{\alpha\beta} - v_0^3 b^{\alpha\beta} \right) \boldsymbol{a}_\alpha \otimes \boldsymbol{a}_\beta + \right. \\ & \left. \frac{1}{2} \left( v_0^\beta b_\beta^\alpha + v_0^{3,\alpha} + \frac{2}{\delta} v_1^\alpha \right) (\boldsymbol{n} \otimes \boldsymbol{a}_\alpha + \boldsymbol{a}_\alpha \otimes \boldsymbol{n}) \right\} + \\ & P_1(\theta) \left\{ \left( d_1^{\alpha\beta} - \frac{\delta}{2} v_0^3 b_\delta^\beta b^{\delta\alpha} + \frac{\delta}{4} \left( v_{0:\delta}^\beta b^{\delta\alpha} + v_{0:\delta}^\alpha b^{\delta\beta} \right) \right) \boldsymbol{a}_\beta \otimes \boldsymbol{a}_\alpha + \right. \\ & \left. \left. \left( v_1^\beta b_\beta^\alpha + \frac{\delta}{2} \left( v_0^\beta b_{\beta\delta} b^{\delta\alpha} + v_{0,\gamma}^3 b^{\gamma\alpha} \right) \right) (\boldsymbol{n} \otimes \boldsymbol{a}_\alpha + \boldsymbol{a}_\alpha \otimes \boldsymbol{n}) \right\} \right] \end{aligned} \tag{3.137}$$

where we have defined the symmetric part of the in-plane velocity gradients as

$$d_i^{\alpha\beta} = \frac{1}{2} \left( v_i^{\alpha:\beta} + v_i^{\beta:\alpha} \right) \ . \tag{3.138}$$

Next, the volume contribution is found after recalling the velocity divergence Eq. (3.67) to be:

$$\boldsymbol{\sigma}_{\text{visc,vol}} = \omega \left\{ P_0(\theta) \left( v_{0:\alpha}^\alpha - 2H v_0^3 \right) + P_1(\theta) \left( v_{1:\alpha}^\alpha + \frac{\delta}{2} \left( v_{0:\alpha}^\beta b_\beta^\alpha - v_0^3 b_\beta^\alpha b_\alpha^\beta \right) \right) \right\} \boldsymbol{a}_\gamma \otimes \boldsymbol{a}^\gamma \ . \tag{3.139}$$

Given Eqs. (3.137) and (3.139), we can find the stress components as we did in the preceding section. This yields:

$$N^{\alpha\beta}_{\text{visc,shear}} = 2\mu^{\text{m}}\left(d_0^{\alpha\beta} - v_0^3 b^{\alpha\beta}\right) \ , \tag{3.140}$$

$$N^{\alpha\beta}_{\text{visc,bulk}} = \mu^{\text{m}}\left(v^{\gamma}_{0:\gamma}a^{\alpha\beta} - 2Hv_0^3 a^{\alpha\beta}\right) \ , \tag{3.141}$$

$$M^{\delta\mu}_{\text{visc,shear}} = -\frac{\delta^2\zeta^{\text{m}}}{2}\left(d_1^{\delta\mu} - \frac{\delta}{2}v_0^3 b^{\mu}_{\gamma}b^{\gamma\delta} + \frac{\delta}{4}\left(v^{\mu}_{0:\gamma}b^{\gamma\delta} + v^{\delta}_{0:\gamma}b^{\gamma\mu}\right) + \frac{\delta}{2}\left(d_0^{\gamma\mu} - v_0^3 b^{\gamma\mu}\right)b^{\delta}_{\gamma}\right) \ , \tag{3.142}$$

$$M^{\alpha\beta}_{\text{visc,bulk}} = -\frac{\zeta^{\text{m}}\delta^2}{4}\left\{\left(v^{\mu}_{1:\mu} + \frac{\delta}{2}\left(v^{\lambda}_{0:\mu} - v_0^3 b^{\lambda}_{\mu}\right)b^{\mu}_{\lambda}\right)a^{\alpha\beta} + \frac{\delta}{2}b^{\alpha\beta}\left(v^{\mu}_{0:\mu} - 2v_0^3 H\right)\right\} \tag{3.143}$$

We are now in place to write down the material dependent equations of motion.

## 3.6 Equations of motion for a lipid bilayer in a viscous medium

In this section, we will derive the material-dependent equations of motion using the results from Sec. 3.5. However, we first turn our attention towards the applied surface tractions.

### 3.6.1 The surface traction terms

To analyze Eqs. (3.120), (3.121) and (3.123), it is essential to correctly assess the surface traction terms. We assume that the surrounding medium, in which the membrane is situated, behaves as an incompressible Newtonian fluid, and its stress is described by the following expression [72, 73]:

$$\boldsymbol{\sigma} = -p\boldsymbol{I} + 2\mu^{\text{b}}\boldsymbol{D} \ , \tag{3.144}$$

Here, $\boldsymbol{\sigma}$ represents the stress tensor, $p$ is the pressure, $\boldsymbol{I}$ is the identity tensor (Eq. (2.30)), and $\mu^{\text{b}}$ is the dynamic viscosity. The term $\boldsymbol{D}$ corresponds to the rate of deformation tensor, which characterizes the velocity gradient within the fluid. This description is suitable for modeling the behavior of the surrounding fluid medium.

Due to our chosen kinematic framework for the membrane (as discussed in Sec 2.2), we have established specific local tangent and dual bases solely on the mid-surface. These tangent vectors, as expressed in Eqs. (2.57) and (2.58), do not directly correspond to a local parametrization because they rely on coordinates defined exclusively on the mid-surface.

To bridge the gap between the mid-surface and points within the membrane, we assume the existence of a mapping. Consequently, we cannot guarantee that the same tangent basis is suitable for points in the bulk of the material. To address this, we employ an arbitrary tangent basis, denoted as $\{\bar{\boldsymbol{g}}_i\}$, and its associated dual basis that best fits the geometric

configuration. This approach allows us to establish a connection between the bulk and the membrane by projecting the relevant quantities onto the appropriate bounding surface.

This projection has notable implications for both velocity and traction boundary conditions. However, we cannot determine these components without initially specifying the geometry of the bulk. For instance, if we have a cylindrical membrane, it may be convenient to parameterize the bulk using cylindrical coordinates. However, this choice is not obligatory. Alternatively, we could opt for Cartesian coordinates for the bulk and project the relevant quantities onto the membrane. It's important to emphasize that the projected quantities remain vectorial or tensorial, and their fundamental properties remain invariant. While their components may change upon projection, the overall solution for the bulk remains unaffected.

In light of these considerations, we express the stress tensor as follows:

$$\boldsymbol{\sigma} = -p\delta^i_j + \mu^{\mathrm{b}} \left[ u^i|_j \; \bar{\boldsymbol{g}}_i \otimes \bar{\boldsymbol{g}}^j + u^i|_j \; \bar{\boldsymbol{g}}^j \otimes \bar{\boldsymbol{g}}_i \right] \; . \tag{3.145}$$

Here, $\boldsymbol{u}$ represents the bulk velocities, and $(\cdot)^i|_j$ signifies the $j^{th}$ three-dimensional covariant derivative (e.g., as defined in Eq. (2.15)) of the $i^{th}$ component of $(\cdot)$ along the $\{\bar{\boldsymbol{g}}_i\}$ direction. It is essential to note that we differentiate from the semi-colon notation for these covariant derivatives as the notations $(\cdot)_{;\alpha}$ and $(\cdot)_{:\alpha}$ are particular to the mid-surface parametrization. In Eq. (3.145), we have inserted the following definition [38, 72]:

$$\boldsymbol{D} = \frac{\mu^{\mathrm{b}}}{2} \left[ u^i|_j \; \bar{\boldsymbol{g}}_i \otimes \bar{\boldsymbol{g}}^j + u^i|_j \; \bar{\boldsymbol{g}}^j \otimes \bar{\boldsymbol{g}}_i \right] \; . \tag{3.146}$$

We now define the surface tractions applied by the bulk onto the membrane:

$$\begin{aligned} \boldsymbol{t}_{\pm} &= \boldsymbol{\sigma}^T|_{\pm\delta/2}\boldsymbol{n}_{\pm} && (3.147)\\ &= \pm \left( -p|_{\mathcal{S}_{\pm}}\boldsymbol{n} + 2\mu^{\mathrm{b}}\boldsymbol{D}^T|_{\mathcal{S}_{\pm}}\boldsymbol{n} \right) && (3.148)\\ &= \boldsymbol{t}_{\pm,\mathrm{press}} + \boldsymbol{t}_{\pm,\mathrm{visc}} \; , && (3.149) \end{aligned}$$

where we identify:

$$\boldsymbol{t}_{\pm,\mathrm{press}} \coloneqq \mp p|_{\mathcal{S}_{\pm}} \; \boldsymbol{n} \; , \tag{3.150}$$

$$\boldsymbol{t}_{\pm,\mathrm{visc}} \coloneqq \pm 2\mu^{\mathrm{b}}\boldsymbol{D}^T|_{\mathcal{S}_{\pm}} \; \boldsymbol{n} \; . \tag{3.151}$$

In these expressions, the positive normal vector corresponds to the upper boundary of the membrane, coinciding with that of the mid-surface (see Fig. 2.2). This approach allows us to decompose the applied tractions into contributions from pressure and viscous terms. We project onto the basis defined with respect to the mid-surface, for which we have developed our effective equations of motion, and evaluate our bulk quantities at the membrane surfaces $\mathcal{S}_{\pm}$. This is possible because we know there is a one-to-one mapping between points on the membrane boundaries and its mid-surface. If we instead projected onto the full

three-dimensional tangent vectors, we simply would get different, but physically equivalent components associated with such a basis. Indeed, we could relate these components to those associated with the mid-surface basis, but choose instead to go the latter route out of convenience.

Using Eqs. (3.151) and (3.146), the in-plane applied tractions are:

$$\begin{aligned} t^{\alpha}_{\pm} &\coloneqq \boldsymbol{t}_{\pm} \cdot \boldsymbol{a}^{\alpha} \\ &= \pm \mu^{\mathrm{b}} \left[ (u^i|_j)|_{\mathcal{S}_{\pm}} \, (\boldsymbol{a}^{\alpha} \cdot \bar{\boldsymbol{g}}_i)(\bar{\boldsymbol{g}}^j \cdot \boldsymbol{n}) + (u^i|_j)|_{\mathcal{S}_{\pm}} \, (\boldsymbol{a}^{\alpha} \cdot \bar{\boldsymbol{g}}^j)(\bar{\boldsymbol{g}}_i \cdot \boldsymbol{n}) \right] . \end{aligned} \tag{3.152}$$

Likewise, the normal components read:

$$\begin{aligned} t^{n}_{\pm} &\coloneqq \boldsymbol{t}_{\pm} \cdot \boldsymbol{n} \\ &= \mp p \pm \mu^{\mathrm{b}} \left[ (u^i|_j)|_{\mathcal{S}_{\pm}} \, (\boldsymbol{n} \cdot \bar{\boldsymbol{g}}_i)(\bar{\boldsymbol{g}}^j \cdot \boldsymbol{n}) + (u^i|_j)|_{\mathcal{S}_{\pm}} \, (\boldsymbol{a}^{\alpha} \cdot \bar{\boldsymbol{g}}^j)(\bar{\boldsymbol{g}}_i \cdot \boldsymbol{n}) \right] . \end{aligned} \tag{3.153}$$

Note that this is consistent with our development of the traction continuity conditions that constrain our use of constitutive relations Eq. (3.12). The jumps and averages over the membrane of the in-plane and normal applied tractions follow as:

$$[\![ t^{\alpha} ]\!] = 2\mu^{\mathrm{b}} \left\langle u^i|_j \, (\boldsymbol{a}^{\alpha} \cdot \bar{\boldsymbol{g}}_i)(\bar{\boldsymbol{g}}^j \cdot \boldsymbol{n}) + u^i|_j \, (\boldsymbol{a}^{\alpha} \cdot \bar{\boldsymbol{g}}^j)(\bar{\boldsymbol{g}}_i \cdot \boldsymbol{n}) \right\rangle , \tag{3.154}$$

$$2 \langle t^{\alpha} \rangle = \mu^{\mathrm{b}} [\![ u^i|_j \, (\boldsymbol{a}^{\alpha} \cdot \bar{\boldsymbol{g}}_i)(\bar{\boldsymbol{g}}^j \cdot \boldsymbol{n}) + u^i|_j \, (\boldsymbol{a}^{\alpha} \cdot \bar{\boldsymbol{g}}^j)(\bar{\boldsymbol{g}}_i \cdot \boldsymbol{n}) ]\!] , \tag{3.155}$$

$$[\![ t^{n} ]\!] = -2 \langle p \rangle + 2 \left\langle u^i|_j \, (\boldsymbol{n} \cdot \bar{\boldsymbol{g}}_i)(\bar{\boldsymbol{g}}^j \cdot \boldsymbol{n}) + u^i|_j \, (\boldsymbol{n} \cdot \bar{\boldsymbol{g}}^j)(\bar{\boldsymbol{g}}_i \cdot \boldsymbol{n}) \right\rangle , \tag{3.156}$$

$$2 \langle t^{n} \rangle = -[\![ p ]\!] + [\![ u^i|_j \, (\boldsymbol{n} \cdot \bar{\boldsymbol{g}}_i)(\bar{\boldsymbol{g}}^j \cdot \boldsymbol{n}) + u^i|_j \, (\boldsymbol{n} \cdot \bar{\boldsymbol{g}}^j)(\bar{\boldsymbol{g}}_i \cdot \boldsymbol{n}) ]\!] , \tag{3.157}$$

where we have used the notation: $[\![ (\cdot) ]\!] \coloneqq (\cdot)_{\mathcal{S}_+} - (\cdot)_{\mathcal{S}_-}$ and $2 \langle (\cdot) \rangle \coloneqq (\cdot)_{\mathcal{S}_+} + (\cdot)_{\mathcal{S}_-}$.

We are now in place to write down the equations of motion.

### 3.6.2 Equations of motion

The material dependent equations of motion are found when inserting Eqs. (3.140) into Eqs. (3.103), (3.104), and (3.123). However, before doing so we will make a few assumptions about the system at hand. First, we will neglect the inertial contributions to the balances as the Reynolds number of nearly flat bilayers are typically very small, as shown in [60]. Upon this assumption and using the results from Sec. 3.6.1, Eqs. (3.103),(3.104), and (3.69) become:

$$\begin{aligned} 0 = {} & \lambda^{\mathrm{eff},\alpha} + \frac{k_{\mathrm{b}}}{2} K^{,\alpha} + 2\mu^{\mathrm{m}} \left( d^{\alpha\beta}_{:\beta} - v_{,\beta} b^{\alpha\beta} - 2v H^{,\alpha} \right) \\ & + \frac{\delta}{2} (b^{\alpha}_{\lambda} - 2\delta^{\alpha}_{\lambda} H) [\![ t^{\alpha}_{\mathrm{visc}} ]\!] + 2 \langle t^{\alpha}_{\mathrm{visc}} \rangle - \delta \langle p \rangle^{,\alpha} , \end{aligned} \tag{3.158a}$$

$$\begin{aligned} 0 = {} & 2H\lambda^{\mathrm{eff}} - k_{\mathrm{b}} H (4H^2 - 3K) - k_{\mathrm{b}} \Delta_s H + 2\mu^{\mathrm{m}} \left( d^{\alpha\beta} b_{\alpha\beta} - v(4H^2 - 2K) \right) \\ & + \frac{\delta}{2} [\![ t^{\alpha}_{\mathrm{visc}} ]\!]_{:\alpha} - [\![ p ]\!] + 2 \langle t^{n}_{\mathrm{visc}} \rangle , \end{aligned} \tag{3.158b}$$

$$0 = v^{\alpha}_{:\alpha} - 2vH \tag{3.158c}$$

where we have made use of the assumptions in Sec. 3.2.2. Additionally, we let $v_0^3 = v$ and $d_0^{\alpha\beta} = d^{\alpha\beta}$ as we realize we need only to solve for the membrane velocity components $v_0^\alpha$ and $v_0^3$. The double bracket notation, $[\![\cdot]\!] \coloneqq (\cdot)^+ - (\cdot)^-$, denotes a jump in quantities evaluated at the membrane surfaces, $\mathcal{S}_\pm$, while the angled bracket notation, $2\langle\cdot\rangle \coloneqq (\cdot)^+ + (\cdot)^-$ refers to the average of such quantities. The surface Laplacian is denoted as $\Delta_s(\cdot) \coloneqq (\cdot)_{;\alpha\beta} a^{\alpha\beta}$ [33]. The applied surface tractions due to bulk viscous forces are given by the in-plane and normal components $t^\alpha_{\text{visc}}$ and $t^n_{\text{visc}}$. The membrane velocity components $\{v^\alpha, v^n\}$ here refer to that of the mid-surface $\mathcal{S}_0$, and are those of the lowest order coefficient in the spectral representation of the total membrane velocity, Eq. (3.57). Finally, $d^{\alpha\beta} = (v^\alpha_{;\gamma} a^{\gamma\beta} + v^\beta_{;\gamma} a^{\gamma\alpha})/2$ is the in-plane strain rate for $i = 0$ in Eq. (3.138), and $\lambda^{\text{eff}} \coloneqq \lambda + \delta\langle p\rangle$ is the effective membrane tension and lumps the tension $\lambda$ and the average applied pressure $\langle p\rangle$ from the surroundings.

In the context of biological membranes, inertia is negligible [74, 75] so that the bulk fluid velocity $\boldsymbol{u}$ and pressure $p$ are governed by the Stokes' equations and continuity as,

$$-\nabla p_\pm + \mu^{\text{b}} \nabla^2 \boldsymbol{u}_\pm = 0 \ , \tag{3.159a}$$

$$\nabla \cdot \boldsymbol{u}_\pm = 0 \ . \tag{3.159b}$$

where the $\pm$ corresponds to the pressure and velocities for the domains located at the top and bottom of the membrane, respectively. The bulk fluid is mainly responsible for relaxing any membrane perturbations through viscous dissipation.

At infinity, the bulk fluid is at rest, leading to the following conditions for the velocities and pressure

$$\boldsymbol{u}_\pm\Big|_{z\to\pm\infty} = 0 \ , \tag{3.160a}$$

$$p_\pm\Big|_{z\to\pm\infty} = \ const. \tag{3.160b}$$

Additionally, at the membrane boundaries, the in-plane and out-of plane no-slip conditions, Eqs. (3.10) lead to

$$u^\alpha_\pm = v^\alpha \mp \frac{\delta}{2}\left(v^{,\alpha} + b^\alpha_\beta v^\beta\right) \ , \tag{3.161a}$$

$$u^n_\pm = v^n \ , \tag{3.161b}$$

where we have used the velocity equations, Eqs. (2.55) and (3.22), to evaluate the total membrane velocity at the bounding surfaces.

## 3.7 Summary

In this chapter, we presented and applied the dimension reduction procedure to the three-dimensional balance laws and constitutive relations governing lipid bilayers. By expressing desired quantities using expansion in Chebyshev polynomials, we arrived at low-order expressions for the material-independent and material-dependent equations of both. At the

end, we arrived at a set of a equations and boundary conditions describing a membrane immersed in an infinite Newtonian medium. In the following chapter, we will use these results to analyze the dynamic behavior of finite thickness membrane fluctuations.

# Chapter 4

# Fluctuations of nearly flat membranes

Building upon the previous chapters, we present here a model that allows us to capture the dynamics of finite thickness membranes in contact with fluid reservoirs, while adhering to the principles of a continuous three-dimensional framework. In order to develop this model, we employ the linear response framework [72] to analyze membrane fluctuations. In this chapter, we first non-dimensionalize the equations of motion presented in Sec. 3.6. We then derive the general perturbation equations for a nearly flat lipid bilayer. Using these equations, we solve for and analyze the dispersion relation that characterizes the decay rate of fluctuations. By investigating the hydrodynamic response of the membrane-fluid system, we pinpoint the effects of thickness resolved in our theory. Finally, we compare our results to the intermonolayer slip model [24].

## 4.1 Dimensionless parameters

We seek a set of nondimensional groupings governing the present physics. We scale all lengths with the typical system size, $L$, the tension with the base state $\Lambda$, the velocity with $U$, and the time with $\tau = L/U$. In what follows, we denote dimensionless quantities with an asterisk, $(\cdot)^*$.

Given the low Reynolds numbers of microbiological systems [74], the bulk is assumed to be governed by the Stokes' equations [73]. The Stokes' equations in terms of non-dimensional quantities are:

$$-\nabla^* p_\pm^* + \nabla^{*2} \boldsymbol{u}_\pm^* = 0 \ , \tag{4.1a}$$

$$\nabla^* \cdot \boldsymbol{u}_\pm^* = 0 \ . \tag{4.1b}$$

from which we chose the bulk pressure scale as $p_c \coloneqq \mu^{\mathrm{b}} U/L$ [33, 73].

Application of the Buckingham $\pi$ theorem tells us that we can express the membrane equations in terms of four unique dimensionless numbers. The resulting dimensionless numbers are the Föppl-von Kármán number [76], $\Gamma \coloneqq \Lambda L^2/k_{\mathrm{b}}$ comparing membrane tension to bending forces, the Scriven-Love number $SL \coloneqq \mu^{\mathrm{m}} V L/k_{\mathrm{b}}$ [60] relating membrane viscous to

bending forces, and the capillary number $\mathrm{Ca} \coloneqq \mu^{\mathrm{b}} U/\Lambda$ contrasting applied viscous traction forces to membrane tension. As the last dimensionless group, we choose the ratio between the membrane thickness $\delta$ and $L$, i.e. $\ell \coloneqq \delta/L$, which characterizes the finite thickness effects. The nondimensional form of membrane equations read:

$$0 = \lambda^{*\mathrm{eff},\alpha} + \frac{1}{2\Gamma} K^{*,\alpha} + 2\frac{SL}{\Gamma}\left(d^{*\alpha\beta}_{:\beta} - v^{*}_{,\beta} b^{*\alpha\beta} - 2v^{*} H^{*,\alpha}\right) + \mathrm{Ca}\Bigg(\frac{\ell}{2}(b^{*\alpha}_{\lambda} - 2\delta^{\alpha}_{\lambda} H^{*})[\![t^{*\alpha}_{\mathrm{visc}}]\!] + 2\left\langle t^{*\alpha}_{\mathrm{visc}}\right\rangle - \ell \left\langle p^{*}\right\rangle^{,\alpha}\Bigg), \tag{4.2a}$$

$$0 = 2H^{*}\lambda^{*eff} - \frac{1}{\Gamma} H^{*}(4H^{*2} - 3K^{*}) - \frac{1}{\Gamma}\Delta_{s} H^{*} + 2\frac{SL}{\Gamma}\left(d^{*\alpha\beta} b^{*}_{\alpha\beta} - v^{*}(4H^{*2} - 2K^{*})\right) + \mathrm{Ca}\Bigg(\frac{\ell}{2}[\![t^{*\alpha}_{\mathrm{visc}}]\!]_{:\alpha} - [\![p^{*}]\!] + 2\left\langle t^{*n}_{\mathrm{visc}}\right\rangle\Bigg), \tag{4.2b}$$

$$0 = v^{\alpha}_{:\alpha} - 2vH\ . \tag{4.2c}$$

Some characteristic values for the physical parameters are $k_{\mathrm{b}} \sim \mathcal{O}(10^2)$ pN $\cdot$ nm [60, 77, 78] and $\Lambda_0 \sim \mathcal{O}(10^{-4} - 10^{-1})$ pN $\cdot$ nm$^{-1}$ [60, 77, 79]. Typical length-scales range from $\mathcal{O}(10^2)$ nm for small lipid vesicles to $\mathcal{O}(1)$ $\mu$m for cellular radii [1, 60, 74, 78] while velocities vary from $\mathcal{O}(10^{-3})$ nm $\cdot$ $\mu$s$^{-1}$ for membrane tube-pulling [60, 80, 81] to $\mathcal{O}(10)$ nm $\cdot$ $\mu$s$^{-1}$ for bacterial gliding on soft substrates [82, 83]. Taking the bulk viscosity to be that of water, the dimensionless groups attain values of $\Gamma \sim 10^{-2} - 10^{3}$, $\mathrm{Ca} \sim 10^{-7} - 10^{2}$, and $\ell \sim 10^{-3} - 10^{-2}$. Note that for $\ell \to 0$, we recover the classical two-dimensional membrane equations [60] up to non-linear terms. However, it is possible that finite thickness effects to contribute to membrane dynamics when $\mathrm{Ca}\ell \sim O(1)$. This may be the case when the membrane is under the presence of a strong shear and/or extensional flow fields. For the ease of notation, we drop the $^{*}$ superscript and consider all quantities to be dimensionless, unless otherwise noted.

We now proceed to derive the general unperturbed and perturbed equations of motion.

## 4.2 Perturbation analysis

In this section, we derive the general base and perturbed state equations for nearly flat membranes. These equations allow us to proceed with studying membrane dynamics using linear response theory. In general, base state and perturbed quantities will be denoted by the scripts (0) and (1), respectively.

### 4.2.1 The general unperturbed equations

In this section, we will derive the general unperturbed equations for a base state where the membrane is initially flat. We choose a Cartesian parametrization: $\theta^1, \theta^2, \theta^3 = x, y, z$. This

choice allows us to express a point on the mid-surface $\boldsymbol{x}_{(0)}^{\text{mid}} \in \mathcal{S}_0$ as

$$\boldsymbol{x}_{(0)}^{\text{mid}} = x\boldsymbol{e}_x + y\boldsymbol{e}_y \ , \tag{4.3}$$

where the set $\{\boldsymbol{e}_i\}$ are Cartesian basis vectors. Using the results from Sec. 2.2, Eq. (4.3) yields the following relationships:

$$\begin{aligned} &\boldsymbol{a}_\alpha^{(0)} = \boldsymbol{e}_\alpha \ , \quad a_{\alpha\beta}^{(0)} = \delta_{\alpha\beta} \ , \quad a_{(0)}^{\alpha\beta} = \delta^{\alpha\beta} \ , \quad \boldsymbol{n}_{(0)} = \boldsymbol{e}_z \ , \\ &b_{\alpha\beta}^{(0)} = 0 \ , \quad H_{(0)} = 0 \ , \quad K_{(0)} = 0 \ , \quad \text{and} \quad {}^0\Gamma_{\lambda\mu}^{\alpha\ (0)} = 0 \ . \end{aligned} \tag{4.4}$$

We note here that the metric tensor is the identity tensor Eq. (2.30). As a result, the reciprocal basis is equivalent to the tangent basis. Therefore, we henceforth assume that repeated indices are summed over, even if they both appear as sub or superscripts (e.g. $u^\beta_{,\alpha\alpha} = u^{\beta,\alpha}_{,\alpha} = u^\beta_{,xx} + u^\beta_{,yy}$). The base state velocity is:

$$\boldsymbol{v}_{(0)} = v_{(0)}^\alpha \boldsymbol{a}_\alpha + v_{(0)}^3 \boldsymbol{n} \tag{4.5}$$

$$= v_{(0)}^\alpha \boldsymbol{e}_\alpha + v_{(0)}^z \boldsymbol{e}_z \tag{4.6}$$

$$= v_{(0)}^\alpha \boldsymbol{a}^\alpha \ , \tag{4.7}$$

where $v_{(0)}^z$ is zero since the membrane is initially flat and therefore moves at most in-plane in the $x-$ and $y-$directions. Similarly, the bulk unperturbed velocities are:

$$\boldsymbol{u}_{(0)} = u_{(0)}^i \boldsymbol{e}_i \ , \tag{4.8}$$

The in-plane surface tractions in Eq. (3.152) are then:

$$t_{(0)\pm}^\alpha = \pm \left( u_{(0),\alpha}^z + u_{(0),z}^\alpha \right) \ , \tag{4.9}$$

and the normal components, Eq. (3.153), become:

$$t_{(0)}^n = -p_{(0)} + 2\mu^{\text{b}} u_{(0),z}^z \ , \tag{4.10}$$

The jumps and averages in the base state Eq. (3.157) can then be written,

$$[\![ t_{(0)}^\alpha ]\!] = 2 \left\langle u_{(0),\alpha}^z + u_{(0),z}^\alpha \right\rangle \ , \tag{4.11}$$

$$2 \left\langle t_{(0)}^\alpha \right\rangle = [\![ u_{(0),\alpha}^z + u_{(0),z}^\alpha ]\!] \ , \tag{4.12}$$

$$[\![ t_{(0)}^n ]\!] = -[\![ p_{(0)} ]\!] + 2[\![ u_{(0),z}^z ]\!] \ , \tag{4.13}$$

$$\left\langle t_{(0)}^n \right\rangle = - \left\langle p_{(0)} \right\rangle + 2 \left\langle u_{(0),z}^z \right\rangle \ . \tag{4.14}$$

We are now proceed to derive the unperturbed equations of motion. The membrane continuity equation Eq. (3.158c) becomes:

$$v_{(0),\alpha}^\alpha = 0 \ . \tag{4.15}$$

The shape equation,Eq. (3.158b), reads:

$$0 = -[\![p_{(0)}]\!] + \ell \left\langle u^z_{(0),\alpha} + u^\alpha_{(0),z} \right\rangle_{,\alpha} + 2[\![u^z_{(0),z}]\!] \ , \tag{4.16}$$

and the in-plane equations, Eq. (3.158a), are:

$$0 = \lambda^{\text{eff}}_{(0),\beta} a^{\alpha\beta} + \frac{\text{SL}}{\Gamma} v^\alpha_{(0),\beta\beta} + \text{Ca}\Big( [\![u^z_{(0),\alpha} + u^\alpha_{(0),z}]\!] - \ell \left\langle p_{(0)} \right\rangle_{,\beta} a^{\alpha\beta} \Big) \ , \tag{4.17}$$

where we employ the membrane continuity, Eq. (3.158c) to simplify the result. The bulk base state continuity equation reads:

$$u^i_{(0),i} = 0 \ , \tag{4.18}$$

and the Stokes equations are,

$$0 = -p_{(0),i} + (u^i_{(0),jj}) \ . \tag{4.19}$$

Eqs. (4.15)-(4.19) represent the general unperturbed equations for planar geometry. We will now consider small perturbations around this base state.

### 4.2.2 The general perturbed equations

Now, let us consider the general perturbed equations. Due to thermal fluctuations, the membrane shape undulates and experiences shape deformations. In this case, we express the mid-surface in terms of a height field quantifying displacement from $z = 0$:

$$\boldsymbol{x}^{\text{mid}} = \boldsymbol{x}^{\text{mid}}_{(0)} + \epsilon h(x, y, t) \boldsymbol{e}_z \ , \tag{4.20}$$

where $\epsilon \ll 1$ is the perturbation parameter. To first order in $\epsilon$, Eq. (4.4) is now

$$\begin{aligned} &\boldsymbol{a}_\alpha = \boldsymbol{e}_\alpha + \epsilon \ h_{,\alpha} \boldsymbol{e}_z \ , \quad a_{\alpha\beta} = \delta_{\alpha\beta} \ , \quad a^{\alpha\beta} = \delta^{\alpha\beta} \ , \quad \boldsymbol{n} = \boldsymbol{e}_z - \epsilon h_{,\alpha} \boldsymbol{e}_\alpha \ , \\ &b_{\alpha\beta} = \epsilon h_{,\alpha\beta} \ , \quad H = \epsilon \frac{1}{2} \Delta_s h \ , \quad K = 0 \ , \quad \text{and} \quad {}^0\Gamma^\alpha_{\lambda\mu} = 0 \ . \end{aligned} \tag{4.21}$$

The membrane velocity and effective surface tension become:

$$v^\alpha = v^\alpha_{(0)} + \epsilon v^\alpha_{(1)} \ , \quad v = \frac{d}{dt} \boldsymbol{x}^{\text{mid}} \cdot \boldsymbol{n} = \epsilon h_{,t} \ , \quad \lambda^{\text{eff}} = \lambda^{\text{eff}}_{(0)} + \epsilon \lambda^{\text{eff}}_{(1)} \ . \tag{4.22}$$

Similarly, we have for the bulk velocities:

$$\boldsymbol{u} = \sum_{\{x,y,z\}} \left( u^i_{(0)} + \epsilon u^i_{(1)} \right) \boldsymbol{e}_i \ . \tag{4.23}$$

The $\mathcal{O}(\epsilon)$ membrane continuity equation becomes:

$$v^\alpha_{(1),\alpha} = 0 \ . \tag{4.24}$$

In order to evaluate the contributions from applied tractions, we calculate the following:

$$\boldsymbol{e}_i \cdot \boldsymbol{a}_\alpha = \delta_{i\alpha} + \epsilon h_{,\alpha}\delta_{iz} \ , \tag{4.25}$$

$$\boldsymbol{e}_i \cdot \boldsymbol{n} = \delta_{iz} - \epsilon h_{,\alpha}\delta_{i\alpha} \ . \tag{4.26}$$

We then find the in-plane components up to linear order in $\epsilon$ to be:

$$\begin{aligned} t^\alpha_\pm &= t^\alpha_{(0)\pm} \pm \epsilon \left( u^z_{(1),\alpha} + u^\alpha_{(1),z} + 2h_{,\alpha} u^z_{(0),z} - h_{,\beta}(u^\beta_{(0),\alpha} + u^\alpha_{(0),\beta}) \right) \\ t^\alpha_\pm &= t^\alpha_{(0),\pm} + \epsilon t^\alpha_{(1),\pm} \ , \end{aligned} \tag{4.27}$$

and the normal components up to the same order are:

$$\begin{aligned} t^n_\pm &= t^n_{(0),\pm} + \epsilon \left( 2u^z_{(1),z} - 2h_{,\alpha}(u^\alpha_{(1),z} + u^z_{(1),\alpha}) - p_{(1)} \right) \ , \\ t^n_\pm &= t^n_{(0),\pm} + \epsilon t^n_{(1),\pm} \ . \end{aligned} \tag{4.28}$$

We can then find the jumps and averages of the perturbed surface traction components:

$$[\![ t^\alpha_{(1)} ]\!] = 2 \left( \left\langle u^z_{(1),\alpha} \right\rangle + \left\langle u^\alpha_{(1),z} \right\rangle + 2h_{,\alpha} \left\langle u^z_{(0),z} \right\rangle - h_{,\beta} \left\langle u^\beta_{(0),\alpha} + u^\alpha_{(0),\beta} \right\rangle \right) \ , \tag{4.29}$$

$$2 \left\langle t^\alpha_{(1)} \right\rangle = \left( [\![ u^z_{(1),\alpha} ]\!] + [\![ u^\alpha_{(1),z} ]\!] + 2h_{,\alpha} [\![ u^z_{(0),z} ]\!] - h_{,\beta} [\![ u^\beta_{(0),\alpha} + u^\alpha_{(0),\beta} ]\!] \right) \ , \tag{4.30}$$

$$[\![ t^n_{(1)} ]\!] = \left( 2[\![ u^z_{(1),z} ]\!] - 2h_{,\alpha} [\![ u^\alpha_{(1),z} + u^z_{(1),\alpha} ]\!] - [\![ p_{(1)} ]\!] \right) \ , \tag{4.31}$$

$$\left\langle t^n_{(1)} \right\rangle = \left( 2 \left\langle u^z_{(1),z} \right\rangle - 2h_{,\alpha} \left\langle u^\alpha_{(0),z} + u^z_{(0),\alpha} \right\rangle - \left\langle p_{(1)} \right\rangle \right) \ . \tag{4.32}$$

Now, the $\mathcal{O}(\epsilon)$ equations for Eqs. (4.2a) and (4.2b) become, respectively:

$$\begin{aligned} 0 =& \lambda^{\text{eff}}_{(1),\alpha} + \frac{\text{SL}}{\Gamma} v^\alpha_{(1),\beta\beta} + \text{Ca} \Big( \delta \Big( h_{,\alpha\lambda} - \delta^\alpha_\lambda \Delta_s h \Big) \left\langle u^z_{(0),\lambda} + u^\lambda_{(0),z} \right\rangle - \ell \left\langle p_{(1)} \right\rangle^{,\alpha} \Big) \\ &+ \Big( [\![ u^z_{(1),\alpha} ]\!] + [\![ u^\alpha_{(1),z} ]\!] + 2h_{,\alpha} [\![ u^z_{(0),z} ]\!] - h_{,\beta} [\![ u^\beta_{(0),\alpha} + u^\alpha_{(0),\beta} ]\!] \Big) \end{aligned} \tag{4.33}$$

and

$$\begin{aligned} 0 =& \Delta_s h \left( \lambda^{\text{eff}}_{(0)} + \ell \text{Ca} \left\langle u^z_{(0),z} \right\rangle \right) - \frac{1}{2\Gamma} \Delta_s^2 h + \frac{\text{SL}}{\Gamma} h_{,\alpha\beta} \left( v^\alpha_{(0),\beta} + v^\beta_{(0),\alpha} \right) + \text{Ca} \big( - [\![ p_{(1)} ]\!] \\ &+ \ell \Big( \left\langle u^z_{(1),\alpha} \right\rangle_{,\alpha} + \left\langle u^\alpha_{(1),z} \right\rangle_{,\alpha} + 2h_{,\alpha\alpha} \left\langle u^z_{(0),z} \right\rangle + 2h_{,\alpha} \left\langle u^z_{(0),z} \right\rangle_{,\alpha} \\ &- h_{,\beta\alpha} \left\langle u^\beta_{(0),\alpha} + u^\alpha_{(0),\beta} \right\rangle - h_{,\beta} \left\langle u^\beta_{(0),\alpha} + u^\alpha_{(0),\beta} \right\rangle_{,\alpha} \Big) \\ &+ \left( 2[\![ u^z_{(1),z} ]\!] - 2h_{,\alpha} [\![ u^\alpha_{(0),z} + u^z_{(0),\alpha} ]\!] \right) \ . \end{aligned} \tag{4.34}$$

In the subsequent sections, we will use these equations to analyze the fluctuations of a membrane immersed in an initially quiescent, infinite medium.

## 4.3 Membrane immersed in an infinite medium

We study the dynamics of finite thickness lipid bilayers by considering an initially flat membrane immersed in a quiescent viscous fluid. The membrane experiences thermal fluctuations that lead to shape perturbations that we express in the Monge gauge $h\,(x, y, t)$ [84] (see Sec. 4.2, as shown in Fig. 4.1. In order to characterize these dynamics, we first state the base state solution. We then proceed to solve the perturbed equations specialized from the results in Sec. 4.2. Finally we analyze the results and compare to other finite thickness theories.

### 4.3.1 Problem solution

First, the base state results are written down. Then, the perturbed equations from the previous section are written in nondimensional form (see Sec. 4.1), and are solved using proper no-slip boundary conditions at the membrane-fluid interfaces and far-field conditions for the perturbations.

### 4.3.2 Membrane Parametrization and Base State

As in Sec. 4.2.1, we describe the membrane mid-surface position Cartesian coordinates where we write (as in Eq. (4.3)):

$$\boldsymbol{x}_0 = \boldsymbol{x}_{(0)} = x\boldsymbol{e}_x + y\boldsymbol{e}_y, \tag{4.35}$$

On average, the membrane remains flat and the surrounding fluid is stagnant, hence choosing that the mid-surface coincides with $z = 0$. Given this assumption and Eqs. (4.16) and (4.17), the 'base' state conditions for the velocities $\left(\boldsymbol{u}_{(0)}, \boldsymbol{v}_{(0)}\right)$, the bulk fluid pressure $p$, and the membrane tension $\lambda$ read:

$$\boldsymbol{u}_{(0)} = 0, \quad \boldsymbol{v}_{(0)} = 0, \quad p_{(0)} = 0, \quad \lambda^{\text{eff}}_{(0)} = 1\ , \tag{4.36}$$

Without loss of generality, we choose to set $p$ to zero (datum value), while the membrane tension for a homogeneous membrane is assumed to be constant, $\lambda^{\text{eff}}_{(0)} = 1$[1]. Though in Sec. 4.2.2 we associated perturbed quantities with the script (1), we will forgo this notation in the following section because the base state is trivial and most quantities are zero. Thus, we avoid cumbersome notation given that it is not necessary here.

### 4.3.3 Perturbation expansion and Linearized Equations

Under the Monge gauge [84], the membrane mid-surface position including shape fluctuations reads:

$$\boldsymbol{x} = \boldsymbol{x}_{(0)} + \epsilon h(x, y, t)\boldsymbol{e}_z\ , \tag{4.37}$$

[1]The constant value is taken to be some $\lambda_0$, by which the effective tension is nondimensionalized.

where $\boldsymbol{x}_0 = x\boldsymbol{e}_x + y\boldsymbol{e}_y$ and $h(x, y, t)$ is the mid-surface height field encoding deviations away from the base state. We require that $\epsilon \ll 1$ so that the fluctuations have small magnitude. Under this decomposition, the membrane normal becomes:

$$\boldsymbol{n} = \boldsymbol{e}_z - \epsilon \left(h_{,x}\boldsymbol{e}_x + h_{,y}\boldsymbol{e}_y\right) \equiv \boldsymbol{n}_0 + \epsilon \boldsymbol{n}_1 \ , \tag{4.38}$$

where $\boldsymbol{n}_0 \equiv \boldsymbol{e}_z$ and $\boldsymbol{n}_1 = -h_{,x}\boldsymbol{e}_x - h_{,y}\boldsymbol{e}_y$. We note this is the result we found in Sec. 4.2.2. As before, the velocity at the membrane mid-surface is:

$$\boldsymbol{v} \cdot \boldsymbol{n} = \epsilon h_{,t} \ , \tag{4.39a}$$

$$\boldsymbol{v} \cdot \boldsymbol{a}^\alpha = \epsilon v^\alpha \ , \tag{4.39b}$$

where Eq. (4.39a) and Eq. (4.39b) correspond to the normal and in-plane velocities, respectively.

The form of Eq. (4.37) motivates us to perform a perturbation expansion for the unknowns in terms of $\epsilon$, which up to $O(\epsilon)$ yields:

$$\boldsymbol{u}_\pm = \boldsymbol{u}_{\pm,(0)} + \epsilon \boldsymbol{u}_{\pm,(1)} = \epsilon \boldsymbol{u} \ , \tag{4.40a}$$

$$p_\pm = p_{\pm,(0)} + \epsilon p_{\pm,(1)} = \epsilon p_\pm \ , \tag{4.40b}$$

$$\boldsymbol{v} = \boldsymbol{v}_{(0)} + \epsilon \boldsymbol{v}_{(1)} = \epsilon \boldsymbol{v} \ , \tag{4.40c}$$

$$\lambda^{\text{eff}} = \lambda^{\text{eff}}_{(0)} + \epsilon \lambda^{\text{eff}}_{(1)} = 1 + \epsilon \lambda^{\text{eff}} \ , \tag{4.40d}$$

where we have omitted the (1) subscript since nearly all base state quantities are zero. Figure 4.1 shows a schematic representation of the membrane before and after fluctuations are considered. From hereon and for the ease of notation, we drop the subscript from all quantities of $O(\epsilon)$.

After applying the perturbation expansions for the pressure and the bulk fluid velocities, Eqs. (4.40a) and (4.40b), the $\mathcal{O}(\epsilon)$ bulk Stokes and continuity equations read:

$$0 = -p_{\pm,i} + u^i_{\pm,jj} \ , \tag{4.41a}$$

$$0 = u^i_{\pm,i} \ . \tag{4.41b}$$

Similarly for the membrane equations, we substitute Eqs. (4.40c) and (4.40d) into , which to $O(\epsilon)$ gives the following equations:

$$0 = \lambda^{\text{eff}}_{,\alpha} + \frac{SL}{\Gamma}\Delta_s v^\alpha + \text{Ca}\left(\left[\!\left[u^\alpha_{,z} + u^z_{,\alpha}\right]\!\right] - \ell \left\langle p \right\rangle_{,\alpha}\right) \ , \tag{4.42a}$$

$$0 = \Delta_s h - \frac{1}{2\Gamma}\Delta_s^2 h + \text{Ca}\left(\frac{1}{2}\ell \left\langle u^\alpha_{,z\alpha} + u^z_{,\alpha\alpha} \right\rangle - \left[\!\left[p\right]\!\right] + 2\left[\!\left[u^z_{,z}\right]\!\right]\right) \ , \tag{4.42b}$$

$$0 = v^\alpha_{,\alpha} \ , \tag{4.42c}$$

where for our parametrization $\Delta_s \equiv \partial_x^2 + \partial_y^2$, and we used that $2H \simeq \Delta_s h$.

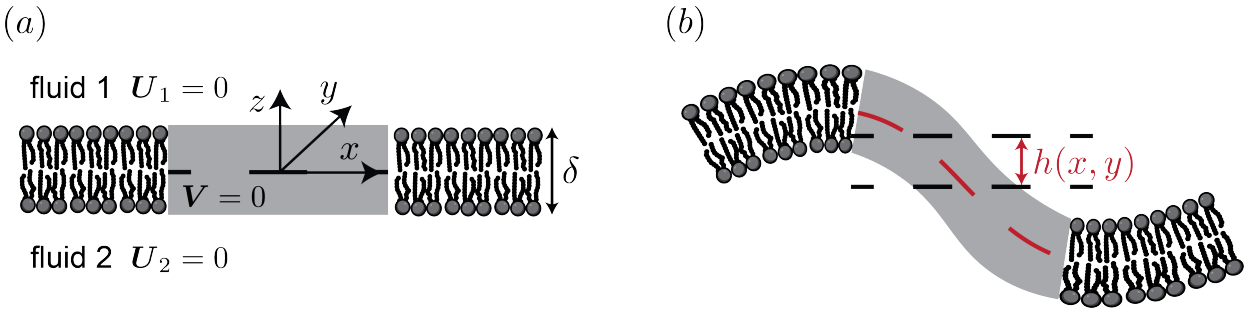


Figure 4.1: Schematic of the perturbation scheme. (a) The unperturbed membrane state. (b) The perturbed state with height field $h(x, y)$.

We use the method of domain perturbations to extrapolate the quantities evaluated at $z = \pm\ell/2 + \epsilon h$ in terms of $z = \pm\ell/2$. In particular, the velocities and pressure become:

$$u^i_\pm = u^i_\pm\Big|_{z=\pm\ell/2} + \left(\frac{\partial u^i_\pm}{\partial z}\right)_{z=\ell/2} \epsilon h + O(\epsilon^2) \ , \tag{4.43a}$$

$$p_\pm = p_\pm\Big|_{z=\pm\ell/2} + \left(\frac{\partial p_\pm}{\partial z}\right)_{z=\pm\ell/2} \epsilon h + O(\epsilon^2) \ , \tag{4.43b}$$

where after substituting the perturbation expansion, we find that only the bare quantities remain.

### 4.3.4 Linear response solution for finite thickness membranes

To proceed with the solution of Eqs. (4.41a), (4.41b) and (4.42a) to (4.42c), we exploit translation invariance of the linear operators in the $x$ and $y$ directions and decompose the unknowns into plane waves as:

$$\boldsymbol{u}_\pm(x, y, z, t) = \sum_q \boldsymbol{u}_{\boldsymbol{q}\pm}(z) e^{i\boldsymbol{q}\cdot\boldsymbol{x}+\omega t} \ , \tag{4.44a}$$

$$p_\pm(x, y, z, t) = \sum_q p_{\boldsymbol{q}\pm}(z) e^{i\boldsymbol{q}\cdot\boldsymbol{x}+\omega t} \ , \tag{4.44b}$$

$$\boldsymbol{v}(x, y, t) = \sum_q \boldsymbol{v}_{\boldsymbol{q}} e^{i\boldsymbol{q}\cdot\boldsymbol{x}+\omega t} \ , \tag{4.44c}$$

$$\lambda^{\text{eff}}(x, y, t) = \sum_q \lambda^{\text{eff}}_{\boldsymbol{q}} e^{i\boldsymbol{q}\cdot\boldsymbol{x}+\omega t} \ , \tag{4.44d}$$

$$h(x, y, t) = \sum_q h_{\boldsymbol{q}} e^{i\boldsymbol{q}\cdot\boldsymbol{x}+\omega t} \ , \tag{4.44e}$$

where $\boldsymbol{q} \cdot \boldsymbol{x} \equiv q_x x + q_y y$. Using the ansatz of Eq. (4.44) in the bulk equations yields the following equations for the bulk fluid unknown coefficients:

$$0 = \; - iq_\alpha p_{\boldsymbol{q}\pm} + (\partial_z^2 - q^2) u^\alpha_{\boldsymbol{q}\pm} \; , \tag{4.45a}$$

$$0 = \; - \partial_z p_{\boldsymbol{q}\pm} + (\partial_z^2 - q^2) u^z_{\boldsymbol{q}\pm} \; , \tag{4.45b}$$

$$0 = \; \partial_z u^z_{\boldsymbol{q}\pm} + iq_\alpha u^\alpha_{\boldsymbol{q}\pm} \; , \tag{4.45c}$$

where $q^2 \equiv q_x^2 + q_y^2$. Similarly, the membrane equations Eqs. (4.42a) to (4.42c) become:

$$0 = iq_\alpha \lambda^{\text{eff}}_{\boldsymbol{q}} - q^2 \frac{SL}{\Gamma} v^\alpha_{\boldsymbol{q}} + \text{Ca} \left( [\![ u^\alpha_{\boldsymbol{q},z} + iq_\alpha u^z_{\boldsymbol{q}} ]\!] - iq_\alpha \ell \, \langle p \rangle \right) \; , \tag{4.46a}$$

$$0 = q^2 h_{\boldsymbol{q}} + \frac{1}{2\Gamma} q^4 h_{\boldsymbol{q}} - \text{Ca} \left( \frac{1}{2} \ell \left\langle iq_\alpha u^\alpha_{\boldsymbol{q},z} - q^2 u^z_{\boldsymbol{q}} \right\rangle - [\![ p_{\boldsymbol{q}} ]\!] + 2 [\![ u^z_{\boldsymbol{q},z} ]\!] \right) \; , \tag{4.46b}$$

$$0 = iq_\alpha v^\alpha_{\boldsymbol{q}} \; . \tag{4.46c}$$

We now proceed with the general solution for the bulk fluid unknowns.

We start by multiplying the in-plane equations Eq. (4.45a) by $iq_\alpha$ and subsequently substituting $iq_\alpha u^\alpha_{\boldsymbol{q}\pm}$ via Eq. (4.45c) to arrive at the following relation between the bulk pressure and $z$-velocity:

$$0 = q^2 p_{\boldsymbol{q}\pm} - (\partial_z^2 - q^2) \partial_z u^z_{\boldsymbol{q}\pm} \; . \tag{4.47}$$

We then derive a pressure equation by first differentiating Eq. (4.45b) with respect to $z$ and then substituting Eq. (4.47), resulting in:

$$\partial_z^2 p_{\boldsymbol{q}\pm} - q^2 p_{\boldsymbol{q}\pm} = 0 \; , \tag{4.48}$$

whose solution is:

$$p_{\boldsymbol{q}\pm} = P_\pm e^{\mp qz} \; , \tag{4.49}$$

in which we have used the condition Eq. (3.160b). The pressure solution of Eq. (4.49) is then introduced into the momentum equations Eqs. (4.45a) and (4.45b), from which the velocity solutions are found:

$$u^z_{\boldsymbol{q}\pm} = \left( U_\pm + P_\pm \frac{z}{2} \right) e^{q\mp z} \; , \tag{4.50a}$$

$$u^\alpha_{\boldsymbol{q}\pm} = \left( V^\alpha_\pm \mp P_\pm \frac{q_\alpha z}{2q} \right) e^{q\mp z} \; , \tag{4.50b}$$

where we have used the condition Eq. (3.160a). We now turn our attention to the coupling conditions at the membrane boundaries to determine the undetermined coefficients $(U_\pm, P_\pm)$.

Using the bulk solutions Eqs. (4.49), (4.50a) and (4.50b) in the no-slip conditions Eqs. (3.161a) and (3.161b), we obtain:

$$\left( U_\pm \pm P_\pm \frac{\ell}{4} \right) e^{-q\ell/2} = \omega h_{\boldsymbol{q}} \; , \tag{4.51a}$$

$$\left( V^\alpha_\pm - P_\pm \frac{q_\alpha \ell}{4q} \right) e^{-q\ell/2} = v^\alpha_{\boldsymbol{q}} \mp iq_\alpha \omega \frac{\ell}{2} h_{\boldsymbol{q}} \; , \tag{4.51b}$$

where we have used the results Eq. (4.39). Combining the in-plane conditions Eq. (4.51b) with the bulk continuity equation Eq. (4.45c) and Eq. (4.50a), we find

$$\frac{1}{4}e^{-q\ell/2}\left(4qU_{\pm} \pm P_{\pm}(q\ell - 2)\right) = \frac{\ell}{2}q^2\omega h_{\boldsymbol{q}} \ . \tag{4.52}$$

We then use Eqs. (4.51a) and (4.52) to eliminate $U_{\pm}$ and find the following:

$$\frac{q\ell - 2}{4q}(P_+ + P_-) + \frac{\ell}{2}(P_+ + P_-) = 0 \ , \tag{4.53}$$

implying that for arbitrary $q$:

$$P_+ = -P_- = P \ . \tag{4.54}$$

Plugging this result back into the $z-$velocity conditions Eqs. (4.51a) and (4.52), we solve for the pressure coefficient as:

$$P = \omega h_{\boldsymbol{q}} q\left(2 - \ell q\right)e^{q\ell/2} \ . \tag{4.55}$$

Substitution of Eq. (4.55) in Eqs. (4.51a) and (4.52) allows us to solve for the $z-$direction velocity coefficients:

$$U_+ = U_- = \frac{1}{4}\omega h_{\boldsymbol{q}}\left(4 + q\ell(q\ell - 2)\right)e^{q\ell/2} \ . \tag{4.56}$$

We now turn our attention to the in-plane equations, Eq. (4.46a). Using the results of Eqs. (4.51a), (4.51b) and (4.55), they become:

$$0 = iq_\alpha\lambda^{\text{eff}}_{\boldsymbol{q}} - q\left(\frac{SL}{\Gamma}q + 2\text{Ca}\right)v^\alpha_{\boldsymbol{q}} \ . \tag{4.57}$$

Along with the membrane continuity equation Eq. (4.46c), Eq. (4.57) implies that for arbitrary wavevectors:

$$v^\alpha_{\boldsymbol{q}} = 0 \ , \tag{4.58}$$

$$\lambda^{\text{eff}}_{\boldsymbol{q}} = 0 \ . \tag{4.59}$$

Equations (4.55) and (4.58) are then plugged into Eq. (4.51b), and the result is used to solve for the bulk $x-$ and $y-$velocity coefficients:

$$V^\alpha_+ = -V^\alpha_- = -\frac{1}{4}i\omega\ell^2 h_{\boldsymbol{q}} q q_\alpha e^{q\ell/2} \ . \tag{4.60}$$

Finally, we use Eqs. (4.55), (4.56) and (4.60) in Eq. (4.46b) to find the following expression for the dispersion $\omega$:

$$\omega = -\frac{\frac{1}{2}q^4 + \Gamma q^2}{\text{Ca}\Gamma q\left(4 + q^2\ell^2\right)} \ . \tag{4.61}$$

The non-zero real-space solutions are summarized:

$$u^z_\pm(x,y,z,t) = \frac{1}{4}\sum_q \omega h_{\boldsymbol{q}} \left(4 + q(\ell \mp 2z)(q\ell - 2)\right) e^{q\left(\frac{\ell}{2}\mp z\right)} e^{(i\boldsymbol{q}\cdot\boldsymbol{x}+\omega t)} \ , \tag{4.62}$$

$$u^\alpha_\pm(x,y,z,t) = \frac{1}{4}\sum_q \omega h_{\boldsymbol{q}} i q_\alpha \left(2z(q\ell - 2) \mp q\ell^2\right) e^{q\left(\frac{\ell}{2}\mp z\right)} e^{(i\boldsymbol{q}\cdot\boldsymbol{x}+\omega t)} \ , \tag{4.63}$$

$$p_\pm(x,y,z,t) = \pm\sum_q \omega h_{\boldsymbol{q}} q \left(2 - q\ell\right) e^{q\left(\frac{\ell}{2}\mp z\right)} e^{(i\boldsymbol{q}\cdot\boldsymbol{x}+\omega t)} \ , \tag{4.64}$$

$$v^\alpha_m(x,y,z,t) = -z\sum_q \omega h_{\boldsymbol{q}} i q_\alpha e^{(i\boldsymbol{q}\cdot\boldsymbol{x}+\omega t)} \ , \tag{4.65}$$

$$v^z(x,y,t) = \sum_q \omega h_{\boldsymbol{q}} e^{(i\boldsymbol{q}\cdot\boldsymbol{x}+\omega t)} \ , \tag{4.66}$$

where $v^\alpha_m$ is the total in-plane membrane velocity, reconstructed using Eq. (3.57) and Eq. (2.55).

### 4.3.5 Dispersion relation and hydrodynamics

In this section, we analyze the linear response of a lipid bilayer membrane immersed in an incompressible, Newtonian fluid subject to shape fluctuations. We first investigate the dispersion relation, where we discuss the regimes characterized by membrane bending, tension, and finite thickness effects on the dynamics. Then, we proceed with understanding the flow fields resulting from applied membrane fluctuations. In particular, we consider the profiles at length scales both much greater and on the order of the membrane thickness, thereby showing the importance of its resolution on the relaxation of membrane itself.

#### 4.3.5.1 Dispersion relation

Motivated by experimental measurements and previous theoretical works [60, 77–79], we choose $L = 200$ nm, a base tension $\Lambda_0 = 10^{-3}$ pN $\cdot$ nm$^{-1}$, which corresponds to moderately tense lipid bilayers, and a bending rigidity $k_\mathrm{b} = 14.3$ k$_\mathrm{B}$T [85]. We take the bulk medium to be water, with viscosity $\mu^\mathrm{b} = 10^{-3}$ pN $\cdot$ nm$^{-2}$ $\cdot$ $\mu$s. Additionally, we choose the characteristic velocity scale $U = \Lambda_0/\mu^b$ such that Ca $= 1$ and take the membrane thickness to be 4 nm [1, 78]. This results in $\Gamma = 0.645$ and $\ell = 0.02$, and sets a characteristic timescale of $\tau = L\Lambda_0/\mu^b = 200$ $\mu$s, by which our dispersion relation is nondimensionalized, $\omega^* = L\Lambda_0\omega/\mu^b$. We further set Ca $= 1$ as it only rescales the value of $\omega(q)$.

Figure 4.2 shows $\omega$ vs. $q$, where we observe three different regimes. The long wavelength regime, for which $q \ll q_1$ and $q_1 \equiv \sqrt{2\Gamma}$, or on length-scales of $\mathcal{O}(10^2 - 10^3)$ nm, corresponds to the relaxation of tension modes. The next regime, marked by $q_1 \ll q \ll q_2$ and $q_2 \equiv 2/\ell$, refers to the relaxation of bending modes whose wavelengths typically typically on $\mathcal{O}(10 - 10^2)$ nm. The third, short wavelength regime, $q \gg q_2$, exhibits a transition from viscous dissipation through normal forces (e.g. pressure difference or $t^n_{visc}$ terms) to that

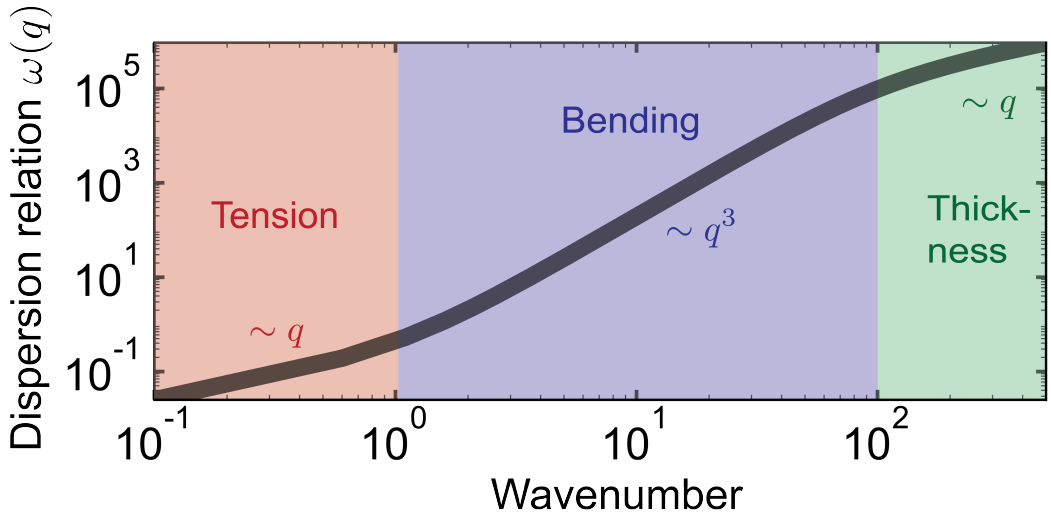


Figure 4.2: The dispersion relation for finite thickness, nearly flat membranes, as given by Eq. (4.61). The tension regime crosses over into bending at $q_1 = \sqrt{2\Gamma} = 0.645$ and the viscous crossover occurs at $q_2 = 2/\ell = 0.02$, where where $\Gamma = \Lambda_0 L^2/k_\mathrm{b}$ and $\ell = \delta/L$. We choose as physical parameters $L = 200$ nm, $k_\mathrm{b} = 62$ pN $\cdot$ nm, $\Lambda_0 = 10^{-3}$ pN $\cdot$ nm$^{-1}$, and $\delta = 4$ nm, and $\mu^\mathrm{b} = 10^{-3}$ pN $\cdot$ nm$^{-2}$ $\cdot$ $\mu$s [1, 78].

through in-plane forces (e.g. $t^\alpha_{visc}$ terms). Following [24], we express the dispersion relation as:

$$-\omega(q) \approx \begin{cases} \dfrac{q}{4}\,, & q \ll q_1 \\ \dfrac{1}{8\Gamma}q^3\,, & q_1 \ll q \ll q_2 \\ \dfrac{1}{\Gamma\ell^2}q\,, & q_2 \ll q \end{cases} \tag{4.67}$$

We find that both the large, $q \ll q_1$, and short, $q \gg q_2$, wavelength regimes scale linearly with $q$ but exhibit different slopes.

Membrane dynamics on nanometer lengthscales are often probed through density fluctuations via structure factor measurements [29, 30, 86–88]. Such analyses require a statistical description of membrane relaxation across a wide range of length-scales, including those at the membrane thickness. The dispersion relation $\omega(q)$ of Eq. (4.61) provides the connection between the current work and the statistics of membrane fluctuations, which can be experimentally studied via techniques such as neutron spin echo, dynamic light scattering, or flicker spectroscopy [77, 89, 90]. To link $\omega\,(q)$ with the dynamics of fluctuating membranes,

we express it as a ratio between conservative and dissipative parts as:

$$\omega(q) = \frac{-\kappa_{\boldsymbol{q}}^{\text{eff}}}{\zeta_{\boldsymbol{q}}^{\text{eff}}} = \frac{-\left(\frac{1}{2}q^4 + \Gamma q^2\right)}{\Gamma q\left(4 + q^2\ell^2\right)} \ , \tag{4.68}$$

where $\kappa_{\boldsymbol{q}}^{\text{eff}} \equiv q^4/2 + \Gamma q^2$ corresponds to the elastic response of the membrane due to out-of-plane bending, and $\zeta_{\boldsymbol{q}}^{\text{eff}} \equiv \Gamma q\left(4 + q^2\ell^2\right)$ describes all dissipative processes coming from both the bulk fluid and the in-plane fluidity. Using Eq. (4.68) and noting that $\partial_t h = \omega h$, we express the dynamic equation for each individual height mode $h_{\mathbf{q}}$ as:

$$0 = -\zeta_{\boldsymbol{q}}^{\text{eff}}\partial_t h_{\boldsymbol{q}} - \kappa_{\boldsymbol{q}}^{\text{eff}} h_{\boldsymbol{q}} + f_{\boldsymbol{q}}(t) \ , \tag{4.69}$$

where $f_{\mathbf{q}}(t)$ is a Gaussian distributed random force with $\langle f_{\mathbf{q}}(t)\rangle = 0$ and $\langle f_{\mathbf{q}}(t) f_{-\mathbf{q}}(t')\rangle = 2k_{\text{B}}T\zeta_{\boldsymbol{q}}^{\text{eff}}\delta(t-t')$ [91].

The form of Eq. (4.69) is that of an overdamped forced oscillator, with drag coefficient $\zeta_{\boldsymbol{q}}^{\text{eff}}$, spring constant $\kappa_{\boldsymbol{q}}^{\text{eff}}$, and forcing $f_{\boldsymbol{q}}(t)$. The crossover between the first two regimes at $q_1$ is interpreted as the change of the restorative force, from that of membrane tension to membrane bending. Consequently, at $q_2$ the dissipative force switches from a linear form to a cubic one, and corresponds to a change in the dissipation mechanism. For $\ell \to 0$, $\zeta_{\boldsymbol{q}}^{\text{eff}} \sim q$, which is the classical result of two-dimensional theories [91–93], while for $q \sim \ell^{-1}$ we find $\zeta_{\boldsymbol{q}}^{\text{eff}} \sim q^3$. While both effects emerge from hydrodynamic interactions between bulk fluid and the membrane [91, 94], the $q^3$ dependence originates from $\ell[\![t_{visc}^{\alpha}]\!]_{:\alpha}/2$, which is the torque that results due to differences in shear forces on the top and bottom boundaries of the membrane. This contribution is a characteristic result of the finite thickness nature of the membrane. Another way to interpret this analysis is that finite thickness modifies the Greens function that encodes the response membrane due to thermal fluctuations in an embedding viscous medium. To see this, we note that $1/\zeta_{\mathbf{q}} = 1/4\Gamma q$ when $\ell \to 0$, which corresponds to the Fourier transform of the Oseen's tensor in the equivalent two-dimensional problem [91, 92, 94]. A two-dimensional membrane may be considered as a collection of independent points, each of which experiences a drag from the bulk fluid as it relaxes from $z = h(x, y)$ back to $z = 0$. The finite-thickness membrane, by contrast, is effectively a collection of rods whose mid-point positions relative to $z = 0$ relax the same way the two-dimensional membrane does, but that also experience an additional drag as they rotate back to an aligned state. This additional effect is encoded in the $(q\ell)^2$ term in the denominator of $\omega(q)$, and becomes the relevant dissipative effect when $q > q_2$, as shown in Eq. (4.67).

#### 4.3.5.2 Induced flow fields for single modes

The observed transition for wavelengths $q > q_2$ of the damping behavior of $h_{\boldsymbol{q}}$ occurs independently of any parameter in our model other than the membrane thickness ratio $\ell$. To gain a deeper understanding of the emergent hydrodynamic phenomena, we analyze the induced flow fields for the limiting cases of $q \to 0$ and $q \sim \ell^{-1} > q_2$. Our primary goal is to identify and characterize the physical mechanisms responsible for the observed finite thickness effects on the hydrodynamics of the membrane and bulk fluid.

We specialize our solutions of Eqs. (4.62) to (4.66) to that of a single mode $q^*$ so as to understand the response of the system to single-mode fluctuations. In particular, we choose the initial height perturbation as:

$$h(x, y, z, 0) = h_0 \sin(q^* x) \ , \tag{4.70}$$

where we let $h_0 = 10^{-2}\ell$. The Fourier transform of Eq. (4.70) leads to the following form of $\hat{h}$:

$$\hat{h} = h_0 \frac{1}{2i} \left(\delta(q_x - q^*) + \delta(q_x + q^*)\right) \delta(q_y) \ . \tag{4.71}$$

Substituting this result into Eqs. (4.62) to (4.66) results in:

$$u^z_\pm(x, y, z, t) = \frac{1}{4}\omega h_0 \left(4 + q^*(\ell \mp 2z)(q^*\ell - 2)\right) e^{q^*\left(\frac{\ell}{2} \mp z\right)} e^{\omega t} \sin(q^* x) \ , \tag{4.72}$$

$$u^\alpha_\pm(x, y, z, t) = \frac{1}{4}\omega h_0 q^* \left(2z(q^*\ell - 2) \mp q^*\ell^2\right) e^{q^*\left(\frac{\ell}{2} \mp z\right)} e^{\omega t} \cos(q^* x) \ , \tag{4.73}$$

$$p_\pm(x, y, z, t) = \pm\omega h_0 q^* \left(2 - q^*\ell\right) e^{q^*\left(\frac{\ell}{2} \mp z\right)} e^{\omega t} \sin(q^* x) \ , \tag{4.74}$$

$$v^\alpha_m(x, y, z, t) = -z\omega h_0 q^* e^{\omega t} \cos(q^* x) \ , \tag{4.75}$$

$$v^z(x, y, t) = \omega h_0 e^{\omega t} \sin(q^* x) \ , \tag{4.76}$$

which are the fields given an applied perturbation of the form Eq. (4.70). With Eqs. (4.72) to (4.76), we are now in position to study the hydrodynamic response of the membrane and the bulk fluid for the two limiting cases, $q \ll q_2$ and $q \sim q_2$

#### 4.3.5.3 Flows in the tension and bending regimes

Here, we present the flow field solutions for two different modes, corresponding to the tension and bending regimes, using the same physical parameters as were chosen for the dispersion relation in Fig. 4.2. For these parameter values, the crossover from tension to bending modes occurs at $q_1 = 1.136$. Since the time dependence is purely exponential, we focus again on the flows at $t = 0$, as they qualitatively remain the same but decrease in magnitude over time. We illustrate the velocity flow fields for $\ell = 0.02$ (the $(2 + \delta)$-dimensional case) and $\ell = 0$ (the $2d$ case) for modes $q = 0.3 < q_1$ and $q = 30.0 < q_2$ in Figure 4.3, utilizing the equations solutions provided by equations Eqs. (4.72) to (4.76).

Figure 4.3 shows that the dominant motion at the membrane surfaces occurs in the normal direction regardless of inclusion of thickness or not at both $q = 0.3$ and $q = 30.0$. The flow is maximum at the height extrema and minimum where the membrane is stationary, i.e. $h = 0$. Given the initial perturbation Eq. (4.70), the flow maxima occur at $x = (2n + 1)\pi/2q$ where $n \in \mathbb{Z}$ when $h = \pm h_0$. Minima in the initial perturbation ($h = -h_0$) push and drag bulk fluid in the positive $z-$direction, while maxima ($h = h_0$) do so in the opposite direction. This is marked by pressure maxima and minima occurring at the height field crests and troughs, respectively. In the tension regime, pressure builds up at the height field troughs monotonically, as shown in Fig. 4.4, where we plot Eq. (4.64) at $(x = 3\pi/2q, z = \ell/2)$ as

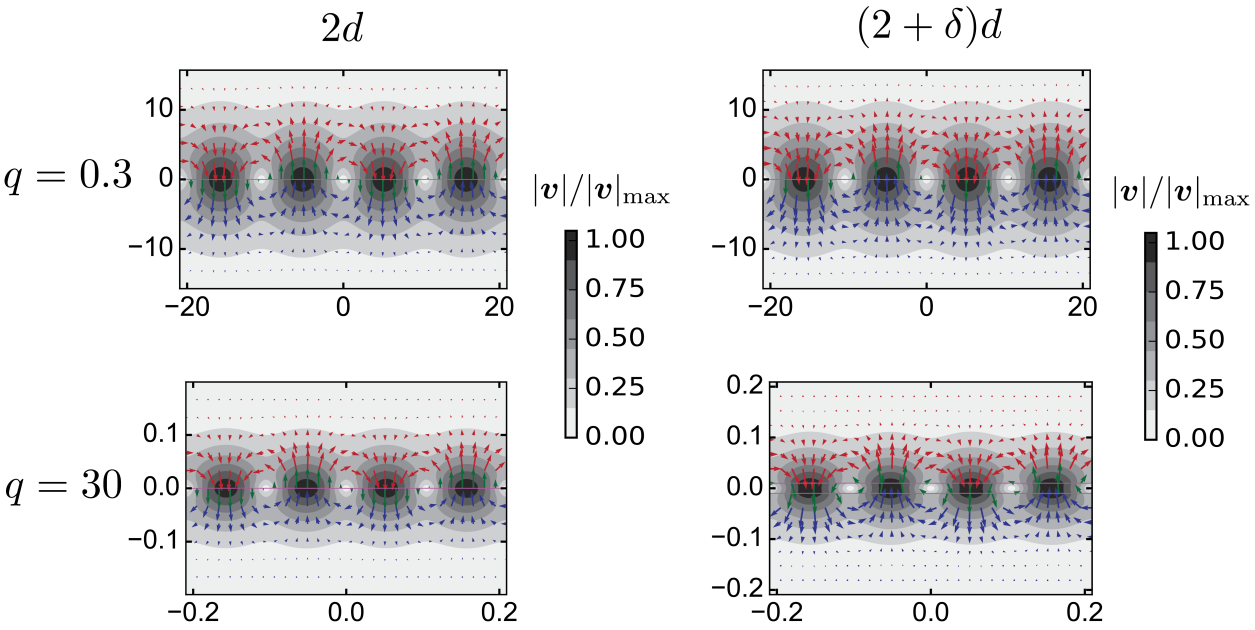


Figure 4.3: The normalized flow fields in the tension ($q = 0.3$) and bending ($q = 30$) regimes. In every case, the predominant surface motion is in the normal, or $z-$, direction. The flow patterns exhibit little difference, with circulations occuring about the membrane. Though the membrane thickness becomes "visible" for $q = 30$, it does not affect the induced hydrodynamics at this wavenumber.

a function of wavenumber. Due to incomprehensibility in the bulk fluids, vortices develop about the membrane, as fluid flows from pressure maximum sources to pressure minimum sinks. In this regime, the perturbations decay spatially on $\mathcal{O}(10L)$.

As we increase the perturbation frequency to the second regime where $q_1 < q^* < q_2$, we find that the flow distributions qualitatively remain similar to the tension regime. The flow patterns remain the same, but the spatial decay length decreases significantly to be of $O(0.1L)$. This reduction in decay length corresponds to the transition from the relaxation of tension to bending modes. However, as noted in Sec. 4.3.5.1, the effects of thickness on the viscous dissipation are still not apparent from the flow fields in this regime.

We gain further insight into the induced hydrodynamics by again considering the surface pressure at at the trough at $(x = 3\pi/2q, z = \ell/2)$, as shown in in Fig. 4.4. Though at lower wavenumbers in the bending regime, the pressure at this trough in the $2d$ and $(2+\delta)d$ theories match, they diverge as the perturbation frequency increases. This is a direct result of the incorporation of thickness effects, which are observed to regulate the pressure at the membrane surfaces. As in-plane surface motion due to lipid reorientations begins to dominate the normal motion due to height field relaxation, the pressure experiences an inversion. This

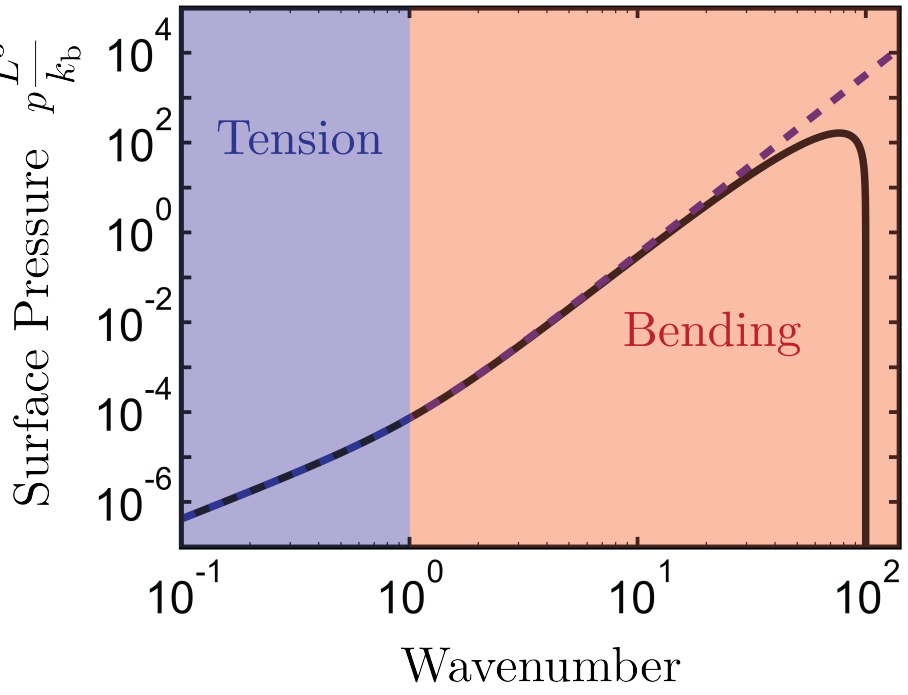


Figure 4.4: The maximum pressure per wavenumber $q$ for the (a) tension and (b) bending regimes. Pressure build up occurs predominantly due to bending fluctuations, indicating high-frequency modes lead to stronger circulations.

marks flow reversal and bulk fluid ciriculations, as shown in the following section.

#### 4.3.5.4 Flows in the thickness regime

In order to discuss the hydrodynamic response in the "thickness" regime, we show in Fig. 4.5 the flow fields for $q = 300$. We note here that the qualitative nature of the $2d$ membrane flow fields does not change with increasing wavenumber. The only change is that the flows decay increasingly closer to the membrane, with decay occurring at $\mathcal{O}(0.02L)$ for $q = 300$. However, the finite thickness membrane shows a qualitatively different flow due to thickness effects. We observe vortices to appear in the vicinity of the membrane. This is marked by the phenomena of pressure inversion at the membrane surface (see Fig. 4.4) and the flow reversal, which we further analyze in the following section.

#### 4.3.5.5 The emergence of flow reversal

Thickness effects lead to the emergence of flow reversal and pressure inversion for high wavenumber modes. These phenomena are accompanied by the emergence of stagnation

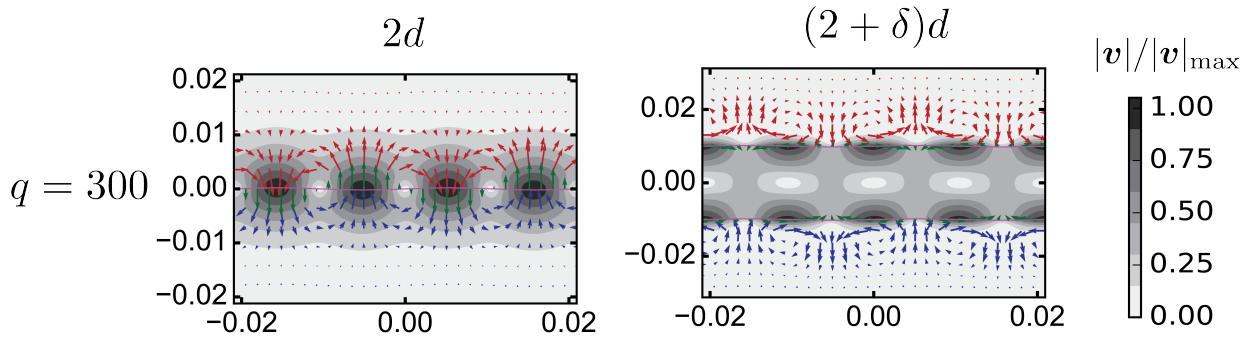


Figure 4.5: The normalized flow fields for $\ell = 0$ and $\ell = 0.02$ at $q = 300$.

points. We focus on the bulk flows of the upper half-plane, or for $z > 0$. We note that due to the periodic nature of the perturbation, it is sufficient to focus on two representative stagnation points. To that end, we set Eq. (4.72) and Eq. (4.73) to zero to find the following set of points:

$$(x,z)_{\text{ext}} = \left(\frac{\pi}{2q},\ \frac{\ell}{2} + \frac{2}{q\,(\ell q - 2)}\right) \tag{4.77}$$

$$(x,z)_{\text{vortex}} = \left(\frac{\pi}{q}, \frac{\ell}{2} + \frac{\ell}{\ell q - 2}\right)\ . \tag{4.78}$$

To understand the physics at these points, we find the strain rates as functions of wavenumber, which is evaluated as $\boldsymbol{D} = \frac{1}{2}(\nabla\,\boldsymbol{u} + \nabla\,\boldsymbol{u}^T)$. We find that at $(x,z)_{\text{vortex}}$, $\boldsymbol{D} = \boldsymbol{0}$, suggesting there is no strain at the vortex stagnation points. However, at $(x,z)_{\text{ext}}$, we have:

$$[\boldsymbol{D}]\Big|_{(x,z)_{\text{ext}}} = \begin{pmatrix} \frac{1}{2}\omega h_0 q(\ell q - 2)\exp\left(\frac{-2}{\ell q - 2}\right) & 0 \\ 0 & -\frac{1}{2}\omega h_0 q(\ell q - 2)\exp\left(\frac{-2}{\ell q - 2}\right) \end{pmatrix} = \begin{pmatrix} \dot{\epsilon} & 0 \\ 0 & -\dot{\epsilon} \end{pmatrix}\ , \tag{4.79}$$

which shows that these stagnation points are indeed marked by extentional flows.

To further understand the nature of the stagnation points, we consider the rotation rate, $\boldsymbol{W} = \frac{1}{2}(\nabla\,\boldsymbol{u} - \nabla\,\boldsymbol{u}^T)$ at each type of point. At the extensional points, we find $\boldsymbol{W} = \boldsymbol{0}$, confirming that there we have pure shear transformations due to hydrodynamic compressive

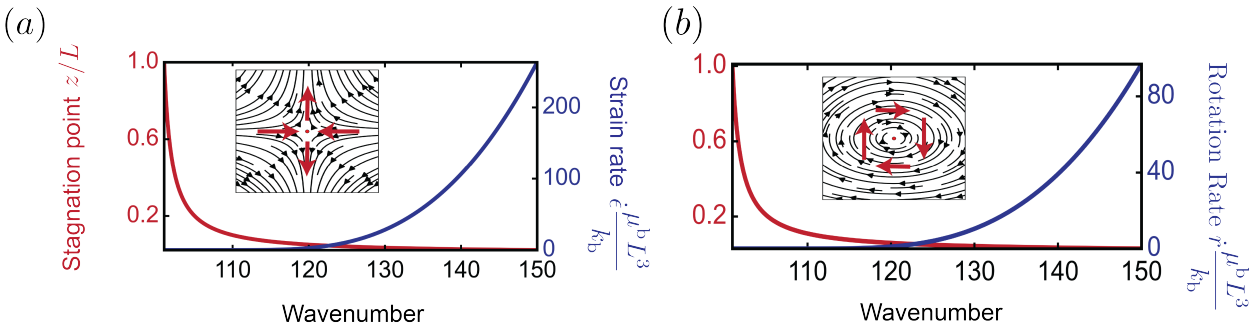


Figure 4.6: (a)– The position of and strain rate at the stagnation point with pure extensional flow. (b) – The position of and rotation rate at the stagnation point with pure circulatory flow. Both panels have insets with the streamlines about each respective stagnation point.

and expansive forces. At the vortex points, the rotation rate reads,

$$[\boldsymbol{W}]\Big|_{(x,z)_{\text{vortex}}} = \begin{pmatrix} 0 & -\frac{1}{4}\omega h_0 q(\ell q - 2)\exp\left(\frac{-2}{\ell q - 2}\right) \\ \frac{1}{4}\omega h_0 q(\ell q - 2)\exp\left(\frac{-2}{\ell q - 2}\right) & 0 \end{pmatrix} = \begin{pmatrix} 0 & -\dot{r} \\ \dot{r} & 0 \end{pmatrix} . \tag{4.80}$$

Because these points exhibit pure rotation and no elongation or shear, they do not contribute to viscous dissipation in the bulk.

The form of the strain in Eq. (4.79) suggests that material points at $(x, z)_{\text{ext}}$ undergo pure compressive stress while points under Eq. (4.80) experience equal and opposing stresses from either side and are simply rotated. To demonstrate these physics, we show in Fig. 4.6 (a) the strain rate as a function of wavenumber relative to the $z-$coordinate of the associated stagnation point.

The stagnation point locations shown by the red lines in Fig. 4.6 and given by Eqs. (4.77) to (4.78) begin infinitely far away from the membrane for $q = q_2 = \ell/2$, i.e. the $z-$coordinates diverge. However, as the wavenumber increases, the stagnation points move closer to the membrane surface. At the same time, the strain and rotation rates are initially close to zero but increase monotonically as the perturbation frequency increases.

Regarding the relevance of our analysis, we expect that our results have implications for biological processes such as mechanosensitive protein function and intercellular contact. For instance, it has recently been observed that increased thickness correlates with smaller membrane permeability to solute molecules [95]. Such observation might be explained due to local mixing induced by circulations caused by finite thickness effects that lead to smaller concentration gradients, and thus smaller permeation rates. Additionally, the predicted pressure inversion phenomenon at $\mathcal{O}$(nm) lengthscales, Fig. 4.4, can lead to hydrodynamic-related forces that might mediate intercellular contact and affect intermembrane junction fluctuations [22, 96].

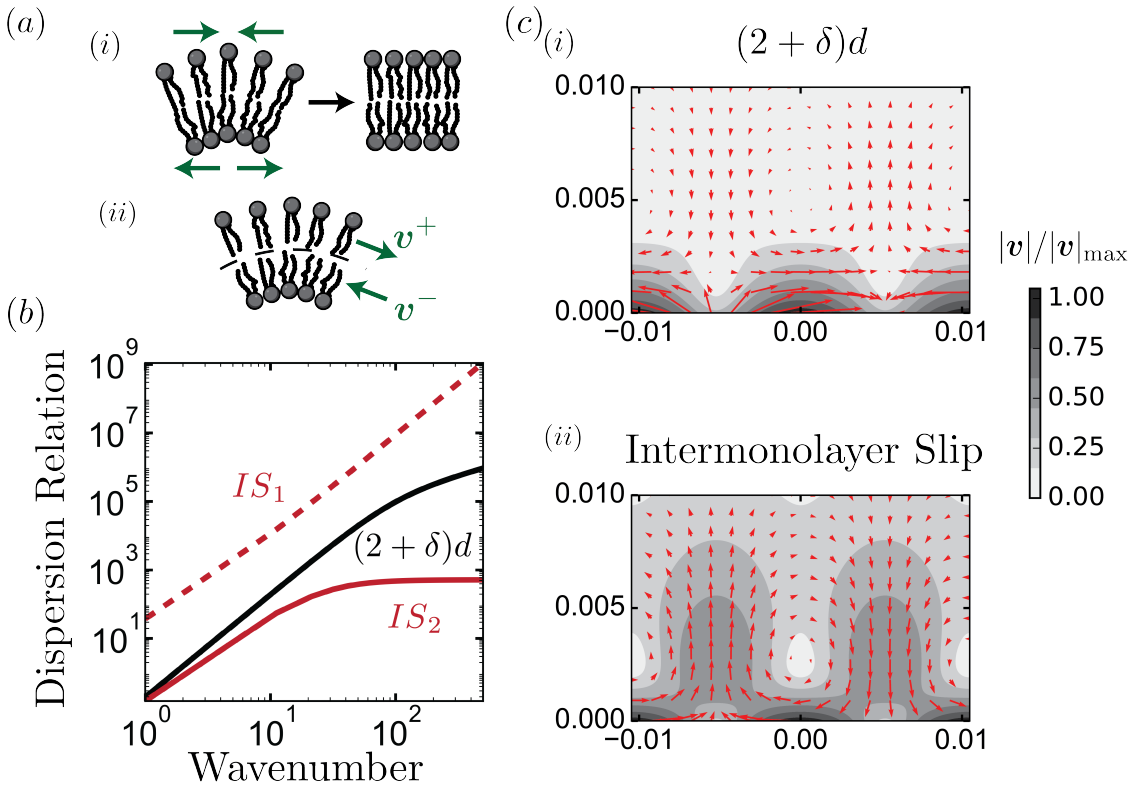


Figure 4.7: (a)–(i),(ii) The lipid reorientiation mechanism proposed in this work and the intermonolayer slip model. (b)– The dispersion relations for the intermonolayer slip model and the finite thickness model of the present work. In the intermonolayer slip model, two dispersion relations are necessary describe the separate density and height mode dynamics. In our work, the height modes alone govern the dynamics of the bilayer. (c)-(i),(ii) Upper half-plane flow fields at $q = 300$ for the present finite thickness theory and the intermonolayer slip model, respectively. For comparison, we used the representative parameters $b = 10^9$ pN $\cdot$ $\mu$s/nm, $\Lambda_0 = 10^{-}8$ pN/nm, $\mu^{\mathrm{b}} = 10^{-}3$ pN $\cdot$ $\mu$s/nm$^2$, $\mu^{\mathrm{m}} = 1$ pN $\cdot$ $\mu$s/nm, $\kappa = 100$ pN $\cdot$ nm, $k_{\mathrm{m}}$ 100 pN/nm[27].

### 4.3.6 Comparison with intermonolayer slip

In this section, we compare our results with the intermonolayer slip model [24, 25]. In this model, the monolayers of the bilayer are considered decoupled, allowing one to slip past the other, as shown in Fig. 4.7 (a)–(ii). This phenomenon is called "intermonolayer slip" and leads to the the existence of two dispersion relations, which we label $\mathrm{IS}_1$ and $\mathrm{IS}_2$ in Fig. 4.7 (b) and resulting in a dissipative friction with coefficient $b$ between the monolayers, $\mathbf{f} := b(\mathbf{v}^+ - \mathbf{v}^-)$, that affects the membrane dynamics. At high wavenumbers (e.g. $q > q_2$), the slower mode becomes constant while it can be shown that the faster mode scales with $q^3$ [24, 29]. Physically, the faster and slower modes correspond to height and density field

relaxations, respectively. It can be shown that the static density density difference between the two monolayers is related to the height field through $\rho_{\mathbf{q}} = \ell q^2 h_{\mathbf{q}}$ [32], where in this model $\ell$ is a measure of thickness that describes the distance between the neutral surfaces of the two layers and $\rho \coloneqq \rho^+ - \rho^-$ is the difference between neutral surface densities of the top ($\rho^+$) and bottom ($\rho^-$) monolayers projected onto the bilayer mid-surface. Because the layers are decoupled, such differences are permitted as each monolayer bends independently. For example, when the top monolayer experiences compression at the bilayer mid-surface, the bottom monolayer experiences expansion so that the bilayer in total undergoes bending. Because the two monolayers are compressible at the mid-surface, in-plane flows develop at the mid-surface due to continuity [27, 28]. This mechanism leads to the familiar flow fields we find with the $(2+\delta)d-$theory.

To study the hydrodynamic response in the bulk, one may follow the steps outlined in [27], where Rayleighian is constructed and minimized with respect to quantities of interest to derive dynamic equations of motion, in accordance with Onsager's variational principle [97]. Figure 4.7 (c)–(i) & (ii) show the flow fields in the upper half plane for the $(2+\delta)d$ and intermonolayer slip theories, respectively. Both exhibit vortex flows above the the points where height field remains zero and where we observe surface in-plane motions. However, as discussed, our theory predicts these phenomena as a result of lipid reorientations, which are three-dimensional. The interemonolayer slip theory treats the two monolayers surfaces located at $z = \{0^+, 0^-\}$, whose in-plane flows are inherentely two-dimensional and result from density mode relaxation. The fundamental difference here is that the in-plane motion we resolve is elastic in nature, resulting from deformations in the bilayer relaxing, while the intermonolayer slip motion is a viscous flow, resulting from the two-dimensional membrane mass balance [27, 28].

Intermonolayer slip has been suggested as a intramembrane dissipative source to account for rapid non-equilibrium dynamics of lipid bilayers [98]. However, it is still a fundamentally two-dimensional framework. We have shown here a model that allows us to capture the three dimensional elastic nature of the lipid bilayer. It is possible the two in unison will allow for a more complete theory for lipid bilayer dynamics across all scales.

## 4.4 Summary

We have shown here that the finite thickness of lipid bilayers affects how they couple with the surrounding media. In particular, shear forces caused by lipid reorientations during bending develop at the membrane surfaces, resulting in in-plane flows that are not observed in pure two-dimensional membrane models. For fluctuations on the order of the membrane thickness, we predict that this coupling results in pressure inversion at the membrane surfaces, which indicates the existence of flow reversal in the vicinity of the bilayer. Stagnation points associated with bulk fluid circulatory and extensional flows mark where the flow reversal occurs. Our analysis shows that as the frequency of the membrane fluctuations increases, the extensional flow stagnation points both localize near the membrane and exhibit increasingly

large rates of viscous dissipation. Finally, we discussed the implication of our results on statistical descriptions of membrane fluctuations and their relevance for biological processes such as membrane permeation and intercellular contact.

# Chapter 5

# Conclusions and future work

Throughout this thesis, we embarked on a scientific journey into the world of finite thickness lipid bilayers, aiming to unravel their intricate properties. Our exploration began in Chapter 1, where we laid the mathematical groundwork using principles of differential geometry. By adopting Kirchhoff-Love kinematics, we established a robust framework to describe the deformations of lipid bilayers, with a particular focus on characterizing their geometry and kinematics through the parameterization of the mid-surface.

In Chapter 2, we introduced a dimension reduction framework that allowed us to derive essential two-dimensional balance laws from their three-dimensional counterparts, resulting in what we termed the $(2+\delta)$-dimensional theory. By applying this framework to the constitutive relations governing viscous elastic membranes, we successfully derived the equations of motion for finite thickness membranes immersed in viscous fluids. This theoretical foundation equipped us with the tools necessary to investigate the complex behaviors of these bilayers.

Chapter 3 marked our investigation of the fluctuations of nearly flat finite thickness lipid bilayers within an infinite medium, employing linear response theory as our guide. Our findings unveiled the influence of finite thickness on the bilayers' interactions with their surroundings. Notably, we uncovered the emergence of shear forces arising from lipid reorientations during bending, leading to in-plane flows that are absent in traditional two-dimensional membrane models. Moreover, for fluctuations of a scale similar to the membrane thickness, we predicted the occurrence of pressure inversion at the bilayer's surfaces, which coincided with the presence of flow reversal in the immediate vicinity of the membrane.

These flow reversals were intrinsically linked to the existence of stagnation points, associated with bulk fluid circulatory and extensional flows. As we increased the frequency of membrane fluctuations, these stagnation points shifted closer to the membrane, accompanied by a marked rate of viscous dissipation. Our analysis has far-reaching implications, particularly for statistical descriptions of membrane fluctuations and their relevance in the context of biological processes such as membrane permeation and intercellular contact.

In conclusion, this thesis represents a comprehensive exploration of finite thickness lipid bilayers. Our investigations spanned from the mathematical characterization of these struc-

tures to their hydrodynamic behaviors and fluctuations. The insights we have gained contribute significantly to our understanding of these complex biological membranes, shedding light on their roles in various physiological processes. The theoretical framework developed here and the applications provide a solid foundation for future research endeavors in the field of membrane science. In particular, applying this theory to systems with multiple membranes may yield interesting results. The linear response results suggest that it is possible that finite thickness effects may lead to attractive forces at short distances, suggesting that hydrodynamics may drive membrane fusion phenomena. Furthermore, the transport of solutes through the membrane may be influenced by these flow fields. To further understand such phenomena, numerical schemes will be required to fully resolve the membrane-fluid dynamics. The theory itself is a low-order, effective framework that can be improved by going beyond K-L kinematics, and allowing for thickness fluctuations. This will require a careful formulation of different kinematic assumptions while retaining analytic tractability.

# Bibliography


1. Alberts, B. *et al. Molecular Biology of the Cell* (Garland Science, New York City, 2002).
2. Dror, R. O. *et al.* Pathway and mechanism of drug binding to G-protein-coupled receptors. en. *Proceedings of the National Academy of Sciences* **108,** 13118–13123 (Aug. 2011).
3. Marrink, S. J., Risselada, H. J., Yefimov, S., Tieleman, D. P. & De Vries, A. H. The MARTINI Force Field: Coarse Grained Model for Biomolecular Simulations. en. *The Journal of Physical Chemistry B* **111,** 7812–7824 (July 2007).
4. Jensen, M. Ø. *et al.* Mechanism of Voltage Gating in Potassium Channels. en. *Science* **336,** 229–233 (Apr. 2012).
5. Lyumkis, D. *et al.* Cryo-EM Structure of a Fully Glycosylated Soluble Cleaved HIV-1 Envelope Trimer. en. *Science* **342,** 1484–1490 (Dec. 2013).
6. Helfrich, W. Elastic Properties of Lipid Bilayers: Theory and Possible Experiments. *Zeitschrift fur Naturforschung - Section C Journal of Biosciences* **28,** 693–703 (1973).
7. Brown, F. L. Continuum simulations of biomembrane dynamics and the importance of hydrodynamic effects. *Quarterly Reviews of Biophysics* **44,** 391–432 (2011).
8. Agrawal, A. & Steigmann, D. J. Modeling protein-mediated morphology in biomembranes. en. *Biomechanics and Modeling in Mechanobiology* **8,** 371–379 (Oct. 2009).
9. Arroyo, M. & Desimone, A. Relaxation dynamics of fluid membranes. *Physical Review E - Statistical, Nonlinear, and Soft Matter Physics* **79,** 1–17 (2009).
10. Steigmann, D. J. Fluid films with curvature elasticity. *Archive for Rational Mechanics and Analysis* **150,** 127–152 (1999).
11. Sahu, A., Sauer, R. A. & Mandadapu, K. K. Irreversible thermodynamics of curved lipid membranes. *Physical Review E* **96,** 1–62 (2017).
12. Watanabe, S. *et al.* Ultrafast endocytosis at Caenorhabditis elegans neuromuscular junctions. *eLife* **2013,** 1–24 (2013).
13. Omar, Y. A., Sahu, A., Sauer, R. A. & Mandadapu, K. K. Nonaxisymmetric Shapes of Biological Membranes from Locally Induced Curvature. en. *Biophysical Journal* **119,** 1065–1077 (Sept. 2020).

14. Saffman, P. G. & Delbrueck, M. Brownian motion in biological membranes. *Proceedings of the National Academy of Sciences of the United States of America* **72,** 3111–3113 (1975).

15. Agrawal, A. & Steigmann, D. J. A model for surface diffusion of trans-membrane proteins on lipid bilayers. *Zeitschrift fur Angewandte Mathematik und Physik* **62,** 549–563 (2011).

16. Steigmann, D. J. On the relationship between the Cosserat and Kirchhoff-Love theories of elastic shells. *Mathematics and Mechanics of Solids* **4,** 275–288 (1999).

17. Deserno, M. Fluid lipid membranes: From differential geometry to curvature stresses. *Chemistry and Physics of Lipids* **185.** Publisher: Elsevier Ireland Ltd, 11–45 (2015).

18. Liu, J., Kaksonen, M., Drubin, D. G. & Oster, G. Endocytic vesicle scission by lipid phase boundary forces. en. *Proceedings of the National Academy of Sciences* **103,** 10277–10282 (July 2006).

19. Dmitrieff, S. & Nédélec, F. Membrane Mechanics of Endocytosis in Cells with Turgor. en. *PLOS Computational Biology* **11** (ed Ewers, H.) e1004538 (Oct. 2015).

20. Phillips, R., Ursell, T., Wiggins, P. & Sens, P. Emerging roles for lipids in shaping membrane-protein function. en. *Nature* **459,** 379–385 (May 2009).

21. Kaizuka, Y. & Groves, J. T. Hydrodynamic Damping of Membrane Thermal Fluctuations near Surfaces Imaged by Fluorescence Interference Microscopy. en. *Physical Review Letters* **96,** 118101 (Mar. 2006).

22. Liu, K. *et al.* Hydrodynamics of transient cell-cell contact: The role of membrane permeability and active protrusion length. en. *PLOS Computational Biology* **15** (ed Asthagiri, A. R.) e1006352 (Apr. 2019).

23. Qi, S. Y., Groves, J. T. & Chakraborty, A. K. Synaptic pattern formation during cellular recognition. en. *Proceedings of the National Academy of Sciences* **98,** 6548–6553 (June 2001).

24. Seifert, U. & Langer, S. A. Viscous modes of fluid bilayer membranes. *Europhysics Letters* **23,** 71–76 (1993).

25. Evans, E. & Yeung, A. Chemistry and Physics of LIPIDS Hidden dynamics in rapid changes of bilayer shape. *Chemistry and Physics of Lipids* **73,** 39–56 (1994).

26. Seifert, U., Shillcock, J. & Nelson, P. Role of Bilayer Tilt Difference in Equilibrium Membrane Shapes. en. *Physical Review Letters* **77,** 5237–5240 (Dec. 1996).

27. Fournier, J. B. On the hydrodynamics of bilayer membranes. *International Journal of Non-Linear Mechanics* **75.** Publisher: Elsevier, 67–76 (2015).

28. Rahimi, M. & Arroyo, M. Shape dynamics, lipid hydrodynamics, and the complex viscoelasticty of bilayer membranes. *Physical Review E - Statistical, Nonlinear, and Soft Matter Physics* **86,** 1–15 (2012).

29. Watson, M. C., Peng, Y., Zheng, Y. & Brown, F. L. The intermediate scattering function for lipid bilayer membranes: From nanometers to microns. *Journal of Chemical Physics* **135** (2011).

30. Kelley, E. G., Frewein, M. P. K., Czakkel, O. & Nagao, M. Nanoscale Bending Dynamics in Mixed-Chain Lipid Membranes. en. *Symmetry* **15,** 191 (Jan. 2023).

31. Nagao, M., Kelley, E. G., Ashkar, R., Bradbury, R. & Butler, P. D. Probing elastic and viscous properties of phospholipid bilayers using neutron spin echo spectroscopy. *Journal of Physical Chemistry Letters* **8,** 4679–4684 (2017).

32. Seifert, U. Configurations of fluid membranes and vesicles. en. *Advances in Physics* **46,** 13–137 (Feb. 1997).

33. Aris, R. *Vectors, Tensors, and the Basic Equations of Fluid Mechanics* (Dover Publications, New York City, 1989).

34. Itskov, M. *Tensor Algebra and Tensor Analysis for Engineers: With Applications to Continuum Mechanics* (Springer Berlin Heidelberg, 2012).

35. Green, A. E. & Zerna, W. *Theoretical elasticity* (Oxford University Press, 1992).

36. Rangamani, P., Agrawal, A., Mandadapu, K. K., Oster, G. & Steigmann, D. J. Interaction between surface shape and intra-surface viscous flow on lipid membranes. *Biomechanics and Modeling in Mechanobiology* **12,** 833–845 (2013).

37. Sahu, A., Omar, Y. A., Sauer, R. A. & Mandadapu, K. K. Arbitrary Lagrangian–Eulerian finite element method for curved and deforming surfaces: I. General theory and application to fluid interfaces. *Journal of Computational Physics* **407,** 109253 (2020).

38. Chadwick, P. *Continuum mechanics: concise theory and problems* (Dover Publications, 1999).

39. Naghdi, P. M. N. in *Handbuch der Physik Vol. I/Ia* (ed Truesdell, C.) 425–640 (Springer-Verlag Berlin Heidelberg, 1972).

40. Ciarlet, P. G. *Theory of shells* (Elsevier, 2000).

41. Steigmann, D. J. On the relationship between the Cosserat and Kirchhoff-Love theories of elastic shells. *Mathematics and Mechanics of Solids* **4,** 275–288 (1999).

42. Omar, Y. A., Lipel, Z. G. & Mandadapu, K. K. The $(2+\delta)$-dimensional theory of the electromechanics of lipid membranes: II. Balance laws. *arXiv preprint arXiv:2309.03863* (2023).

43. Popov, E. P. *Engineering mechanics of solids* (Prentice Hall, 1990).

44. Gurtin, M. E., Fried, E. & Anand, L. *The mechanics and thermodynamics of continua* (Cambridge university press, 2010).

45. Truesdell, C. & Toupin, R. A. in *Principles of Classical Mechanics and Field Theory, Handbuch der Physik, Vol. III/I* (ed Flugge, S.) (Springer-Verlag Berlin Heidelberg, 1960).

46. Casey, J. On the derivation of jump conditions in continuum mechanics. *The International Journal of Structural Changes in Solids* **3,** 61–84 (2011).
47. Jackson, J. D. *Classical Electrodynamics* (Wiley, New York City, 1962).
48. Wheeden, R. L. *Measure and integral: an introduction to real analysis* (CRC press, 2015).
49. Boyd, J. P. *Chebyshev and Fourier spectral methods* (Courier Corporation, 2001).
50. Omar, Y. A., Lipel, Z. G. & Mandadapu, K. K. The $(2+\delta)$-dimensional theory of the electromechanics of lipid membranes: I. Electrostatics. *arXiv preprint arXiv:2301.09610* (2023).
51. Green, A. E. & Shield, R. Finite elastic deformation of incompressible isotropic bodies. *Proceedings of the Royal Society of London. Series A. Mathematical and Physical Sciences* **202,** 407–419 (1950).
52. Chien, W.-Z. The intrinsic theory of thin shells and plates. III. Application to thin shells. *Quarterly of Applied Mathematics* **2,** 120–135 (1944).
53. Evans, E. A. & Skalak, R. *Mechanics and Thermodynamics of Biomembranes* (CRC Press, Boca Raton, Fl, 1980).
54. Nichol, J. A. & Hutter, O. F. Tensile strength and dilatational elasticity of giant sarcolemmal vesicles shed from rabbit muscle. *Journal of Physiology* **493,** 187–198 (1996).
55. Scriven, L. E. Dynamics of a fluid interface Equation of motion for Newtonian surface fluids. *Chemical Engineering Science* **12,** 98–108 (1960).
56. Oldroyd, J. G. On the formulation of rheological equations of state. *Proceedings of the Royal Society of London. Series A. Mathematical and Physical Sciences* **200,** 523–541 (1950).
57. Sahu, A., Glisman, A., Tchoufag, J. & Mandadapu, K. K. Geometry and dynamics of lipid membranes Supplemental Material I . Theoretical Considerations, 1–34.
58. Rajagopal, K. R. On implicit constitutive theories. *Applications of Mathematics* **48,** 279–319 (2003).
59. Rajagopal, K. R. & Srinivasa, A. R. On the nature of constraints for continua undergoing dissipative processes. *Proceedings of the Royal Society A: Mathematical, Physical and Engineering Sciences* **461,** 2785–2795 (2005).
60. Sahu, A., Glisman, A., Tchoufag, J. & Mandadapu, K. K. Geometry and dynamics of lipid membranes: the Scriven-Love number. *Physical Review E* **101,** 052401 (2020).
61. Lacoste, D., Menon, G., Bazant, M. & Joanny, J. Electrostatic and electrokinetic contributions to the elastic moduli of a driven membrane. *The European Physical Journal E* **28,** 243–264 (2009).

62. Shibly, S. U. A., Ghatak, C., Karal, M. A. S., Moniruzzaman, M. & Yamazaki, M. Experimental estimation of membrane tension induced by osmotic pressure. *Biophysical journal* **111,** 2190–2201 (2016).

63. Vlahovska, P. M. Electrohydrodynamics of Drops and Vesicles. *Annual Review of Fluid Mechanics* **51,** 305–330 (2018).

64. Bassereau, P., Sorre, B. & Lévy, A. Bending lipid membranes: Experiments after W. Helfrich's model. *Advances in Colloid and Interface Science* **208.** Publisher: Elsevier B.V., 47–57 (2014).

65. Rangamani, P., Mandadapu, K. K. & Oster, G. Protein-induced membrane curvature alters local membrane tension. *Biophysical Journal* **107.** Publisher: Biophysical Society, 751–762 (2014).

66. Truesdell, C. A. *Foundations of continuum mechanics* in *Delaware seminar in the foundations of physics* (1967), 35–48.

67. Deseri, L., Piccioni, M. D. & Zurlo, G. Derivation of a new free energy for biological membranes. *Continuum Mechanics and Thermodynamics* **20,** 255–273 (2008).

68. Saffman, P. G. Brownian motion in thin sheets of viscous fluid. *Journal of Fluid Mechanics* **73,** 593–602 (1976).

69. Faizi, H. A., Dimova, R. & Vlahovska, P. M. A vesicle microrheometer for high-throughput viscosity measurements of lipid and polymer membranes. arXiv: 2103.02106, 1–20 (2021).

70. Landau, L. D. & Lifshitz, E. M. *Fluid Mechanics* (Pergamom Press, 1959).

71. Happel, J. & Brenner, H. *Low Reynolds number hydrodynamics* (Prentice Hall, 1965).

72. Leal, L. G. *Advanced transport phenomena: fluid mechanics and convective transport processes* (Cambridge University Press, Cambridge, 2010).

73. Deen, W. M. *Analysis of Transport Phenomena* (Oxford University Press, 2011).

74. Purcell, E. M. Life at low Reynolds number. *American Journal of Physics* **45,** 3–11 (1977).

75. Sahu, A., Glisman, A., Tchoufag, J. & Mandadapu, K. K. Geometry and dynamics of lipid membranes: The Scriven-Love number. *Physical Review E* **101,** 1–16 (2020).

76. Lidmar, J., Mirny, L. & Nelson, D. R. Virus shapes and buckling transitions in spherical shells. *Physical Review E - Statistical Physics, Plasmas, Fluids, and Related Interdisciplinary Topics* **68.** arXiv: cond-mat/0306741, 1–10 (2003).

77. Pécréaux, J., Döbereiner, H. G., Prost, J., Joanny, J. F. & Bassereau, P. Refined contour analysis of giant unilamellar vesicles. *European Physical Journal E* **13,** 277–290 (2004).

78. Phillips, R. Membranes by the Numbers. *Physics of Biological Membranes,* 73–105 (2018).

79. Dai, J., Sheetz, M. P., Wan, X. & Morris, C. E. Membrane tension in swelling and shrinking molluscan neurons. *Journal of Neuroscience* **18,** 6681–6692 (1998).

80. Shi, Z., Graber, Z. T., Baumgart, T., Stone, H. A. & Cohen, A. E. Cell Membranes Resist Flow. en. *Cell* **175,** 1769–1779.e13 (Dec. 2018).

81. Leduc, C. *et al.* Cooperative extraction of membrane nanotubes by molecular motors. en. *Proceedings of the National Academy of Sciences* **101,** 17096–17101 (Dec. 2004).

82. Nan, B. & Zusman, D. R. Uncovering the Mystery of Gliding Motility in the Myxobacteria. en. *Annual Review of Genetics* **45,** 21–39 (Dec. 2011).

83. Tchoufag, J., Ghosh, P., Pogue, C. B., Nan, B. & Mandadapu, K. K. Mechanisms for bacterial gliding motility on soft substrates. en. *Proceedings of the National Academy of Sciences* **116,** 25087–25096 (Dec. 2019).

84. Monge, G. *Application de l'analyse à la géométrie* (Bernard, Paris, 1807).

85. Takatori, S. C. & Mandadapu, K. K. Motility-induced buckling and glassy dynamics regulate three-dimensional transitions of bacterial monolayers. arXiv: 2003.05618 (2020).

86. Zilman, A. G. & Granek, R. Membrane dynamics and structure factor. *Chemical Physics* **284,** 195–204 (2002).

87. Yi, Z., Nagao, M. & Bossev, D. P. Bending elasticity of saturated and monounsaturated phospholipid membranes studied by the neutron spin echo technique. *Journal of Physics: Condensed Matter* **21,** 155104 (Apr. 2009).

88. Nagao, M. Observation of local thickness fluctuations in surfactant membranes using neutron spin echo. en. *Physical Review E* **80,** 031606 (Sept. 2009).

89. Monzel, C. & Sengupta, K. Measuring shape fluctuations in biological membranes. *Journal of Physics D: Applied Physics* **49,** 243002 (June 2016).

90. Brochard, F. & Frequency, J. F. L. erythrocytes (1975).

91. Granek, R. From Semi-Flexible Polymers to Membranes: Anomalous Diffusion and Reptation. *Journal de Physique I* **7,** 1761–1788 (1997).

92. Takatori, S. C. & Sahu, A. Active Contact Forces Drive Nonequilibrium Fluctuations in Membrane Vesicles. *Physical Review Letters* **124,** 158102 (2020).

93. Lin, L. C. & Brown, F. L. Brownian dynamics in Fourier space: Membrane simulations over long length and time scales. *Physical Review Letters* **93,** 1–4 (2004).

94. Doi, M. & Edwards, S. F. *The Theory of Polymer Dynamics-Oxford University Press* Pages: 391 Place: New York City. 1988.

95. Frallicciardi, J., Melcr, J., Siginou, P., Marrink, S. J. & Poolman, B. Membrane thickness, lipid phase and sterol type are determining factors in the permeability of membranes to small solutes. en. *Nature Communications* **13,** 1605 (Mar. 2022).

96. Lin, L. C.-L., Groves, J. T. & Brown, F. L. Analysis of Shape, Fluctuations, and Dynamics in Intermembrane Junctions. en. *Biophysical Journal* **91,** 3600–3606 (Nov. 2006).

97. Doi, M. Onsager's variational principle in soft matter. *Journal of Physics Condensed Matter* **23** (2011).

98. Evans, E. & Yeung, A. Hidden dynamics in rapid changes of bilayer shape. en. *Chemistry and Physics of Lipids* **73,** 39–56 (Sept. 1994).